Inaugural dissertation

for

obtaining the doctoral degree

of the

Combined Faculty of Mathematics, Engineering and Natural Sciences

of the

Ruprecht - Karls - University

Heidelberg

Presented by

M.Sc. Julia Zaman

Born in: Neu-Ulm

Oral examination: 18.02.2022

GENETICALLY ENGINEERED MURINE NSCS

MIMIC

HUMAN IDH-MUT ASTROCYTOMA

Referees: PD Dr. Karin Müller-Decker

Prof. Dr. Andreas von Deimling

Declaration

The work presented in the following dissertation was carried out from July 2018 until December 2021 in the Clinical Cooperation Unit Neuropathology at the German Cancer Research Center (DKFZ) in Heidelberg (Germany) and was supervised by Dr. Stefan Pusch and Prof. Dr. Andreas von Deimling.

I hereby declare that I have written this dissertation myself and that I have not used any other sources than those indicated. I further have not applied to be examined at any other institution, nor have I submitted the dissertation in this or any other form at any other institution as an examination paper, nor it to any other faculty as a dissertation.

Heidelberg, 2nd December 2021

Julia Zaman

Table of content

Summary

Gliomas are the most frequent adult central nervous system (CNS) tumors. The 2016 published WHO CNS classification update implemented the mutational status of the enzyme isocitrate dehydrogenase (IDH) as important diagnostic marker in glioma. Thus it became defining of *IDH*-mutant astrocytoma (IDH-mut A) WHO grade 2-4 and oligodendroglioma WHO grade 2-3. The genetic and epigenetic landscape of glioma with *IDH*-mutant vs. *IDH* wild-type varies significantly and is used for tumor classification.

These glioma samples carry heterozygous point mutations in IDH1 or IDH2. The most frequently observed variant is IDH1 R132H mutation occurring in >90% of astrocytoma. In this case the arginine residue in codon 132 is substituted by a histidine causing a gain-of-function. While wild-type IDH enzymes naturally catalyze the production of alpha-ketoglutarate (α-KG) from isocitrate, mutant IDH1 convert α-KG into D-2-hydroxyglutartate (2-HG). 2-HG acts as a competitive inhibitor of α-KG dependent enzymes and in doing so influences several tumor-promoting processes and by this acts as an oncometabolite. Most important, it inhibits DNA demethylases leading to a global hypermethylation phenotype.

IDH mutations are considered as an early event as well as tumor driver in the development of glioma. Besides this IDH-mut A harbor loss-of-function mutations in TP53 and ATRX in high frequencies.

Much is known about the genetics of IDH-mut A. However, to gain deeper insights into their development and progression, a representative and biological relevant model is needed, which is still lacking. Especially how biological mechanisms behind common alterations synergize, is not fully understood yet. All current models have weak points regarding various aspects. But the opportunity to identify new targets and test treatment options also integrating the tumor microenvironment will allow research to progress and patients to benefit. To close this gap, I aimed to establish an innovative comprehensive mouse model harboring not only the typical mutations but crucial IDH-mut A features.

To model IDH-mut A I used neural stem cells (NSCs) derived from genetically engineered mice. The mice harbor an inducible heterozygous $Idh1^{R132H}$ knock-in alteration as well as loxP based homozygous $p53^{ko}$ and $Atrx^{ko}$ alleles in all possible combinations. Using this model, the effect of $Idh1^{R132H}$ and its associated alterations can be investigated in a well-defined *in vitro* setting. My findings showed that $Idh1^{R132H}p53^{ko}Atrx^{ko}$ leads to a more tumorigenic behavior, evidenced by increased viability and decreased apoptosis. Furthermore, it points out that induction of $Idh1^{R132H}$ is sufficient to develop the typical hypermethylation phenotype over time. By comparing methylation data of murine and human samples the advanced analysis revealed important pathways related to differentiation and tumorigenicity being altered. Furthermore the proteome data reveal adaptions seen most clearly in

the cells' metabolism. The following *in vivo* part was divided into a pilot experiment and the main experiment. The pilot experiment mainly aimed at identifying a for my purpose suitable immunodeficient strain, what turned out to be important. Within the main experiment I injected the murine NSCs intracranial into the brains of immunocompetent animals. After 10 months a higher lesion developing rate in $Idh1^{R132H}p53^{ko}Atrx^{ko}$ was detected by MRI.

Although my current work focused on generation, validation and characterization of the model it offers first valuable insights into the complex interplay between genetic, epigenetic and proteomic changes in IDH-mut A. Moreover the established model itself provides the basic framework for a future profound understanding of these tumors with additional treatment testing option.

Zusammenfassung

Gliome sind die häufigsten Tumore des zentralen Nervensystems bei Erwachsenen. Die 2016 erschienene Gehirntumor Klassifikation der WHO führte erstmals den Mutationsstatus des Enzyms Isocitrat-Dehydrogenase (IDH) als wichtigen Marker zur Gliom-Diagnose auf. Seitdem definiert diese Mutation die IDH mutierten Astrozytome WHO Grad 2-4 sowie Oligodendrogliome WHO Grad 2-3. Sowohl die genetische als auch epigenetische Signatur von IDH mutierten und IDH wildtyp Gliomen unterscheidet sich so markant, dass sie zur Tumorklassifikation verwendet wird.

Diese Tumorproben weisen alle eine heterozygote Punktmutation in IDH1 oder IDH2. Dabei handelt es sich bei der IDH1 R132H Variante mit einem Vorkommen von > 90% in Astrozytomen, um die meist verbreitetste. Der Austausch des Argininrests an Position 132 durch Histidin führt zu einem Funktionszugewinn. Während das wildtyp IDH-Enzym natürlicherweise die Produktion von Alpha-Ketoglutarat (α-KG) aus Isocitrat katalysiert, wandelt das mutierte Enzym α-KG in D-2-Hydroxyglutarat (2-HG) um. 2-HG fungiert als kompetitiver Inhibitor aller α-KG abhängigen Enzyme und beeinflusst dabei mehrere tumor-fördernde Prozesse und zählt daher als Onkometabolit. Besonders bedeutend dabei ist die Hemmung von DNA und Histonedemethylasen, was zu einem globalen Hypermethylierungs-Phänotyp führt.

In der Entwicklung von Gliomen wird die IDH Mutation als sehr frühes und tumor-treibendes Ereignis angesehen. Daneben zeigen IDH-mut A sehr häufig Veränderungen von TP53 und ATRX, die zum Funktionsverlust führen.

Wir kennen die Genetik dieser Tumore heute zwar sehr präzise, zur genauen Erforschung der Entwicklung und Progression, fehlt es aber aktuell an einem repräsentativen und vor allem biologisch relevanten Modelsystem. Ein bis heute nicht verstandener Aspekt ist das synergistische Zusammenspiel der biologischen Mechanismen, die die charakteristischen Veränderungen hervorrufen. Alle aktuell verwendeten Modelle haben verschiedene Schwachpunkte. Eine Möglichkeit neue Therapieoptionen zu identifizieren und zu testen und dabei auch das Mikromilieu des Tumors nicht zu vernachlässigen, würde die Forschung einen großen Schritt voranbringen und vielen Patienten zu Gute kommen. Um diese Lücke zu schließen, habe ich mir in dieser Arbeit zum Ziel gesetzt ein innovatives, umfassendes Mausmodel zu etablieren, welches nicht nur die IDH-mut A-typischen Mutationen trägt, sondern auch seine entscheidenden Eigenschaften abbildet.

Um dies zu erstellen, habe ich Neurale Stammzellen (NSCs) verwendet, die aus gentechnisch veränderten Mäusen stammen. Die Mäuse tragen heterozygot ein induzierbares $Idh1^{R132H}$ knock-in Konstrukt, sowie homozygote loxP basierte knock-out Konstrukte für p53 und Atrx in allen möglichen Kombinationen. Dank dieses Model kann der Effekt von $Idh1^{R132H}$ und seinen assoziierten

Veränderungen innerhalb eines klar definierten *in vitro* Systems untersucht werden. Meine Forschungsergebnisse zeigen, dass Idh1^{R132H}p53^{ko}Atrx^{ko} ein tumorigeneres Verhalten der Zellen auslöst, was sich in erhöhter Vitalität und verminderter Apoptose darstellen lässt. Außerdem konnte ich zeigen, dass die Induktion von Idh1^{R132H} in den Zellen ausreicht, um mit der Zeit den bekannten Hypermethylierungs-Phänotyp auszubilden. Durch die fortgeschrittenen Analysen des Vergleichs von humanen und murinen Methylierungsdaten hat sich hierbei die Beteiligung elementarer Signalwegen ergeben, die besonders Zelldifferenzierung und Tumorigenität beeinträchtigen. Auf Proteome-Ebene sieht man die größten Veränderungen bei Proteinen, die in Metabolismus involviert sind. Der darauffolgende in vivo Teil lässt sich in Pilot- und Hauptexperiment aufteilen. Wobei das Pilotexperiment zum Ziel hatte einen allen Anforderungen entsprechenden immundefizienten Mausstamm zu finden, was sich als durchaus wichtig herausstellte. Im Hauptexperiment habe ich die murinen NSCs intrakraniell in immundefiziente Mäuse injiziert. Am Ende des Versuchs wurde in der Idh1^{R132H}p53^{ko}Atrx^{ko} Gruppe eine höhere Läsions-Entstehungsrate im MRT nachgewiesen.

Auch wenn sich meine aktuelle Arbeit mehr auf die Generation, Validierung und Charakterisierung des Modells fokussiert hat, habe ich erste wichtige Einblicke in das komplexe Zusammenspiel von genetischen, epigenetischen und proteomischen Veränderungen IDH-mutierter Astrozytome erhalten können. Außerdem bietet mein generiertes Modell die Grundlage um zukünftig ein fundiertes Verständnis dieser Tumore zu erhalten und Behandlungsmöglichkeiten zu testen.

Figures

Abbreviations

°C	celsius
µ	micro
2-HG	D-2-hydroxyglutarate
4-OHT	4-hydroxytamoxifen
5hmC	5-hydroxymethylcytosine
5mC	5-methylcytosine
A	ampere
A, C, T, G, U, (N)	adenine, cytosine, guanine, thymine, uracile, (N: any nucleotide)
ALT	alternative lengthening of telomeres
ALT	alternative lengthening of telomeres
AML	acute myeloid leukemia
Amp	ampicillin
AMPK	AMP-activated protein kinase
ATAC-seq	assay for transposase-accessible chromatin with high-throughput sequencing
ATP	adenosine-5´-triphosphat
ATRX	human alpha thalassemia/mental retardation Syndrome X-Linked
Atrx	murine alpha thalassemia/mental retardation Syndrome X-Linked
B6	C57BL/6 N
bFGF	basic fibroblast growth factor
bp	base pair
BSA	bovine serum albumin
C	cysteine
Ca^{2+}	calcium ion
CDKN2A/Cdkn2a	Cyclin Dependent Kinase Inhibitor 2A
cDNA	complementary DNA
ChIP-seq	chromatin immunoprecipitation coupled with sequencing
chr.	chromosome
CpG	cytosine-phosphate-guanine
CreERT2	Cre recombinase fused to estrogen ligand-binding domain mutant 2
CTG	CellTiterGlo
ctrl	control
DMEM	Dulbecco's modified eagle's medium
DMSO	dimethylsulfoxid
DNA	desoxyribonucleic acid
DNase	desoxyribonuclease
dNTP	2'-deoxyribonucleoside 5'-triphosphate
dsDNA	double-stranded DNA
DTT	dithiothreitol
E. coli	Escherischia coli
EDTA	ethylendiamintetraacetic acid, Na-salt
EGF	epidermal growth factor
ER	endoplasmic reticulum
et al.	et alii (and other)
EtOH	ethanol

FACS	fluorescence activated cell sorting
FBS/FCS	fetal bovine serum/fetal calf serum
FDR	false discovery rate
g	gram
G	gauge
GBM	glioblastoma
G-CIMP	glioma CpG island methylator phenotype
GFP	green fluorescent protein
GO	gene ontology
gRNA	guide RNA
h	hour(s)
H	histidine
H3/4/2A/2B	histone 3/4/2A/2B
HBSS	Hanks' Balanced Salt Solution
HEPES	4-(2-hydroxyethyl)-1-piperazineethanesulfonic acid
hg19	human genome 19
HPLC	high performance liquid chromatography
HRP	horse reddish peroxidase
HxKy	histone x at lysine residue y
HxKyme3	trimethylation of histone x at lysine residue y
IDH	human isocitrate dehydrogenase
Idh	murine isocitrate dehydrogenase
$IDH1^{R132H}$	IDH1 point mutation at codon 132 (R->H substitution)
IDH-mut	IDH mutant
Il2ry	interleukin 2 receptor, gamma chain
IPA	$Idh1^{R132H}p53^{ko}Atrx^{ko}$
Jmjc	Jumonji C
kb	kilo base
kDa	kilo dalton
KEGG	kyoto encyclopedia of genes and genomes
KO	knockout
l	liter
L	leucine
LC-MS/MS	Liquid chromatography tandem-mass spectrometry
log	logarithmic scale
m	milli
M	molar
Mb	mega base
methyl-seq	methylation sequencing
Mg^{2+}	magnesium ion
min	minute(s)
mRNA	messenger RNA
mTOR	mammalian Target of Rapamycin
n	nano
NaCl	sodium chloride

NP-40	nonyl phenoxypolyethoxylethanol
NRAS	neuroblastoma Ras (Rat sarcoma)
NRG	NOD rag gamma (NOD-Rag1^{null} Il2ry^{null})
NSCs	Neural stem cells
NSG	NOD scid gamma (NOD-*Prkdc*^{scid} Il2ry^{null})
NShelf/NShore	North Shore/Shelf (upstream)
P/S/A	Penicillin/Streptomycin/Antimycotic
p53	Cellular tumor antigen p53
PAGE	polyacrylamide gel electrophoreses
PBS	phosphate-buffered saline
PCR	polymerase chain reaction
PHD	plant homeodomain
post-mortem	after death
Prkdc	Protein Kinase, DNA-Activated, Catalytic Subunit
PTEN/Pten	phosphatase and tensin homolog
Q	glutamine
R	arginine
Rag 1/Rag 2	recombination activating 1/2
RNA	ribonucleic acid
rpm	rotation per minute
RT	room temperature
s	second(s)
SDC	sodiumdeoxycholate
SDM	side-directed mutagenesis
SDS	sodiumdodecylsulfat
shRNA	short hairpin RNA
SShore/SShore	South Shore/Shelf (downstream)
SWI/SNF	SWItch/Sucrose Non-Fermentable
Tam	tamoxifen
TBE	Tris/Borat/EDTA
TBS	Tris buffered saline
TCGA	The Cancer Genome Atlas
TET enzymes	ten-eleven translocation methylcytosine dioxygenases
Tlx	tailless
Tris	tris-(hydroxymethyl)-aminomethan
Triton X-100	octyl-phenoxy-ethylenoxide
t-SNE	t-distributed stochastic neighbor embedding
TSS	transcriptional start site
Tween 20	Polyoxyethylen-20-sorbitanmonolaurat
U	unit (enzyme activity)
ULA	ultra-low attachment
UV	ultraviolet
V	volt
W	watt
w	with

w/o	without
WB	western blotting
WGS	whole genome sequencing
YAP	yes-associated protein
β	beta

1. Introduction

1.1. IDH-mutant astrocytoma (IDH-mut A)

1.1.1. Background

Gliomas account for 80.8% of all primary malignant tumors of the brain and central nervous system and thus are the most frequent malignant entity (Ostrom et al., 2020). The most common location of glioma is supra-tentorial including frontal, temporal, parietal and occipital lobes (Ostrom et al., 2020).

Isocitrate dehydrogenase (IDH) mutations depict an essential and class-defining genetic event in adult-type diffuse glioma. (Louis et al., 2021) Since the Classification of Tumors of the CNS WHO 2016, glioma are stratified for their molecular signature: IDH mutant (IDH-mut) or IDH wild-type. The IDH-mut gliomas can further be subdivided into astrocytoma (IDH-mut A) or oligodendroglioma based on the co-occurrence of additional alterations such as *ATRX* and *TP53* mutations characteristic for IDH-mut A and 1p/19q codeletion in oligodendroglioma. (Louis et al., 2016; Louis et al., 2021) IDH-mut A occur in WHO grades 2-4 based on number of mitoses, necrosis and microvascular proliferation. Additionally, *CDKN2A/B* status, *PDGFRA*, *CDK4* or *MYCN* amplifications are associated with higher malignancy and shorter survival of IDH-mut glioma patients (Shirahata et al., 2018; Yang et al., 2020).

According to the EANO patients with this diagnosis currently receive a surgical resection of the tumor followed by radiotherapy and chemotherapy as standard-of-care. (Weller et al., 2021) A complete gross resection of all tumor cells is almost impossible due to the highly infiltrative growth behavior of glioma. (Cancer Genome Atlas Research et al., 2015). The diagnosis IDH-mut glioma predict a better prognosis and longer overall survival duration for patients compared to corresponding IDH wild-type tumors (for example 65 months vs. 20 months). (Jiao et al., 2012; Yan et al., 2009). The typical patient with the diagnosis adult-type IDH-mut A is a young adult with a median age between 36 and 38 years (grades 2/3 and grade 4). (Molinaro et al., 2019) This is, compared to typical glioblastoma patients with a median of 50-60 years, rather young. (Molinaro et al., 2019)

Besides the molecular signature IDH-mut A can be characterized by their genome-wide hypermethylation. Specific hypermethylation of cytosine phosphate guanine (CpG) islands characterizes the glioma CpG island methylator phenotype (G-CIMP). (Noushmehr et al., 2010)

Even though the presence of the IDH mutation is a favorable diagnosis, currently the recurrence rate of IDH-mut A is very high and relapse often return not only at the resection site but more remote. While recurring tumors are often connected with progression, the episodes between relapses shortens and still no curing treatment is found. (Cancer Genome Atlas Research et al., 2015; Miller et al., 2019)

1.1.1. Novel molecular treatment options for IDH-mut A

Because of their distinct composition IDH mutant tumors provide the opportunity for specialized treatment options.

Besides targeting epigenetic modulators, DNA repair enzymes, redox homeostasis, or metabolic enzymes (reviewed by: (Han et al., 2020; Karpel-Massler et al., 2019) the focus of the following section will lie on using mutant IDH as therapeutically weak point.

Mutant IDH1 inhibitors

IDH1 and IDH2 mutations as direct target have been investigated extensively, since it would be a smart and very tumor-specific solution to attack the tumor. AGI 5198 is the first small-molecule inhibitor that was synthesized to specifically inhibit the 2-HG production and treatment is described to induce growth suppression in IDH1 mutant xenograft models. (Rohle et al., 2013) The next generation of AGI inhibitors AG-120 (ivosidenib) and AG-881 (vorasidenib) recently got the FDA approvement as IDH-mutant AML therapy. (Dhillon, 2018; DiNardo et al., 2018b) Further clinical trials are running to demonstrate efficacy and expand the therapy by new entities such as glioma. (Konteatis et al., 2020; Mellinghoff et al., 2020)

Additionally, there are a number of other IDH1 inhibitors with reported tumor growth impairment in an experimental set-up. One of these is BAY-1436032, a small-molecule-inhibitor identified and established in our lab in cooperation with Bayer. The pan-compound of IDH1 mutations depicts a very low IC_{50} particularly for IDH1 R132H and R132C mutations. Further the *in vitro* efficiency has been demonstrated by treatment-induced reduction of 2-HG concentrations in several IDH1mutant cell lines. The patient-derived IDH-mut A (grade 4) cell line NCH 551b additionally had a decreased viability and increased differentiation markers. (Pusch et al., 2017). Under pre-clinical *in vivo* settings daily, BAY-1436032-therapy was sufficient to penetrate the blood-brain barrier and significantly prolonged the survival of mice observing an orthotopic NCH 551b injection. (Pusch et al., 2017)

However, the initially promising treatment option also has several limitations. These include resistance against radiation and chemotherapy induced by 2-HG inhibitor treatment. (Molenaar et al., 2015; Sulkowski et al., 2017) Consequently the combination with different classes of drugs such as epigenetic modulators should also be fostered and further combination screens seem to be essential in the glioma context. (Dinardo et al., 2018a)

Immunotherapies

In the past few years, clear evidence on the interference of the IDH mutation and 2-HG with the immunological tumor microenvironment evolved. The basis is the described immuno-suppressive function of 2-HG against infiltrating T cells, natural killer cells, macrophages and other leucocytes

(Amankulor et al., 2017; Bunse et al., 2018; Friedrich et al., 2021; Ren et al., 2019). This suppressive effect also explains why the down regulation of negative immune system regulators such as PD-L1 does not result in stronger anti-tumor immune system activation. (Wang et al., 2016). Thus combinations such as BAY-1436032 combined with anti-PD-1-derived immunotherapy results in decreased tumor volumes and longer survival in vivo. (Bunse et al., 2018) Despite testing further immune checkpoint inhibitors the IDH1 R132H mutation opens up new possibilities by presenting an immunogenic epitope. (Schumacher et al., 2014) Consequently a IDH1 peptide vaccine was developed and after successful extended survival in mice the first clinical trials (NCT02454634) are running. (Platten et al., 2018) For the immunotherapy approach combination therapies might even increase the efficiency and thereby be promising for all tumor patients with an IDH mutation.

1.2. Core mutations of IDH-mut A

1.2.1. *IDH1* and IDH2 mutation

The discovery of mutations in *IDH1* and *IDH2* in a subset of gliomas in 2008 caused further research on these enzymes. (Parsons et al., 2008) Besides gliomas other malignancies such as acute myeloid leukemia (Mardis et al., 2009; Paschka et al., 2010), intrahepatic cholangiocarcinoma (Borger et al., 2012; Farshidfar et al., 2017), chondrosarcoma (Amary et al., 2011) and melanoma (Shibata et al., 2011) harbor *IDH* mutations.

These *IDH* mutations are supposed to be early or even initiating events in the tumorigenesis. (Watanabe et al., 2009)

Wild-type enzymatic function of IDH

In a human cell three isoforms of IDH can be found: IDH1 found in the cytoplasm and peroxisome and IDH2 and IDH3 located in the mitochondria. IDH3 is not involved in any cancer-related cases, so that the further focus lies on IDH1 and IDH2 and how they impact tumor biology.

IDH1 and *IDH2* have highly similar DNA sequences, both form homodimers and promote the same reaction. In their wild-type state these enzymes catalyze the oxidative decarboxylation of isocitrate to alpha-ketoglutarate (α-KG) in a $NADP^+$ dependent manner. The reduced form, NADPH, is described as protective factor against reactive oxygen species and thereby prohibits DNA damage. (Lee et al., 2002)

Whereas α-KG is an essential co-factor for over 60 enzymes and related cellular reactions such as histone modifications, fatty acid metabolism, collagen biosynthesis, hypoxia sensing and more. (Loenarz and Schofield, 2008)

IDH mutations

Cancer-associated mutations in *IDH* occur at an arginine side that is important for isocitrate recognition and lies within the enzymatic active pocket of the enzyme: R132 for IDH1 and R172 for IDH2 (most common residues). (Yan et al., 2009) In glioma IDH1 R132H forms the majority of detected alterations. Thereby this point mutation leads to the exchange of the strong, positive charged arginine with amino acids exhibiting a lower polarity (for R132H: histidine (H)). Histidine replaced by cysteine (C), leucine (L), serine (S) and glycine (G) also happens but with decreasing incidence. (Yan et al., 2009) The frequencies of the substitutions are different in distinct tumor entities, but in the general result of the cancer-associated missense mutation, IDH enzyme shows a lower substrate binding affinity. (Zhao et al., 2009)

Due to the always heterozygous occurrence of the missense mutation, *IDH1* is supposed to be more likely an oncogene than a tumor suppressor gene where a both allelic inactivation would be necessary. (Stratton et al., 2009)

The major appearance of IDH1 dimers in mutated cells contains the combination of one wild-type and one mutant element. While the wild-type part functions as α-KG producer, the mutant component loses this function, but shows a neomorphic activity. Mutant IDH1/2 gains the function to reduce the previous product α-KG into D-2-hydroxyglutarate (2-HG) consuming NADPH. (Dang et al., 2010) In glioma cells this reduction leads to 100-fold increased 2-HG levels, which is nowadays referred to as oncometabolite. (Dang et al., 2010; Losman and Kaelin, 2013). Thus the heterozygous fashion of IDH1 is described to be necessary for considerable 2-HG production (Jin et al., 2013).

The biological impact of 2-HG

The effect of losing one wild-type enzyme and the additional consumption of α-KG and NADPH leading to reduced α-KG and NADPH levels result in imbalance in metabolism, biosynthesis and oxidative stress response (Grassian et al., 2014b; Reitman et al., 2011)

However, the novel modulated enzyme activity occurring in cancer-associated context has been shown to additionally effect the whole cellular system on several levels and thereby promote tumorigenicity.

The similar structures of 2-HG and α-KG who only differ in the oxidation status of the second C-atom entails a competitive inhibition of many α-KG dependent dioxygenases, a family with over 60 members. (Rose et al., 2011; Xu et al., 2011)

The most important changes will be discussed in detail to highlight some explanations for the tumorigenic role of mutant IDH1.

IDH mutation induces DNA hypermethylation phenotype

Within the group of IDH-mut glioma, but also across IDH-mut entities, hypermethylation can uniformly be detected. (Figueroa et al., 2010; Unruh et al., 2019) Investigating promoter methylation, a remarkable subgroup was identified among a TCGA data set of 272 glioma. (Noushmehr et al., 2010) All these tumors depicted a hypermethylation phenotype of a distinct CpG pattern, now known as G-CIMP, additionally this group was closely associated with *IDH1* mutations. The explaining mechanism behind this hypermethylation is based on the ten-eleven translocation (TET) family of 5-methylcytosine hydroxylases. TET enzymes normally work α-KG dependent and are involved in DNA demethylation by converting 5-methylcytosine (5mC) into 5-hydroxymethylcytosine (5hmC). Under IDH-mut conditions the described competitive inhibition of these enzymes by 2-HG entails decreased 5hmC levels and by this lead to a hypermethylated genome. (Figueroa et al., 2010; Losman and Kaelin, 2013; Turcan et al., 2012; Xu et al., 2011) DNA methylation consequently promotes tumorigenic potential by various effects on the gene expression landscape, especially reported in terms blocking differentiation. (Flavahan et al., 2016; Modrek et al., 2017)

IDH mutation promotes histone methylation

Another class of α-KG dependent dioxygenases are the Jumonji C (JmjC) histone lysine demethylases which are associated with pathogenicity in various tumor entities and are also assumed to be a 2-HG target. (Chowdhury et al., 2011; D'Oto et al., 2016) Histone demethylases are involved in altered gene expression since the methylation status of histones defines chromatin structure and DNA accessibility. Histone methylation marks such as H3K4, H3K36 and H3K79 are often found in euchromatic prevalently transcriptional active regions, while methylation of H3K9, H3K27 and H4K20 residues are closely related to heterochromatic regions with silenced transcription. (Margueron et al., 2005)

Several studies showed an increase of hypermethylated H3K4, H3K9 and H3K27 H3K36 in cell culture models and a close relation to differentiation processes. (Lu et al., 2012; Rohle et al., 2013; Turcan et al., 2012)

However, the patient situation seems to be less clear since the histone demethylases are known to either suppress or even promote tumor growth and perform differently depending on the tissues and cell types this might be one reason why *IDH* mutations are very tumor specific. (Losman and Kaelin, 2013)

In conclusion, 2-HG induced DNA and histone hypermethylation support tumor development by modifying several gene functions and changing biological processes.

It has to be mentioned that, besides the epigenetic alterations, IDH mutation also induces metabolic reprogramming resulting in dysregulated DNA damage repair, oxidative stress response, lipogenesis, collagen maturation, cell death and much more. (reviewed in: (Du and Hu, 2021a; Ye et al., 2018)

However, the *IDH* mutation alone seems to be insufficient to initiate *in vivo* tumor formation reported in several studies. (Amankulor et al., 2017; Bardella et al., 2016; Philip et al., 2018; Sasaki et al., 2012) Thus additional defining genetic alterations are the logical consequence.

1.2.2. *TP53 mutation*

Since *TP53* is mutated in over 50% of all cancer cases, or at the very least a related pathway is inactivated in nearly every human tumor, the importance of *TP53* in tumorigenesis is noncontroversial.

TP53 is the gene encoding the 53 kDa tumor suppressor protein located on human chromosome 17p13.1. The wild-type p53 protein contains five domains. (Harris, 1996)

The transactivation domain, which is important for its function of responding to stress like DNA damage or activity of oncogenes and suppressing tumor development, can bind several cofactors. (Brady et al., 2011) The proline-rich domain, which is reported to be associated with procedures in undergoing apoptosis, also binds DNA (Sakamuro et al., 1997). The central DNA binding domain, which is essential for T53 to carry out its sequence-specific transcription factor activity. (el-Deiry et al., 1992) The tetramerization domain, which allows protein interactions as well as the identification of DNA sequences, for both a proper tetramer formation is essential. (Gabizon et al., 2012; Halazonetis and Kandil, 1993) And lastly the regulatory domain, which interferes with the DNA binding domain until it is modulated by stress-induced post translational alterations. (Hupp et al., 1992)

With all these features p53 is involved in many biological responses and processes comprising apoptosis, cell cycle arrest, senescence, DNA repair, cellular metabolism, autophagy, angiogenesis, development, differentiation and more (Aubrey et al., 2016). Understanding all these functions reveals how p53 can exert its tumor-suppressive task. With a loss of functionality, the whole molecular balance of the cell is disturbed and multiple of the associated pathways are probably involved in the resulting tumorigenesis. While the biology behind it is well-examined, the translation of this knowledge into a clinical benefit remains challenging.

Lower-grade gliomas harboring an *IDH* mutation and no 1p/19q deletion, meaning IDH-mut A, in almost all cases (94%) have a *TP53* mutation. (Cancer Genome Atlas Research et al., 2015) This data led to the conclusion that a *TP53* mutation can be seen as entity defining. In diagnostic routine this is often evaluated by an immunohistochemistry staining with >10% of tumor cell nuclei showing a strong positive nuclear staining or a fully negative loss of p53 staining. (Takami et al., 2015) In glioma most

identified alterations were missense mutations in the DNA binding domain (Louis, 1994; Takami et al., 2015)

1.2.3. *ATRX* mutation

More than 25 years ago *ATRX* was described as responsible gene for the Alpha Thalassemia/mental Retardation syndrome X-linked (ATRX) syndrome, a rare neurodevelopmental disorder. (Gibbons et al., 1992)

However, *ATRX* gained importance since mutations nowadays are identified in about 15 cancer entities such as neuroblastoma, glioma and pancreatic neuroendocrine tumors. (Cheung et al., 2012; Jiao et al., 2011; Liu et al., 2012)

The location of the *ATRX* gene is position q21.1 on the X chromosome resulting in two major transcripts related to the full-length protein of 282 kDa and the smaller truncated protein of 180 kDa localized in the nucleus. (Garrick et al., 2004)

The structure of ATRX, which is a member of the SWI/SNF protein family, shows three domains: C-terminal, a α-helicase/ATPase domain, which is essential for the DNA-dependent ATPase activity and its association to the SNF2 family. (Picketts et al., 1996) The central region with alternating hydrophilic and –phobic parts represents the DAXX-binding motif. (Tang et al., 2004; Xue et al., 2003)

Lastly the N-terminal hydrophilic part with the nuclear localization signal, which contains three subparts, summarized as ADD-domain: the GATA-like domain playing a role in DNA binding; the PHD-like domain associated with chromatin-mediated transcriptional regulation; the α-helix important for the globular structure. (Argentaro et al., 2007; Gibbons et al., 1997)

With all these features ATRX is involved in several biological processes. ATRX in complex with its important interaction partner DAXX mediates the replication independent deposition and inset of histone variant H3.3 at telomeres, pericentromeric chromatin, and other silenced regions enriched in H3K9me3, H4K20me3 or DNA methylation in promyelocytic leukemia nuclear bodies. (Tang et al., 2004; Xue et al., 2003) Moreover, the accessibility of chromatin can change due to absent ATRX resulting in transcriptional activity of prior suppressed regions. (Danussi et al., 2018; Liang et al., 2020) ATRX here promotes the formation and maintenance of pericentromeric and telomeric heterochromatin. (Voon and Wong, 2016)

Another process ATRX takes part in is to prevent replicative stress and maintain genome stability in specific regions particularly G-rich sequences. (Clynes et al., 2014; Juhász et al., 2018)

In the oncogenesis context, lacking ATRX expression is connected to a loss of described protein functions (impaired DNA repair, genetic instability etc.) and in particular to the alternative lengthening of telomeres (ALT) phenotype. (Heaphy et al., 2011; Koschmann et al., 2016)

Meaning *ATRX* mutated tumors often reach an immortalization state by activating a telomerase-independent mechanism of telomere lengthening. (Amorim et al., 2016) The maintenance and extension of telomere length is achieved by a homologous recombination repair mechanism and not by telomerase activity as seen in other tumors with for example *TERT* promoter mutations. (Cesare and Reddel, 2010)

Furthermore, *TP53* mutations and alterations in the *ATRX* gene, often resulting in loss of detectable expression, became classifying markers for IDH-mut A. (Liu et al., 2012; Reuss et al., 2015; van den Bent et al., 2017)

Inactivating *ATRX* alterations in IDH-mut A include mostly mutations and deletions without a local hot spot (Cancer Genome Atlas Research et al., 2015; van den Bent et al., 2017)

1.3. Model systems

To have a reliable model is absolutely essential to obtain a better understanding of the biology behind IDH-mut A, their development and progression to discovering, developing and testing new therapeutical targets and treatment options. Therefore, a model investigating brain tumors must fulfill

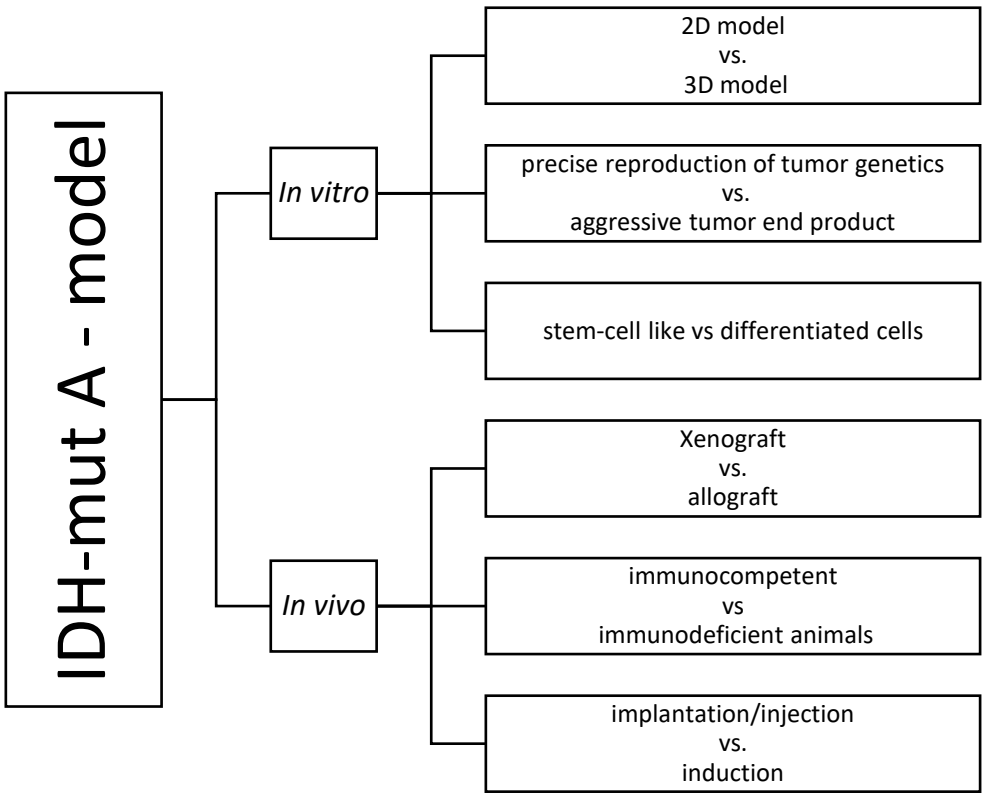

certain criteria such as genetic landscape, tumor microenvironment and much more. In the following I want to discuss the pros and cons of an assortment of model options that are currently used in this field and important for my work.

1.3.1. Neurosphere 3D cultures

In vitro cultures offer the advantages of having a nearly unlimited access to material, low costs and time consumption, defined conditions, the possibility to screen in high through-put and easily manipulate the model. The classical adherent cell cultures were the best tool to investigate molecular mechanisms and biological processes taking place in all kind of cells in detail over decades. But this approach of cultivation in serum conditions is shown to cause genetic drifts and other disadvantages. So the interest in a novel approach increased: cultivating cells instead of under serum conditions, with defined growth factors. (Reynolds and Weiss, 1992)

Years ago first reports then showed that surgically removed glioma as well as neural stem cells (NSCs) can be taken into culture under specialized medium (epidermal growth factor (EGF), basic fibroblast growth factor (bFGF) and neuronal viability supplement B27) where they form and grow as three-dimensional floating spheroids. (Brewer et al., 1993; Lee et al., 2006)

This method harbors certain advantages. The 3D configuration mimics the tissue context of tumors with surrounding cell contacts better. (Pinto et al., 2020) Secondly these neurospheres stably maintain the genetic profile and the expression status. (Lee et al., 2006; Tunici et al., 2004)

Further patient-derived spheres preserve the ability to initiate the formation of tumors and diffusely infiltrate the brain. (Lee et al., 2006)

Nevertheless, this system has some limitations that should be kept in mind. One disadvantage is the selectivity. Generation of IDH-mut A cultures is challenging and only few successes are reported and still the loss of heterozygosity of *IDH1* always remains a problem. (Dao Trong et al., 2018; Luchman et al., 2013; Piaskowski et al., 2011) Even if the cells are in culture, the conditions introduce a bias favoring certain (fast growing) subpopulations. The lacking influence of the tumor-microenvironment further limits the *in vitro* system and weakens the prediction of drug susceptibility. Several works have been showing how important the immune system for example is in context with IDH-mut tumors. (Amankulor et al., 2017; Bunse et al., 2018; Richardson et al., 2019)

1.3.2. Transgenic mouse models

Advantages of in vivo mouse studies

We have learned a lot from *in vitro* experiments, but cell cultures also have their limitations. Modelling infiltration and invasion, vascularization, blood-brain-barrier, tumor-microenvironment-interactions and drug response with pharmacokinetics is not possible in a pure *in vitro* setting. So the next logical step after making the most out of cell culture data is to switch into animals. One of the most advantageous cancer model systems is the mouse by offering a variety of possibilities and showing comprehensive similarity to humans including physiological and molecular features as well as nearly identical genetics especially in protein-coding regions. (Chinwalla et al., 2002; Mural et al., 2002)

Genetically engineered mouse models

One requirement for a good model system is the occurrence of the tumor-associated genetic status especially since the driver mutations of IDH-mut A are well defined (e.g. heterozygous IDH1 R132H mutation). That is why carcinogen-induced mouse models were no option, not recapitulating the genetics and the morphological characteristics the corresponding human tumor harbors.

But the requirement can be met by using genetically engineered mouse models. Innovative technologies, latest CRISPR/Cas approaches, manipulate the mouse genome. Thereby it opens up beneficial possibilities. Due to the precise engineering this system is applicable for investing effects of selected modulated genes and the interaction of defined genetic alterations on tumor formation, progression and drug responses. (Richmond and Su, 2008)

Inbred mouse strains such as C57BL/6 (B6) mostly form the basis for these kinds of systems. Animal experiments in an immune competent setting confers a huge advantage on genetically engineered mouse models against xenograft models. Tumor formation in the brains of these mice also offers the opportunity to particularly examine how the microenvironment influences the tumor and how itself is influenced.

After learning a lot from these models about tumor biology genetically engineered mouse models are also suitable for testing potential therapeutic compounds established *in vitro* before. The mice provide an intact blood-brain barrier and the treatment administration, brain penetration and drug distribution can be tested and monitored.

Conditional mouse model

Since the expression of oncogenes or loss of tumor suppressors is important for a valuable cancer model, this frequently leads to difficulties. Often somatic mutations initiate tumorigenesis, but modelling this by a permanent exposure to the whole mouse organism as germline mutation can cause

defects in developmental processes, embryo lethality or unwanted impact on other tissues and organs. Therefore, the discovery and development of a conditional model system brought considerable advantages. One possibility to achieve the induction of alterations controlled in a temporal and spatial manner presents in the CreERT2 system.

Cre/lox system

Traditional approaches of constant knock-outs have had several disadvantages such as burdened breeding, but this was overcome by conditional knock-out methods. For that purpose, using the Cre/loxP system is commonly the first choice. (Hall et al., 2009; Sauer, 1998) Cre, derived from bacteriophage P1, is a DNA recombinase that site-specifically recognizes a 34 bp target sequence known as loxP site. *(Nagy, 2000)* After recognition the DNA section between two loxP sites is inverted or excised depending on the orientation of the loxPs. (Hoess et al., 1990)

Besides the wild-type loxP sequence, mutant versions were identified, such as the 511 *loxP* sequence at position 2 of the core region the C is change into a T. (Hoess et al., 1986) These mutant loxP sites only recombine successfully with loxP sites of the identical sequence. Thereby wild-type and 511 loxP can efficiently be used to have a double recombination resulting in a knock-in by transferring DNA sections into target regions. (Trinh and Morrison, 2000) To use this feature as a tool to obtain conditional knock-outs and -ins, transgenic mice have to be generated. Flanking loxP sites need to be inserted intronical up- and downstream of the chosen exon of the gene of interest. Thereby the gene will stay wildtype while Cre is not present.

The expression of Cre recombinase can either be under control of a promoter of a gene that is cell type or tissue specific or ubiquitously expressed. To add the temporal control feature, the fusion protein of Cre with a mutant (G521R) ligand binding domain of the estrogen receptor (ER) was developed (Metzger and Chambon, 2001). The activation of this fusion protein known as $CreER^T$ depends on the administration of the synthetic ligands tamoxifen (Tam) and 4-hydroxytamoxifen (4-OHT), common estrogen receptor agonists. (Metzger and Chambon, 2001) Due to the fusion, $CreER^T$ is disabled to translocated from the cytoplasm into the nucleus and catalyze loxP recombination. (Feil et al., 1996) By exposing the cells to Tam or 4-OHT, the preventing binding with heat-shock protein 90 can be reversed and $CreER^T$ follows its nuclear translocation signal. Since this approach still showed some leakiness problems, the ligand specificity towards 4-OHT was improved by introducing three new mutations in the ligand binding domain of the ER in a second generation, known as $CreER^{T2}$. (Feil et al., 1997; Indra et al., 1999) The CreERT2/loxP system offers the possibility to control gene expression or deletion temporally and spatially which is particularly important for studies including early lethal or tumor promoting genes. For that a number of commonly used models are based on this system. But it

has to be mentioned that even for the second generation several limitations are reported. (Álvarez-Aznar et al., 2020; Fonseca et al., 2017; Kristianto et al., 2017; Sandlesh et al., 2018)

1.3.3. Current *in* vivo IDH-mut A models

Searching in the contemporary literature for IDH-mut A models various approaches can be found. On the one hand, few studies tried to use human glioma material by isolating and expanding tumor cells in culture and propagate them in NOD SCID mice. (Luchman et al., 2012) Or by directly implanting biopsies as orthotopic xenografts required additional alterations such as PDGFRA amplification. (Wakimoto et al., 2014a)

One the other hand, applying the RCAS/tv-a system is a prevailed approach to generate murine models. Philip et al. 2018 used this system to overexpress IDH1 R132H and additionally PDGFA combined with a loss of Cdkn2a, Atrx and Pten comparable to what Amankulor et al. 2017 and Ruiz-Rodado et al. 2020 also used (with p53 instead of Atrx). The resulting not physiological expression of ectopical *IDH* mutation can be prevented by using Cre-based knock-in models. (Bardella et al., 2016; Sasaki et al., 2012)

Here only the studies are mentioned that are close enough to IDH-mut A and can be considered as comparison. All the other models in some cases not even expressing IDH1 R132H were neglected.

1.3.4. Requirements for my IDH-mut A model system

The lack of suitable models is one of the major problems we are challenged with doing research in this field. All published models show certain aspects that complicate a convincing analysis of tumor development (initiation) and progression. Listed here are all requirements that a satisfying IDH mutant astrocytoma model has to fulfill:

- A good model should mimic the genetic landscape of the human counterpart as accurate as possible
- The field needs a cellular model that offers the opportunity to investigate the development of IDH-mut A from the beginning.
- Since the tumor microenvironment is getting more important in the brain tumor field, the model has to allow a comprehensive analysis of this. Especially IDH mutant tumors interact strongly with the microenvironment. In particular the relevance of the immune system has been shown in the recent past. This connection is not understood in depth, so that a model should offer the opportunity to further investigate this area/field

1.3.5. Overall project aims and previous work

The necessity of developing a proper model is clear. What has been done beforehand was the development of an Idh1^{R132H} knock-in mouse (generated by the MCI). This mouse ensures the endogenous expression of the mutant Idh1 and was used alone or in combination with p53^{ko} for initial *in vitro* and *in vivo* experiments (work of Viktoria Brendel). During this project several limitations became clear including the genetic loss of the Idh1^{R132H} mutation in long-term cultures as well as the unsuitability of the mouse strain used for the *in vivo* experiments. But as the preliminary data revealed the potential, further effort could have and pointed out what to avoid my follow-up project developed.

I wanted to approach two big objectives during my PhD project: the model generation and validation and the detailed progressive/gradual model investigation.

Thereby the following questions arose:

- How can I generate a reliable model?
- How accurately do I reproduce the different characteristics of IDH-mut A?
- And how to deal with the detected limits?

After establishing a model I wanted to get more insights into the following aspects by analyzing the *in vitro* data on several levels in detail:

- How does the IDH1 mutation impacts cancer biology and therapy?
- What are the tasks of the other two additional core mutations, *TP53* and *ATRX*?
- How do they act jointly?
- Are there dependencies and necessities between the alterations?
- And finally, which cellular changes are promoted by these three core mutations?

And as a last step I wondered

- Can I initiate tumor formation in animals by the established model?
- Are there differences between immunocompetent and immunodeficient mice?
- How does the model behave regarding IDH-mut A characteristics *in vivo*?

2. Material and Methods

2.1. Material

2.1.1. Chemicals and consumables

*Table 1: **Chemicals, reagents and consumables.** Collection of chemicals, reagents and consumables with corresponding suppliers.*

Product	Supplier
0.45 µm nitrocellulose membrane	Novex, Invitrogen
1% Ethidiumbromide (in deionized water)	Roth
4-10% Bis-Tris protein gels	Novex, Invitrogen
4-Hydroxytamoxifen (4-OHT) [Stock concentration: 1mM diluted in Ethanol]	Sigma-Aldrich
5 x Loading dye	ThermoFisher Scientific
Acetone	Sigma-Aldrich
Agarose	Sigma-Aldrich
Ampicillin Na-salt research grade	Serva
Coffee	Hotspot
Dimethylsulfoxide (DMSO)	Roth
Dithiothreitol (DTT)	ThermoFisher Scientific
Dulbecco's Phosphate-Buffered Saline (DPBS)	Gibco
Eppis (1.5, 2 ml)	Eppendorf
Ethanol (EtOH)	VWR Chemicals
Falcons (15, 50 ml)	Flacon
FastRuler DNA Ladder (low, middle, high range)	ThermoFisher Scientific
Filter tips, graduated (10, 100, 200, 1000 µl)	Star Lab
Formic acid	ThermoFisher Scientific
Formaldehyde	Sigma Aldrich
Hanks' Balanced Salt Solution (HBSS) (w and w/o Mg^{2+} and Ca^{2+})	Gibco
Infinium Mouse Methylation BeadChip	Illumina
Iodoacetamide (IAA)	Sigma-Aldrich
Isopropanol	Sigma Aldrich
LUNA Cell Counting Slides	Logos Biosystems
PCR tubes	Biozym
Prime Surface 96U white plate	S-bio
Proteinase inhibitor cocktail, EDTA	Roche Diagnostics
Serological pipettes (5, 10, 25, 50 ml)	Greiner
Superfrost plus Slides	ThermoFisher Scientific
TrueGuide™ Synthetic gRNA	ThermoFisher Scientific
Trypan Blue	Gibco
TrypLE™ Select	Gibco
ultra-low attachment (ULA) 6-well plates	Greiner
ultra-low attachment (ULA) 96-well plates	Corning
ultra-low attachment (ULA) T25 flasks	Corning

ultra-low attachment (ULA) T75 flasks	Corning
Western Bright Chemiluminescent Substrate Sirius	Biozym
Whatman filter paper	Sigma-Aldrich
White 96-well plates	Falcon
Needles (20G, 30G)	Braun
Bepanthen	Bayer
Scalpel (No.21)	Feather
Sterile apllicators	Boettger
Single-use fine dosage syringes	Luer Solo
Tissue adhesive	Braun

2.1.2. Buffers and Solutions

*Table 2: **Buffers and Solutions**. Collection of all buffers and solutions used with corresponding contents and suppliers.*

Buffers and Solutions	Contents	Supplier
Blocking milk	5% milk powder in TBS-T	AppliChem
MOPS buffer	20x MOPS buffer in deionized water	Novex, Invitrogen
NP-40 lysis buffer	150 mM NaCl 50 mM Tris-HCL 0.1 % Nonidet-P40 in deionized water	Sigma-Aldrich Roth AppliChem
PBS/Glucose	PBS (w/o Ca und Mg) 0.5 % Glucose	Gibco Merck
PDD-Solution	HBSS (w/o Magnesium and Calcium) 0.1% Dispase II 0.01% Papain 0.01% DNAse 12.4 mM $MgSO_4$	Gibco Roche Sigma-Aldrich Roche AppliChem
Proteomics lysis buffer	100 mM triethylammonium bicarbonate (TEAB) buffer 1% sodium deoxycholate (SDC) 1% sodium dodecyl sulfate (SDS) protease and phosphatase inhibitor cocktail	ThermoFisher Scientific Sigma-Aldrich Sigma-Aldrich ThermoFisher Scientific
Sample buffer for SDS-PAGE	4 x LDS sample buffer 10 x sample reducing agent in deionized water	Novex, Invitrogen Novex, Invitrogen
TBE buffer	89 mM Trizma Base 89 mM Boric acid 2 mM EDTA in deionized water	Sigma-Aldrich Sigma-Aldrich Sigma-Aldrich
TBS-T	20 x Tris-buffered saline (TBS) powder	AppliChem

	0.05 % Tween 20 in deionized water	MP Biomedicals
Transfer buffer for semi-dry blots	20x Transfer buffer 1% Methanol 0.01 % Antioxidant 0.05% SDS in deionized water	Novex, Invitrogen Sigma-Aldrich Novex, Invitrogen Sigma-Aldrich
MS resuspension buffer	0.1% formic acid 2.5% acetonitrile in mass spectrometry grade water	ThermoFisher Scientific Biosolve Biosolve

2.1.3. Kits

*Table 3: **Kits**. Collection of all used kits with corresponding suppliers.*

Kits	Supplier
Caspase-Glo 3/7 3D Assay	Promega
Qubit dsDNA Assay kit	Invitrogen
Qubit Protein Assay kit	Invitrogen
2-HG Assay Kit	Our lab
SampleIN direct PCR Kit	HighQu
NucleoSpin Gel and PCR Cleanup	MACHEREY-NAGEL
NucleoSpin Plasmid	MACHEREY-NAGEL
NucleoSpin Tissue	MACHEREY-NAGEL
Maxwell RSC Cultured Cells DNA Kit	Promega
pGEMT T-Easy Vector System	Promega
CellTiter-Glo 3D Cell Viability Assay	Promega

2.1.4. Primer

*Table 4: **Primers**. Collections of all used primers with sequence and recommended annealing temperature.*

Primer number	Sequence	Annealing temperature [°C]
P1029	ACTAAGTAGCTTGTCTTTTTGTATACTATTATATAAG	55
P1031	GGATCTACTAGGGTTGGATAGATG	55
P1033	CGTATAATGTATGCTATACGAAGTTATTTTAAAGTATAGTGTTCTTGCTTTTATCACT	58
P1034	CGTATAGCATACATTATACGAAGTTATCACTGGACTACTTCAAGAAACTG	50
P1035	CGTATAATGTATGCTATACGAAGTTATAAATCCGAGGCGCTAGTGAG	47
P1036	CGTATAGCATACATTATACGAAGTTATCCAAGGGTAAATACACACAATTG	50
P1118	GGATCTACTAGGGTTGGATAGATG (phosphorylated)	55
P259	AAGAGTTCTCAGCTCTTTTGGCACGG	62
P262	GCATCACGATTCTCTATGC	45
P258	CACCATTACCACCAACAGCAACATCTC	62

P261	TGCAAAAATATCCCCCGGCTAGTGA	63
P307	GGTTAAACCCAGCTTGACCA	66
P305	GCTGAAACCTCTCAAAGTGGTATTAGAGAC	59
P626	CAAGAAAGCTGGGTTTCAGTCTGAGTCAGGCCCCACTTTC	56.5
P1030	CATTCCATCTGAGTCACGG	55
P1032	GCACTATCACTCTTGCTAGATTCC	56
P1456	CCAGTTCAAGATTTCAAGGAGG	58
P268	AAAGTCGCTCTGAGTTGTTAT	64
P269	GGAGCGGGAGAAATGGATATG	64
P270	CCTGATCCTGGCAATTTCG	64
P277	CACCGGAGAATGGGAAGCCGA	58.5
P278	TCCACACAGATGGAGCGTCCA	58.5
P352	TGGGACTGGTGACAATTGTC	58
P353	GAGTACAGGTGTGCAGCTCT	58

2.1.5. Media

*Table 5: **Media**. Collection of the used media with contents and suppliers.*

Medium	Contents	Supplier
murine NSC-Medium	Neurobasal medium	Gibco
	5% B27 Supplement	Gibco
	1% GlutaMAX	Gibco
	1% Penicillin/Streptomycin/Antimycotic	Gibco
	20 ng/ml Murine basic-FGF	Peprotech
	20 ng/ml Murine EGF	Peprotech
human GSC-Medium	DMEM/F-12, GlutaMAX™ supplement medium	Gibco
	5% B27 Supplement	Gibco
	1% Penicillin/Streptomycin/Antimycotic	Gibco
	20 ng/ml human basic-FGF	Peprotech
	20 ng/ml human EGF	Peprotech

2.1.6. Cell lines

*Table 6: **Cell lines**. Collection of all used cell lines with genotype and origin.*

Name	Genotype	Origin
Proli 25/28/29	$Idh1^{R132H}$	murine NSCs
Proli 18/19/20	$Idh1^{R132H}$ $p53^{ko}$	murine NSCs
Proli 103/116/118	$Idh1^{R132H}$ $Atrx^{ko}$	murine NSCs
Proli 106/108/ 110/140	$Idh1^{R132H}$ $p53^{ko}$ $Atrx^{ko}$	murine NSCs
Proli 129/130/131	$p53^{ko}$ $Atrx^{ko}$	murine NSCs
Proli 132 & #19	$p53^{ko}$	murine NSCs
Proli 117/148/152	$Atrx^{ko}$	murine NSCs
NCH 551b	IDH1-mut A grade 4	Patient-derived GSCs

2.1.7. Antibodies

*Table 7: **Antibodies**. Collection of primary and secondary antibodies with corresponding species, dilutions, clonality, size and suppliers.*

Antibody	Species	Dilution	Clonality	kDa	Supplier
Primary:					
IDH1 R132H	mouse	1:300	monoclonal	47	Dianova
p53	mouse	1:300	monoclonal	53	Cell Signaling
Atrx	rabbit	1:500	polyclonal	280	Abcam
Vinculin	rabbit	1:1 000	monoclonal	124	Cell Signaling
Secondary:					
Anti-rabbit IgG HRP-linked	Goat	1:4 000			Cell Signaling
Anti-mouse IgG HRP-linked	Horse	1:4 000			Cell Signaling

2.1.8. Laboratory equipment

*Table 8: **Laboratory equipment**. Collection of all devices and products used in the lab with corresponding suppliers.*

Devices and products	Supplier
Pipetboy/girl	Integra Bioscience
Nano-Drop 1000	Peq-Lab
Hamilton Syringe 10 µl, 701N	Hamilton
FLUOstar Omega plate reader	BMG Labtech
LUNA Automated Cell Counter	Logos Biosystems
SDS-PAGE chamber	C Cell Sure Lock, Invitrogen
Semi-dry Blotting device	FastBlot B44, Biometra
c400 Imaging System	Azure
Maxwell RSC48	Promega
Biometra TAdvanced Thermal Sycler	Analytik Jena
iScan™ System	Illumina
9.4T small animal MRI	Bruker Daltonik GmbH
Ventana BenchMark ULTRA Immunostainer	Roche
FastBlot B44	Biometra
9.4 T small animal MRI	Bruker Daltonik GmbH

2.1.9. Enzymes, polymerases and bacteria

*Table 9: **Enzymes, polymerases and bacteria**. Collection of all used enzymes, polymerases and bacteria with corresponding suppliers.*

Product	Supplier
2x All In HS Red Taq Mastermix	HighQu
GoTaq® G2 Colorless Master Mix	Promega
Q5 Hot Start High-Fidelity 2xMM	NEB
Lambda Exonuclease	ThermoFisher Scientific
Sequencing Grade Modified Trypsin	Promega
One Shot™ TOP10 Chemically Competent *E. coli*	ThermoFisher Scientific
NEB® 5-alpha Competent *E. coli* (High Efficiency)	NEB
TrueCut Cas9 Protein v2	Invitrogen
Anza 10 DpnI	Invitrogen
Anza 11 EcoRI	Invitrogen
Anza 28 MluI	Invitrogen

2.2. Methods

2.2.1. Atrx^{ko} *In vivo* CRISPR approach

gRNA design and test

The selection of the targeting exon was done based on Ensembl research (Atrx, ENSMUSG00000031229, GRCm39:CM001013.3). The 68 bp long exon (Chromosome X: 104,922,040-104,921,973; exon 8: ENSMUSE00000622873 of Atrx transcript: ENSMUST00000113573.8) is shared by most protein coding transcript versions of Atrx and thereby became the target exon. The needed gRNA upstream and downstream of this exon were identified comparing results of CHOP-CHOP (https://chopchop.cbu.uib.no/), E-CRISP (http://www.e-crisp.org/E-CRISP/) and CRISPOR (http://crispor.tefor.net/) including specificity, efficiency, off target effects etc.

*Table 10: **gRNA sequences**. Selected 5' and 3' gRNA sequences.*

gRNA	Sequence
gRNA 5'	gaacactatactttaaacac tgg
gRNA 3'	actagcgcctcggatttcca agg

The selected gRNAs cutting 5' and 3' of the target exon were then tested on a vector system. The plasmid SP1504 contains a 1kb region around the exon. This plasmid was incubated with several combinations of Cas9, gRNA 5', gRNA3' and a digestion enzyme (MluI).

*Table 11: **Process of gRNA test**. Reagents with corresponding volumes and concentrations and steps to test gRNA*

	Volume	Concentration
Cas9 protein	1 µl	1 µM
gRNA 5'	1.5 µl	300 nM
gRNA 3'	1.5 µl	300 nM
MluI	1 µl	
Anza-Buffer	3 µl	
Nuclease-free water	add 27 µl	
25°C for 10 min		
SP1504	3 µl	100 ng/µl
37°C for 15 min		
Proteinase K	1 µl	
Room temperature (RT) for 10 min		

The samples were loaded on a 1% agarose gel with 120 V for 40 min. The expected band for adding both gRNAs would be 640 bp long, for cutting with Mlu and gRNA 5' 1700 bp and Mlu and gRNA 3' 1100 bp. The conditions without Cas9 protein should only show the SP1504 plasmid.

ssDNA construct design and generation

Based on the *Easi*-CRISPR protocol I designed my customized repair cassette. (Miura et al. (2018) The principal design of such a construct consists of two homologous arms (5' and 3') and the middle region containing the sequence that's new and should be exchanged. In my case the arms are 100 bp long and the middle region includes the wildtype exon 8, flanked by two loxP sites. To avoid interferences with splicing donor or acceptor sites, branch sites or other regulatory sequences the loxP sites were inserted over 125 bp away from the exon-intron border. The insertion of the loxP sequence at the cleavage site leads to a split of the gRNA recognition site, so that re-cleaving of the repair cassette by the Cas9-gRNA-complex can be prevented. In total my repair cassette has a length of 955 bp.

To generate the repair construct several steps had to be performed. First I amplified the wildtype template of the defined region from genomic DNA (PCR 1, following GoTaq protocol with listed accommodations). This product was ligated into a pGEM-T Easy backbone and transformed into TOP10 E.coli applying blue-white selection (according to the manufacture's protocol). After plasmid purification done using the NucleoSpin Plasmid Kit the correct insertion was tested with an EcoRI digest (following Anza's restriction enzyme protocol). To add the loxP sites flanking the exon two side-directed-mutagenesis (SDM) PCRs (SDM-PCR 5' and SDM-PCR 3') were performed using the wildtype region as template. DpnI was used to digest the wildtype plasmid so that the transformation into TOP10 *E.coli* lead to the final repair construct in the pGEM-T Easy backbone. The successfully insertion of both loxP sites was validated by Sanger Sequencing performed at GENEWIZ.

*Table 12: **PCR summary for construct generation**. Collection of used polymerases, primers, annealing temperatures (AT) and elongation time.*

	Polymerase	Primer	AT	Elongation
PCR 1	GoTaq	P1029/P1031	55°C	1 min
SDM-PCR 5'	Q5	P1033/P1034	55°C	1 min
SDM-PCR 3'	Q5	P1035/P1036	55°C	1 min
PCR 2	Q5	P1029/P1118	55°C	1 min

By PCR 2 the modified region can be amplified as dsDNA. Since P1118 is a phosphorylated primer the cleaned-up PCR product can then be digested by a lamda exonuclease into ssDNA.

Microinjection

For the injection the synthesized ssDNA is used together with the other reagents. Before performing injection gRNA that consists of two parts: crRNA and tracrRNA was annealed following the protocol for TrueGuide™ Synthetic gRNA from ThermoFisher.

Thereafter the mixture of all reagents was injected into the cytoplasm of zygotes (one-cell stage). The Core Facility Transgenic Service (headed by Dipl.-Ing. Frank van der Hoeven) performed the

experimental part of *in vivo* microinjection and mouse transgenesis (based on Miura et al. (2018)). After successful knock-in the born pups were transferred into my hands for further breeding.

2.2.2. Genotyping

All samples (blastocysts, ear punches, tails and cells) were lysed using a 50 µl approach of the SampleIN Direct PCR Kit (highQu) according to the manufacturer's protocol. For the PCRs 10 µl of ALLin™ HS Red Taq Mastermix with respective primer pairs (listed 2.1.4 and below) and water was mixed with 1 µl sample template DNA. Besides sample DNA I prepared corresponding positive and negative controls. The PCRs ran following this procedure:

*Table 13: **PCR procedure for genotyping**. Collection of all steps necessary for genotyping PCRs.*

Steps	Temperature	Time
Initial denaturation	95°C	2 min
➔ followed by 35 cycles of		
Denaturation	95°C	15 sec
Annealing	Adjusted	15 sec
Extension	72°C	9 sec

Depending on what to investigate and identify this PCRs were designed, established, validated and used:

*Table 14: **Genotyping summary**. Collection of all genes or constructs the purpose and corresponding primers, annealing temperatures and expected results.*

Gene/ construct	Purpose	Primer	AT	Expected results
Idh1^{R132H}	genotyping	P259/P262	58°C	529 bp = WT; 579 bp = construct
	validating knock-in	P258/P261	60°C	425 bp = WT; 500 bp = KI
p53	genotyping	P307/P308	66°C	425 bp = WT; 600 bp = construct
	validating knock-out	P307/P626	55°C	676 bp = KO
Atrx	genotyping	P1030/P1456	55°C	228 bp = WT; 262 bp = construct
	validating knock-out	P1030/P1456/ P1032	57°C	262 bp = construct or 196 bp = KO
Rosa CreERT2	genotyping	P268/P269/ P270	55°C	603 bp= WT; 800 bp = construct
Y-Chromosome	Sex	P277/P278/ P352/P353	58°C	402 bp = ♂ 294 = control

To visualize the PCR products I prepared a 2% agarose gel (with TBE) with 0.02 µl/ml ethidium bromide and loaded the samples together with 10 µl low range marker. After 60-90 min of electrophoresis (125 V), the gels were imaged and documented using the Azure c400 biosystems.

2.2.3. Generation of NSCs

Neonatal pups were used to prepare NSCs from their brains. After decapitation and removing cerebellum and olfactory bulb the brain were stored in PBS/Glucose solution before I cut it into small pieces and digested the tissue for 30 min at RT using 5 ml PDD solution. Cell suspension was centrifuged (5 min, 500 rpm) and washed with PBS twice before resuspended cells were transferred into ULA flasks (T25) containing murine NSC cultivation medium.

2.2.4. Cultivation of NSCs and GSCs

Murine NSCs and human GSCs were cultured in corresponding medium, under standard cell culture conditions (37°C, 5% CO_2). Medium was changed twice per week and every 2 weeks I passaged the spheres via mechanical dissociation. To seed the cells for experiments TrypLE Select was used for enzymatic dissociation (37°C, 6 min). To stop the digest 5ml HBSS with Mg^{2+} and Ca^{2+} was added. The single cell suspension was stained with trypan blue and counted (Luna CellCounter) to seed proper numbers of vital cells into suitable ULA plates or flasks.

To induce the genetic recombination of the murine constructs the cells were treated with 1 µM 4-OHT (1:1000 from stock of 1 mM). As control cells were applied to same amounts of the solvent, EtOH.

2.2.5. 2-HG Assay

Uninduced NSC spheres were dissociated and counted, before 150 000 cells/well were seeded into a ULA 6-well plate. Every experiment contained 9 time points (0, 3, 7, 10, 14, 21, 28, 42 and 56 days). Backwards induction enabled a common harvest. After washing the cells with PBS they were lysed in NP-40 lysis buffer (120 µl) applying a freeze-thaw extraction approach. Brain tissue was prepared and processed exactly the same.

To determine the protein concentrations of my samples I used the Qubit protein assay (according to manufacturer's protocol). The lysates offered material to measure intracellular 2-HG levels whereas the measured concentrations in the supernatant depict the extracellular 2-HG that the cells transported out. For the enzymatic 2-HG assay the protocol established in our lab was followed (Balss et al., 2012). For calculating intracellular concentrations the measured result [pmol/µl] was normalized to the determined protein concentrations [µg/µl]. To approximate the 2-HG level per cell the pmol/µg were multiplied by 0.2 $\frac{\mathrm{mM}}{\mathrm{pmol/\mu g}}$ to obtain 2-HG concentrations in mM. Statistic was done with an unpaired t-test with Welch's correction (using GraphPad Prism 9.2.0)

2.2.6. Western Blot

For western blot experiments protein lysates from cells lysed either with NP-40 lysis buffer as described before or any other lysis buffer were used. After Qubit protein assay 20-50 µg protein were prepared with 'Sample buffer for SDS-PAGE' before load onto a ready-to-use 4 - 12% Bis-Tris gel with additional proper protein markers. For running the SDS-PAGE I used MOPS buffer. 60 min and 200 V were standard conditions for a run. To transfer the proteins after separation onto a membrane I performed semi-dry blot with a 0.45 µm nitrocellulose membrane. The blotting conditions were 1 h, 30 V and 100 mA per gel. Afterwards the membrane was blocked for 1 h with blocking milk at RT, followed by overnight incubation of the diluted chosen primary antibody (2.1.7). The membrane was washed 3 times with TBS-T before I incubated the corresponding secondary antibody (2.1.7) for 1 h at RT. For signal detection chemiluminescent substrate was applied to the membrane and visualization was performed by the c400 Imaging System.

2.2.7. CellTiterGlo 3D

200.000 NSCs were seeded into 2 wells per culture of a ULA 6-well plate. One well was induced with 4-OHT, the other well with EtOH as corresponding solvent control. Thereby I ensured that the starting conditions for both were most comparable. 2 weeks later induced and control cells were dissociated and 1 000/2 000 cells per well were seeded into two white 96 well plates. For measurements CTG substrate was pipetted 1:1 into each well. The luminescence data were acquired using the BMG reader (5% and 80% gain). The first plate was measured at d0 to have a start point for normalization. 72h later acquisition of the data from plate two was performed to detect the changes in cell numbers based on ATP levels. For analysis 72h data were normalized to 0h before put into proportion to solvent control. For every genotype 3 different cultures were investigated with 3 biological replicates (≥ 6 technical replicates). Statistic was done by either comparing control and induced cells per genotype with an one-sample test or the different induced genotypes were compared using an One-way ANOVA with an Tukey post test (using GraphPad Prism 9.2.0).

2.2.8. Caspase 3/7 assay

Uninduced NSCs were dissociated and directly seeded into ULA 96-well plates. At d0 the induced condition was treated with 4-OHT while the control wells got EtOH. After 14 days the Caspase activity was measured by using the Cas3/7 activity assay (Promega) according to the manufacturer's protocol for 3D cultures. For this assay 2 cultures/genotype and 2 biological (with ≥ 3 technical replicates) were performed and analysis was done as described in CTG section.

2.2.9. Methylation

Sample preparation and data acquisition

Dissociated cells were seeded into ULA 6-well plates and as described for the 2-HG samples backwards induced. To harvest the DNA of the cells, the spheres were collected in 400 µl medium and DNA purification was performed using the automated Maxwell instrument in combination with the Maxwell RSC Cultured Cells DNA Kit following the producer's instructions. For determination of the DNA concentration I used the Qubit dsDNA Assay kit according to the manufacturer's guidelines. The DNA samples (250 ng) were subjected to bisulfite conversion step of the methylation analysis applying the Illumina Mouse Methylation BeadChip readout with the iScan device. The complete preparation was performed by the technical staff of the neuropathology similar to the human EPIC procedure

All computational analyses were performed using R (http://www.R-project.org, R Development Core Team; R version 4.1.1). The raw data from the Illumina Mouse Methylation Chip were processed using the R package sesame (Zhou et al., 2018). Background subtraction was done using normal-exponential deconvolution using out-of-band probes noob (Triche et al., 2013) and non-linear dye bias correction was applied. Probes with a detection p-value >0.05 were masked as "NA". For further analyses probes located on chromosomes X or Y and SNP probes for distinction of mouse strains were removed and only probes detected in all samples according to the detection p-value test were kept. From multiply hybridized probes each only the probe with the lowest detection p-value was selected (as recommended by Illumina). In summary, out of 287 693 probes on the chip 251 646 were kept for subsequent analyses.

DNA methylation data from human tumor samples was by default generated as described before (Capper et al., 2018). The idat-files were processed using the R package sesame similar to the mouse methylation samples.

2.2.10. Proteomics

Sample preparation

The cells were prepared as described for the CTG: one solvent control well and one 4-OHT induced well for 14 days after seeding in a density of 250.000 cells/well. The sample preparation finally followed this protocol:

After collecting the cells and washing them with PBS I added 200-300 µl hot lysis buffer containing 1% SDS and 1% SDC in 100 mM TEAB supplemented with protease and phosphatase inhibitor cocktail. The samples were boiled for 5 min at 95°C and sonification on ice applying 5 times for 20 sec (1 sec on/off) at 35% power using a single sonotrode sonicator. Followed by 10 min centrifugation at max. speed and

4°C lead to the final lysate I used and determined protein concentration from. After the Protein Qubit assay (following the manufactures' protocol) I went on with 100 µg protein in a total volume of 50 µl (ad 100 mM TEAB buffer). By adding 500 mM DTT with a final concentration of 10 mM for 20 min, 57°C the proteins were reduced. Thereafter a final concentration of 40 mM of 500 mM IAA was used incubating for 30 min at RT in the dark to prevent reformation of disulphide bonds. Afterwards to precipitate and eventually desalt the protein 4 volumes of acetone were added for 60 at -20°C. Next, the samples were centrifuged for 5 min at max. speed and 4°C. The precipitated was washed once with 90% acetone before I resuspended it in 50 µl TEAB buffer. Next, the trypsin digestion followed, using trypsin at a ratio of 1:25 (1 µg trypsin per 25 µg protein). After 16h at 37°C the digestion 1 µl formic acid was added. The peptides contained in the supernatant were concentrated for 70 min at 33°C in a speed vac device. After resuspending the peptides in 40 µl MS resuspension buffer, the samples were applied to a precooled sonication bath for 15 min and subsequently centrifuged for 10 min. With NanoDrop results the concentration was set to 250 ng/µl using mass spectrometry resuspension buffer. 2 µl sample volume were then injected into the thermal ionisation mass spectrometry time of flight (timsTOF) mass spectrometer.

LC-MS/MS acquisition

For mass spectrometric analysis a timsTOF pro mass spectrometer was used. The operation mode was set in the following way: Setting for ion accumulation and ramp time was 50 ms each and the range of ion mobility from 1/K0 = 1.3 Vs cm^{-2} to 0.85 Vs cm^{-2} was analyzed. Suitable precursors were identified on the basis of an intensity threshold of 1500 arbitrary units (a.u.). Low abundant precursors were resequenced until 20.000 a.u. ('target value') was reached, taking a dynamic exclusion of 40s into consideration. Mass range was set from m/z 100 to 1700. For MS/MS analysis precursor ions were isolated within a 2 Th window of m/z < 700 and 3 Th for m/z >700 by synchronizing quadrupole switching events with the precursor elution profile from the TIMS device. The collision energy was lowered linearly as a function of increasing mobility starting from 59 eV at 1/K0 = 1.6 VS cm^{-2} to 20 eV at 1/K0 = 0.6 Vs cm^{-2}. By applying the polygon filter, singly charged precursor ions were excluded.

Data processing

The data received after every run were analysed by MaxQuant (version 1.6.17.0) using carboxymethyl as a fixed modification and oxidation as variable modification. The maximal number of missed cleavages was determined to 2. Quality control was done applying the R-based pipeline, Proteomics Quality Control- (PTXQC, Bielow, Mastrobuoni and Kempa, 2016) Only samples that passed the quality control with more than 3 500 identified proteins were used for this data set. Further processing was done in R such as filtering for missing values and imputation (done by k-nearest neighbours (k = 10) of the R package DEP). In the downstream analysis significant proteins were defined by >20% change in

LFQ and adjusted p-value <0.05 (comparing 4-OHT induced cells vs uninduced controls). R packages such as complex heatmap were used to generate the illustrated graphs. This analysis part was mainly done by David Vonhören, supported by Dennis Friedel.

2.2.11. Animal experiments

Mice

C57BL/6 N (B6), BALB/c nude, NSG, NRG, SCID Beige, B6 Rag2 KO, BALB/c RAG2 KO, B6 Rag2 Il2ryc and BALB/C Rag2 Il2ryc animals were purchased from Charles River, Jackson Laboratories and Taconic. My mice were used between 4-6 weeks of age and housed in specific pathogen-free environment. Before experiment start all mice had 2 weeks after arrival to adapt to the new location without stress. Animal care and all experimental procedures were approved by the local government authorities (RP Karlsruhe) (License number G-12/20).

Intracranial stereotaxic injections

For recombination NSC cultures were treated with 4-OHT 14 days before surgery. On the day of surgery dissociated cells were counted and resuspended in PBS with a cell concentration of 100 000 cells/µl (pilot experiment) to 250 000 cells/µl (main experiment). The cell suspension was kept on ice before drawing up and being injected with a Hamilton syringe using stereotactic and injector devices.

Mice at the age of 4-6 weeks were anesthetized with isoflurane (2-4 % for anesthesia induction and 1-2 % for maintenance). At the beginning I verified the surgical anesthesia stage by the absent pedal reflex, covered the eyes with Bepanthen and monitored the breathing during the whole surgical process. The mouse was placed into the stereotact and fixed so that the skull was plane and any movement of the head was impeded. To expose the skull surface I made small incision through the midline of the skin (rostral to caudal) using a sterile scalpel. I drilled a small hole through the skull with a 20G needle at the predetermined coordinates (2mm anterior and 1mm lateral into the right hemisphere, using the bregma as zero). 2 µl cell suspension was injected (200 000 or 500 000 cells in total) with a flow rate of 1µl/min into a depth of 3 mm (below dura). After the cells settled the syringe was slowly removed and tissue adhesive was used to close fresh wounds. For pain relief 5µg/g Carprofen in 0.9% sterile NaCl solution were subcutaneously injected.

For health control each mouse was monitored for behavioral abnormalities, weight was checked once a week and animals were taken out of the experiment as soon as they reached the termination criteria (see G-12/20)

MRI

The animals were routinely screened for lesions via MRI every two weeks starting from week 4-6 after the implantation. The screens were performed by the animal imaging core facility of the DKFZ (mainly done by Dr. Viktoria Eichwald, Inna Babushkina and Hermann Stammer).

MRI was carried out using a Bruker BioSpec 3Tesla. Mice were anesthetized with 3.5% sevoflurane in air. T2 weighted imaging were performed using a T2_TurboRARE method with following settings: TE = 48.0 ms, TR = 3350 ms, FOV 20x20 mm, slice thickness 1mm, averages = 3, Scan Time 3m 21s, echo spacing 12ms, rare factor 8, slices 20, image size 192x192

For the advanced spectrometry analysis in cooperation with Dr. Andreas Korzowski and Justyna Platek (Department of Medical Physics in Radiology, NMR spectroscopy group). The measurements therefore were done at the 9.4 T small animal MRI. Since no final protocol is established everything is still in a very preliminary state and multiple parameters were tested.

Histological and immunohistochemical analysis

Mice were euthanized by cervical dislocation either at the determined experiment end or when defined termination criteria were achieved. Brains were collected and stored in fresh 4% paraformaldehyde overnight. Thereafter they were bisected frontally at the approximate point of injection. The tissue was dehydrated and embedded in paraffin before 0.5 – 1 µm thick slices were cut. Every 10th slices was stained with hematoxylin and eosin (HE) and histologically reviewed. To detect tumor formation frontal sections from suspicious animals were used to perform further analysis. Immunohistochemical staining was done on a Ventana BenchMark ULTRA Immunostainer. IDH1 R132H specific antibody applying the Ventana-specific protocol recommended from dianova was used to identify positive cells within the mouse brain.

After removing slides the slides from the stainer, they were mounted and scanned with the Aperio AT2 device (Leica). Further image analysis was done with Aperio ImageScope and Fiji-ImageJ.

2.2.12. Statistical analysis

Data were analyzed as mentioned in the respective section using either GraphPad Prism 9.2.0 or R Studio (R version 4.1.1). Results were expressed as mean, with standard deviation or as described below the figures. To verify normal distribution Shapiro-Wilk test was used ($p>0.05$). Significance was determined by applying the data-matching tests such as unpaired t tests with Welch's correction or One-way ANOVA with a Tukey post test. Identification of differentially methylated CpGs over time was performed by using Spearman's rank correlation coefficient. The functional enrichment analysis was mainly done with ShinyGO v.0.65 and v0.741 (Ge et al., 2020) and partly g:Profiler (g:Profiler version

e104_eg51_p15_3922dba). (Raudvere et al., 2019) As multiple testing correction methods Benjamini-Hochberg FDR (False Discovery Rate) was used with a significance threshold of 0.05 was applied.

3. Results

3.1. Generation of an inducible Atrx^{ko} mouse

In a previous work I have seen that Idh1^{R132H}p53^{ko} was not successful in developing a tumor in BALB/C nude mice. Since the analysis of the IDH-mut A samples showed Atrx as third important alteration, I decided to improve my model by adding the possibility to mimic the loss of ATRX expression. The first trails using a shRNA were not very efficient over longer time periods (done during my masters). Since Idh1^{R132H} and p53^{ko} were already available in a CreERT2 system in mice, my first aim was to generate a suitable conditional Atrx^{ko} mouse.

I ended up using a novel *in vivo* CRISPR/Cas approach in cooperation with the Transgenic Service at the DKFZ. (Miura et al., 2018) I did research on the murine *Atrx* and identified exon 8 (exon 8: ENSMUSE00000622873 of Atrx transcript: ENSMUST00000113573.8) as the best option to target most isoforms of *Atrx*. After selecting suitable guideRNAs (gRNAs) as described in 2.2.1.1 I tested how reliable their prediction was (Figure 1 A). Based on the chosen gRNA a template DNA was designed (Figure 1 B) containing exon 8 that should be exchanged, flanked by two loxP sites and ending in homologous arms (100 bp long). The detailed requirements are described in 2.2.1.2. To create this ssDNA, the wanted part was copied from murine DNA, subcloned in a pGEM-T backbone vector and loxP sites were added by SDM-PCR (2.2.1.2)

The second step was mainly performed by the Transgenic Service: the *in vivo* injection (G-116/19). Therefore the gRNAs, Cas9 protein and my designed ssDNA construct were directly injected into the cytoplasm of the zygote (Figure 1 C).

To check the efficacy of the CRISPR insertion, I genotyped the DNA of not implanted but altered blastocytes. As expected the PCR band mostly detected wildtype allele but some DNA samples showed a positive shift indicating a successful integration of my construct with the additional loxP sites (Figure 1 D). Next the pups born by the foster mother were genotyped. Those animals whose samples showed the successful integrated construct I finally used as founder for further breeding with the aim to get a homozygote strain (Figure 1 E).

A

	DNA template (SP1504)	Cas9 protein	gRNA 5‘ arm	gRNA 3‘ arm	Enzym Mlu
1	+	+	+	+	-
2	+	-	+	+	-
3	+	+	+	+	+
4	+	-	+	+	+
5	+	+	+	-	+
6	+	+	-	+	+

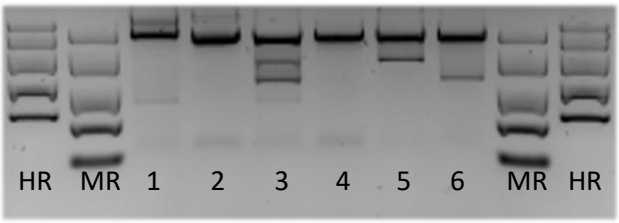

B

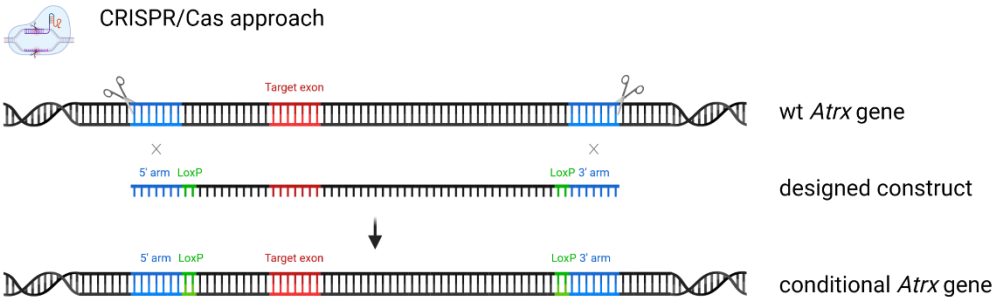

C

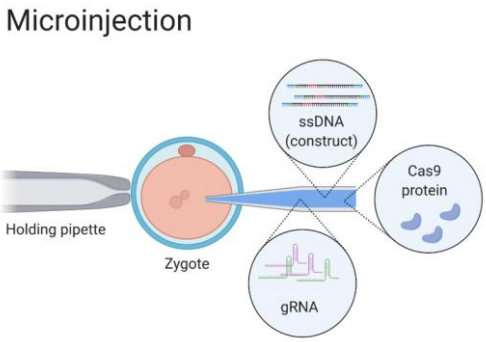

D

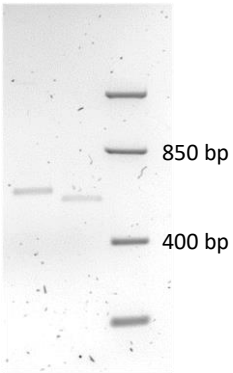

E

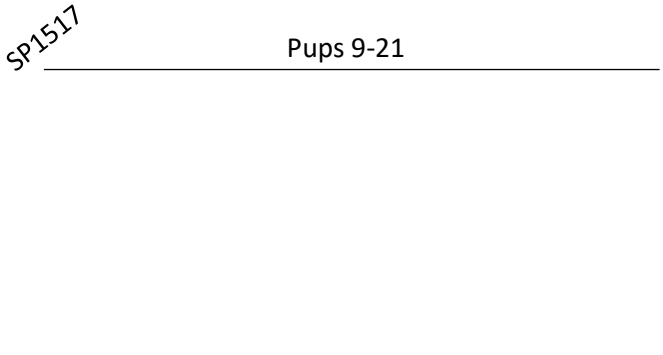

*Figure 1: **Steps to establish a novel Atrx^{ko} mouse strain applying the Easi-CRISPR protocol.** (**A**) The efficiency of the chosen gRNAs was tested using a DNA template containing the sequence of interest (SP1504). As control reactions were performed without Cas9 protein (2, 4). The piece cutted by 3' and 5' gRNA should be 640 bp (1); the combination of 5' gRNA and Mlu should result in 1700 bp and 3' gRNA plus Mlu in 1 100 bp (3, 5, 6). To determine the pieces' length HR=high range marker (10 000/4 000/2 000/1 000/500 bp) and MR=middle range marker (5 000/2 000/850/400/100 bp) were used. (**B**) My CRISPR/Cas approach is based on a ssDNA construct I designed and generated by adding loxP sites flanking exon 8 which finally should lead to a conditional allele of Atrx. (**C**) To germline modulate the Atrx gene the specific construct together with Cas9 protein and the specific gRNAs were injected into the cytoplasm of zygotes, so that the reagents can enter the nucleus and exchange the wt allele of Atrx with the conditional construct. (**D**) The extracted DNA gained from lysed blastocytes was screened for band shifts of the Atrx PCR product as seen in B29 indicating a positive integration of a 34 bp long loxP site (shift from 552 bp to 586 bp). (**E**) Two PCRs were established to clearly detected wildtype, heterozygous and homozygous altered animals for further breeding approaches. The upper panel reveals results applying PCR seen in (E) clearly detecting the heterozygous genotypes (e.g. Pup 17). For the lower PCR the shifts from wild-type to conditional became slightly clearer whereas it was difficult to distinguish heterozygous and homozygous animals (e.g. Pup 17 vs. 18 vs. 19).*

3.2. Generation and Validation of Idh1^{R132H}p53^{ko}Atrx^{ko} Rosa CreERT2 NSCs

After generating a mouse strain with my third alteration, the period of crossbreeding started. Aim was to get Idh1^{R32H} heterozygous p53^{ko} homozygous Atrx^{ko} homozygous animals and all possible combinations out of the tree alterations (in total seven genotypes, Figure 2 A). Thereafter I harvested cells to generate in vitro cultures from pups taken directly after birth (P0). The NSCs isolated from their brains were cultured and expanded under spheroid conditions because it is clearly shown that spheres approximate tumor behavior better than adherent 2D cultures (Figure 2 B).

As I used a CreERT2 based system, the induction of recombination via 4-OHT needed to be validated before starting further analysis. 4-OHT treatment lead to positive results on DNA and protein level showing that the mutant Idh1^{R132H} was successfully induced as well as p53 and Atrx were knocked out as expected (Figure 2 C). The PCR specifically designed to detect the efficient recombination or wildtype alleles verified the induction for all three alterations (Figure 2 D). On protein level I verified the knock-in of Idh1^{R132H} with a mutation specific antibody and both knock-outs with the loss of protein expression compared to the wild-type controls (Figure 2 E)

For validating the knock-in of Idh1^{R132H} and knock-out of p53, I were also able to use the changes of the target surrounding CpGs mapped on the mouse methylation array (Figure 2 F). As an example here the clear drop after 4-OHT treatment indicates the recombination of p53^{ko} for the corresponding genotypes.

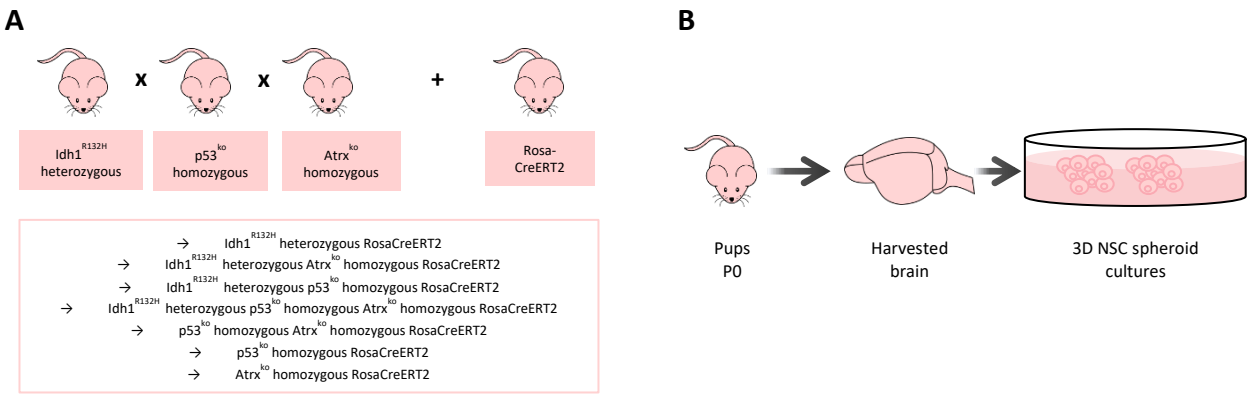

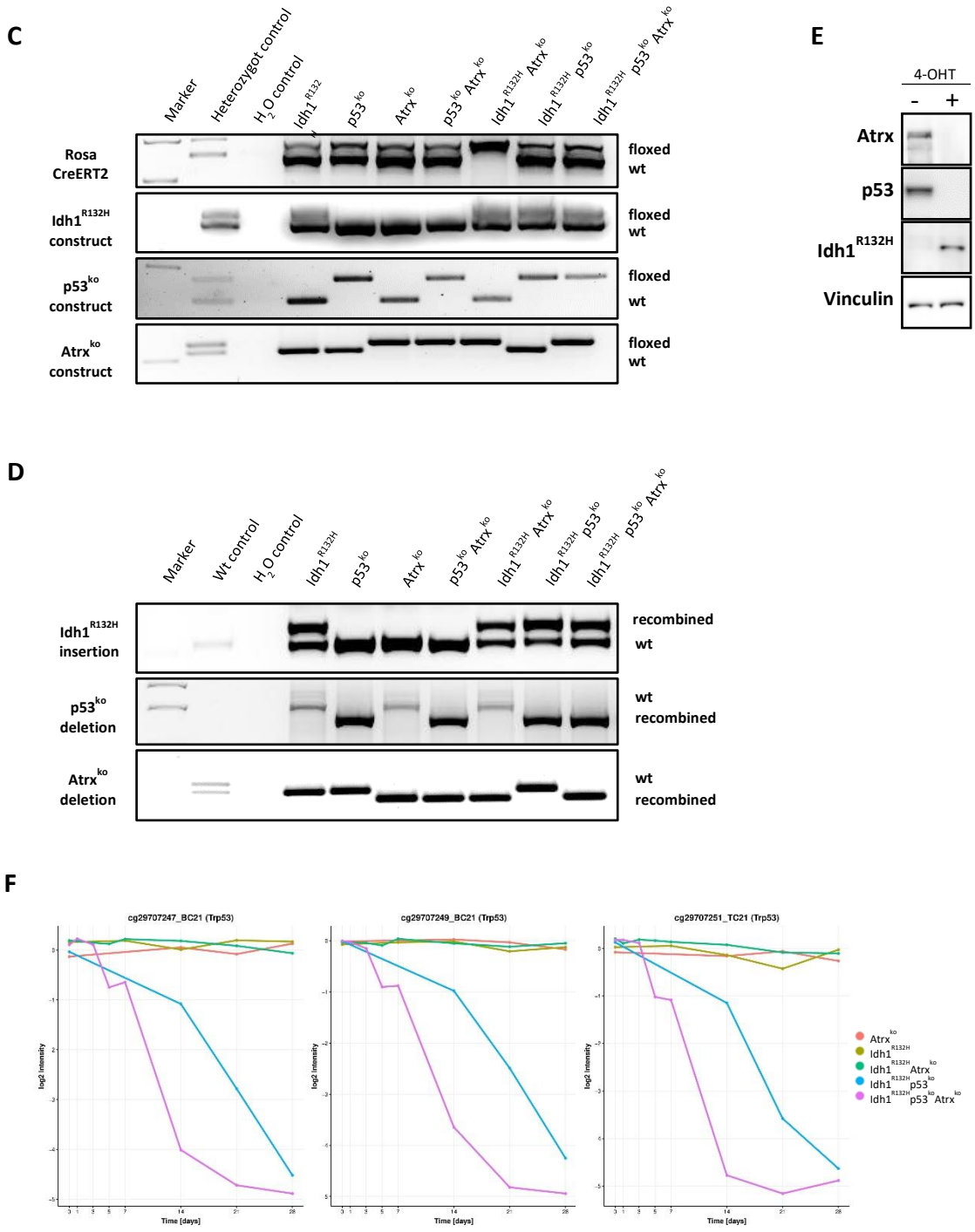

Figure 2: ***Generation and validation of my NSC model****. (**A**) Crossbreeding of Idh1^{R32H} heterozygous, p53^{ko} homozygous and Atrx^{ko} homozygous mice in a RosaCreERT2 background in a way that all 7 possible genotype-combinations are obtainable. (**B**) Litter of respective parents are taken at P0 and NSC cultures are generated from their brains, meaning each culture belong to one pup, for each genotype I generated at least spheroids from 3 different pups. Established PCRs to validate the genetic status distinguishing between wild-type and conditional alleles for all 4 conditions (**C**) or successful recombination (**D**). The shown gel images were generated by Caroline Birr. An additional tool to verify ko induction provides the Illumina mouse methylation chip (**E**). Exemplaric the 3 p53 associated CpG are mapped comparing the methylation intensity of the different genotypes over 28 days (**F**)*

3.3. Monitoring 2-HG levels

The production of the oncometabolite 2-HG is one of the most important IDH-mut A characteristics. Therefore, the first requirement needed to be fulfilled by my model, was increased 2-HG concentrations after induction. Using an enzymatic assay, these levels were intra- and extracellularly detectable for all cells harboring $Idh1^{R132H}$ ($Idh1^{R132H}$, $Idh1^{R132H}Atrx^{ko}$, $Idh1^{R132H}p53^{ko}$ and $Idh1^{R132H}p53^{ko}Atrx^{ko}$).

All cells were induced and monitored over 56 days. For every time point I collected supernatant as well as a cell pellets and finally measured all samples together to decrease assay variance. The intracellular levels were obtained from cell lysates and normalized on the protein content of every sample. All 4 conditions lead to a strong increase over the first seven days. However, $Idh1^{R132H}$ and $Idh1^{R132H}p53^{ko}$ picked at values over 30 mM whereas cells with $Atrx^{ko}$ ($Idh1^{R132H}Atrx^{ko}$ and $Idh1^{R132H}p53^{ko}Atrx^{ko}$) stayed at maximum values of around 10 mM (Figure 3 A) After reaching their maximal levels 2-HG concentrations of all decreased around day 14-21. The measurements from d28 on showed lower intracellular levels than on day 3 (around the quantification limit) for all genotypes.

Since 2-HG can leave the cell via several channels, 2-HG can also be measured outside the cell, in the supernatant (Figure 3 B). The curve pattern for the extracellular levels was comparable to what I observed intracellularly. The pick with the highest values shifted more to day 10-14 but also decreased afterwards. But in general I measured extracellular levels at d28, 42 and 56 that were higher than at day 3 and in a reliable measuring range. So that I can say also 56 days after induction I was able to measure extracellular 2-HG.

In order to identify possible differences between the genotypes in terms of varying oncometabolite distribution, I calculating the ratio between intra- and extracellular 2-HG concentrations (Figure 3 C-F). The ratio determined for $Idh1^{R132H}$ cells was lower compared to the 3 others at early time points, amount to proportional higher extracellular 2-HG concentrations. The ratio curves look comparable for $Idh1^{R132H}Atrx^{ko}$, $Idh1^{R132H}p53^{ko}$ and $Idh1^{R132H}p53^{ko}Atrx^{ko}$, even though the genotypes had dissimilar maximum values. The first rate of day 3 for $Idh1^{R132H}Atrx^{ko}$ is located between $Idh1^{R132H}$ and the two others.

Taken together, these results indicate that *in vitro* the Idh1 mutation effectively producing 2-HG in all matching genotypes although the 2-HG concentrations reach different maxima.

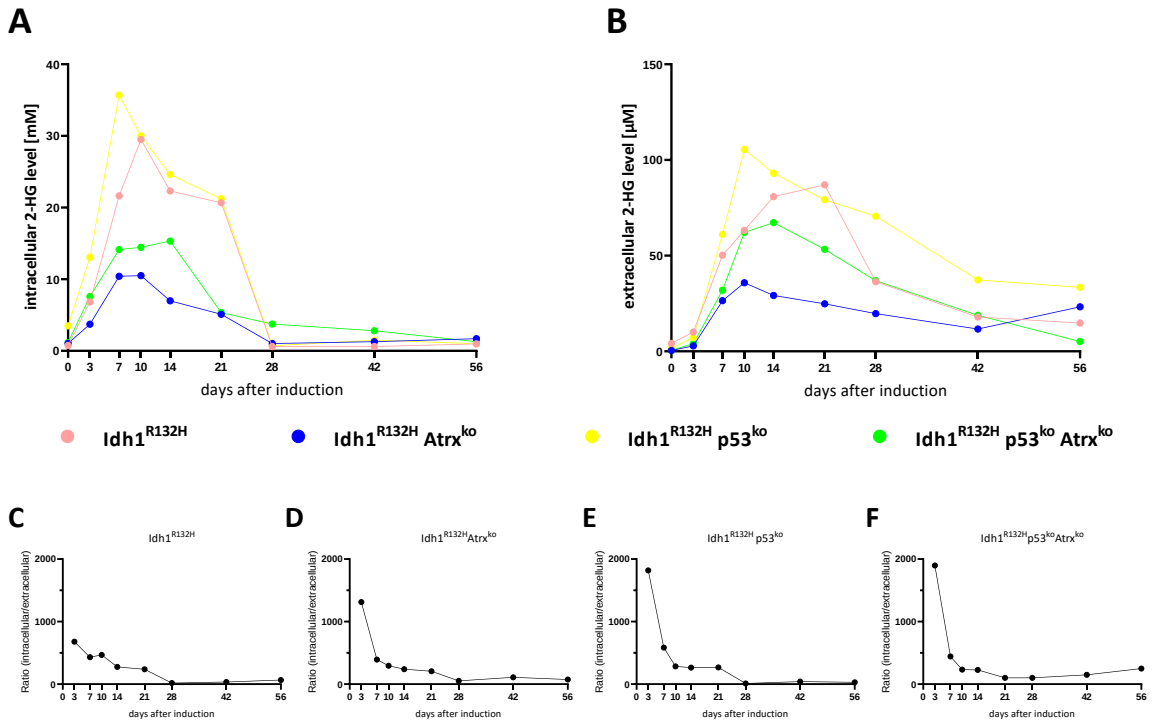

Figure 3: ***2-HG monitoring over time.*** *After induction of Idh1^{R132H} with and without additional alterations NSCs started to produce 2-HG detected using an enzymatic 2-HG assay. From lysates intracellular levels were determined (**A**), while extracellular 2-HG is present in the supernatant (**B**). For each genotype three different cell lines were included. Depending on the time point between 3 (for the later ones) and 12 (for the first 21 days) biological replicates were performed. The intracellular concentrations were normalized to the protein content of the lysate. The ratio between intracellular and extracellular 2-HG was calculated for Idh1^{R132H} (**C**), Idh1^{R132H}Atrx^{ko} (**D**), Idh1^{R132H}p53^{ko} (**E**) and Idh1^{R132H}p53^{ko}Atrx^{ko} (**F**).*

3.4. Apoptotic behavior

Besides the specific features of 2-HG production, a convincing IDH-mut-A model needs to fulfill common cancer hallmarks (Hanahan and Weinberg, 2011). Therefore I first focused on cell death in terms of apoptosis, constituting a natural barrier for tumor development.

Taking the 2-HG measurements into account, I chose d14 after induction as time point for all further experiments. By then the cells still express mutant Idh1, had some time to adapt to the altered genetics and to modulate their cellular processes.

A functional assay targeting the activity of Caspase 3/7 specialized to 3D cultures was applied to detect varying effects of genotypes on NSC behavior.

$Idh1^{R132H}$ alone showed a slight but no significant activity increase of 9% compared to the corresponding (solvent) control 14 days after recombination (Figure 4 A; p = 0.29). The results for $Idh1^{R132H}Atrx^{ko}$ were not significantly different from their control cells (Figure 4 B; p = 0.77). Adding $p53^{ko}$ leads to significantly decreased Caspase levels detected in both genotypes $Idh1^{R132H}p53^{ko}$ and $Idh1^{R132H}p53^{ko}Atrx^{ko}$ (Figure 4 C: 24.8% lower activity levels with p= 0.007; Figure 4 D: 32.3% lower with p = 0.02).

Consequently apoptotic activity in these two was also significantly lower in direct comparison with $Idh1^{R132H}$ NSCs (Figure 4 E; p = 0.02 (*) and p = 0.009 (**)). Consulting Caspase 3/7 activity data of pure $p53^{ko}$ for comparison purpose (Data shown in Supplement 1), $Idh1^{R132H}p53^{ko}$ and $Idh1^{R132H}p53^{ko}Atrx^{ko}$ showed a similar decrease.

This suggests that $p53^{ko}$ is necessary for Idh1 mutant cells to resist cell death, fitting with the high level of co-occurrence in my tumor entity.

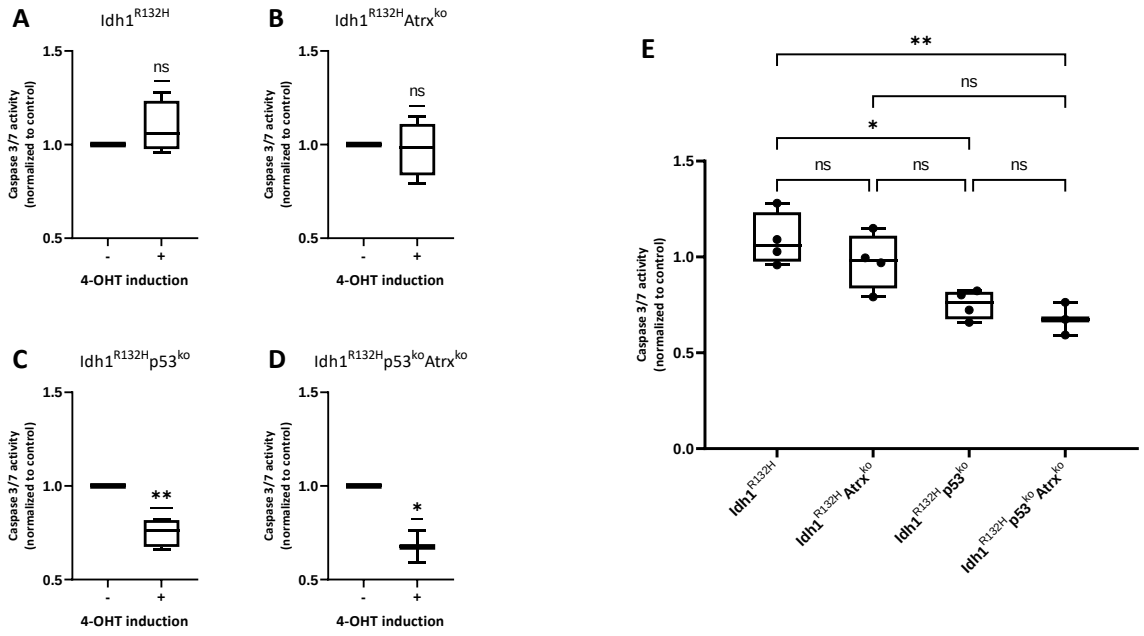

*Figure 4: **Apoptotic activity differs between murine genotypes**. NSCs (2 000/well) of all genotypes were treated with or without 4-OHT. After 14 days apoptosis was assayed using the luminescence-based Caspase-Glo 3/7 assay to reveal activity differences. Fold changes from solvent control cells of each genotype was calculated for all measurements and plotted for (**A**) Idh1^{R132H} (**B**) Idh1^{R132H}Atrx^{ko} which not deviate with and without 4-OHT whereas (**C**) Idh1^{R132H}p53^{ko} and (**D**) Idh1^{R132H}p53^{ko}Atrx^{ko} murine NSCs depict significant changes. (**E**) illustrates the differences in activity directly comparing the 4 induced genotypes. Data are shown as box and whiskers-graphs, where the middle line plots the median, the box extends from the 25th to 75th percentiles and the whiskers go down to the smallest and up to the highest value. For each genotype two independent cell lines were used and two biological replicates with ≥ 3 technical replicates were performed. The normal distribution of the measurements was tested applying the Shapiro-Wilk test, before one sample t test was used in (A)-(D) to compare the 4-OHT treated conditions against the normalized (to 1) control. Ordinary one-way ANOVA followed by a Tukey's multiple comparisons test was performed for the comparison of (E); ns = not significant, * p ≤ 0.033, ** p ≤ 0.002, *** p < 0.001*

3.5. Viability and proliferation behavior

Next important hallmark I examined in my model was proliferation to identify how viability and growth was influenced by the detected apoptosis. The therefore applied CellTiterGlo (CTG) assay measures ATP levels per well specially adapted for 3D cultures and thus permits the comparison of vital cells over time and between conditions. I kept every culture under 4-OHT or solvent treatment for 14 days and monitor their behavior than for 72 hours.

Expression of Idh1^{R132H} alone lead to a highly significant signal decrease (p<0.001). Meaning NSCs with mutant Idh1 showed a 30.7 % reduced cell number after 72h normalized to experiment start and compared to the solvent treated NSCs of the same culture (Figure 5 A). The same emerged for additional Atrx^{ko} (Figure 5 B). Similar to Idh1^{R132H} the viability after the observation period significantly decreased by 30.6 % (p<0.001). However, the opposite was the case for Idh1^{R132H}p53^{ko} and Idh1^{R132H}p53^{ko}Atrx^{ko}. Idh1^{R132H}p53^{ko} alteration leads to a 63 % (p=0.001) higher CTG results than the solvent controls (Figure 5 C). The increase in viability/proliferation came to 205% (p<0.001) for Idh1^{R132H}p53^{ko}Atrx^{ko} cells (Figure 5 D).

In a direct comparison (Figure 5 E) the mean values of Idh1^{R132H} and Idh1^{R132H}Atrx^{ko} did not differ significantly. Whereas comparing them to Idh1^{R132H}p53^{ko} and Idh1^{R132H}p53^{ko}Atrx^{ko}, both showed significant differences. Likewise I measured significant higher numbers (42 %, p=0.05) of cells in Idh1^{R132H}p53^{ko}Atrx^{ko} than under Idh1^{R132H}p53^{ko} conditions.

To see if this effect is only caused by p53^{ko} I again considered pure p53^{ko} NSCs as additional control. p53^{ko} alone resulted in higher viability measurements (against the control) but in direct comparison with both Idh1^{R132H} combinations the increase was less marked. Idh1^{R132H}p53^{ko}Atrx^{ko} NSCs for instance yielded 14.4 % higher CTG results (p<0.001). This observations hint at synergistic effects occurring in the triple combination.

Summarizing apoptosis results and CTG data, Idh1^{R132H}p53^{ko}Atrx^{ko} exhibited highest proliferation capacity. Whereas Idh1^{R132H} mutation alone was not beneficial to approach tumorigenicity.

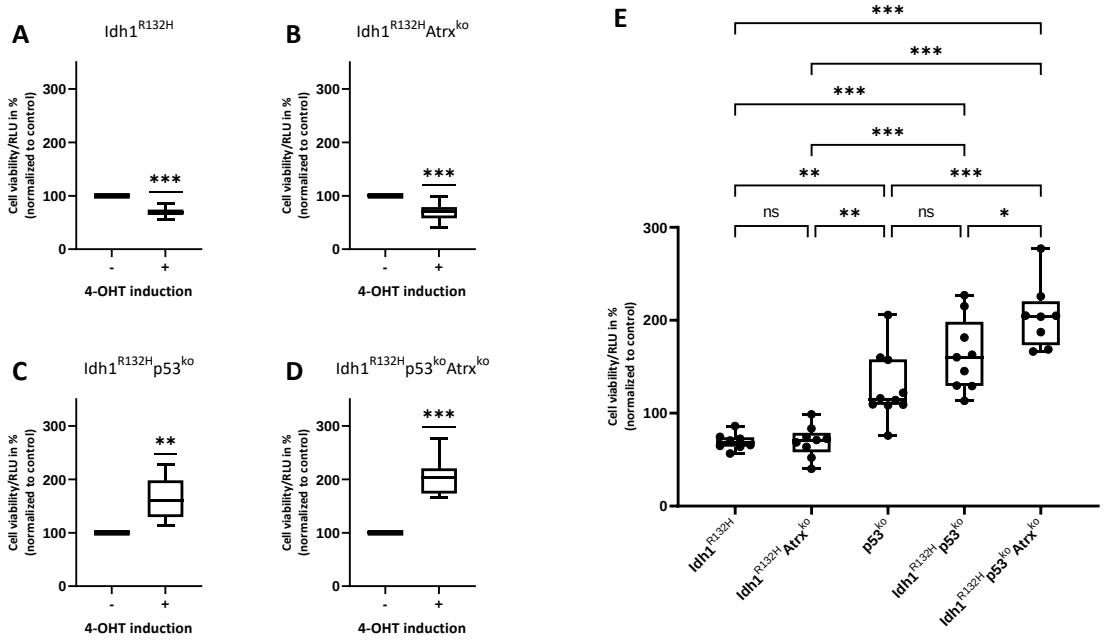

*Figure 5: **Proliferation capacity is impacted by alterations**. All genotypes were treated for 14 days with and without 4-OHT before 2 000 cells/well were seeded. 72h later viability was assayed applying the luminescence-based CTG 3D assay to detect changes in grown cell numbers. Percental fold changes normalized to the solvent control data of each genotype was calculated for all data points and plotted for (**A**) Idh1^{R132H} (**B**) Idh1^{R132H}Atrx^{ko} (**C**) Idh1^{R132H}p53^{ko} and (**D**) Idh1^{R132H}p53^{ko}Atrx^{ko} murine NSCs. 4-OHT induction resulted in significant changes for all 4 genotypes while (A) and (B) revealed decreased proliferation, (C) and (D) strongly increased their viability over 72h. The comparison of all genotypes including a p53^{ko} control (**E**) illustrates the differences between the alteration combinations. All data are shown as box-and-whiskers plots, where the middle line reveals the median, the box extends from the 25th to 75th percentiles and the whiskers go down to the smallest and up to the highest value. For each genotype three cell lines were used in independent experiments with ≥ 6 technical replicates. One sample t test was used in (A)-(D) to compare the 4-OHT treated conditions against the normalized 100 % control. Prior normal distribution was confirmed by Shapiro-Wilk test. Ordinary one-way ANOVA followed by a Tukey's multiple comparisons test was performed to compare the different conditions in (E); ns = not significant, * p ≤ 0.033, ** p ≤ 0.002, *** p < 0.001*

3.6. Methylation analysis

3.6.1. Induction of global hypermethylation

A further very individual hallmark defining IDH-mut A is hypermethylation. This is caused by dysfunctional demethylases, which are inhibited in their catalytic activity. DNA demethylases like TET proteins count into the group of enzymes, called α-KG dependent dioxygenases. Since α-KG and 2-HG have a quiet similar molecule structure, 2-HG competitively inhibit this dioxygenases leading to impaired DNA demethylation and epigenetic deregulations.

For this reason I analyzed how my murine NSC model response to their expression of mutant Idh1 and the increased 2-HG concentrations on methylome level by applying the recently released Illumina Mouse Methylation BeadChip.

The first analyzed aspect was the genome wide mean methylation after 4-OHT induced recombination over time (Figure 6) . Immediately after the expression of mutant Idh1, beta values changed similar to the 2-HG level patterns. Already during the first 21 days the mean methylation reached high beta level within cells either harboring $Idh1^{R132H}$ alone or the three other combination genotypes. Observation periods longer than 28 days resulted in subsequently decreasing beta-values since the cells lose their 2-HG producing mutation during long term cultivation. Therefore I focused on the changes occurring during the first phase. Considered as negative control samples of $Atrx^{ko}$ alone were analyzed. Contrary to expectations these NSCs developed a hypomethylation over 28 days with constantly decreasing beta-values.

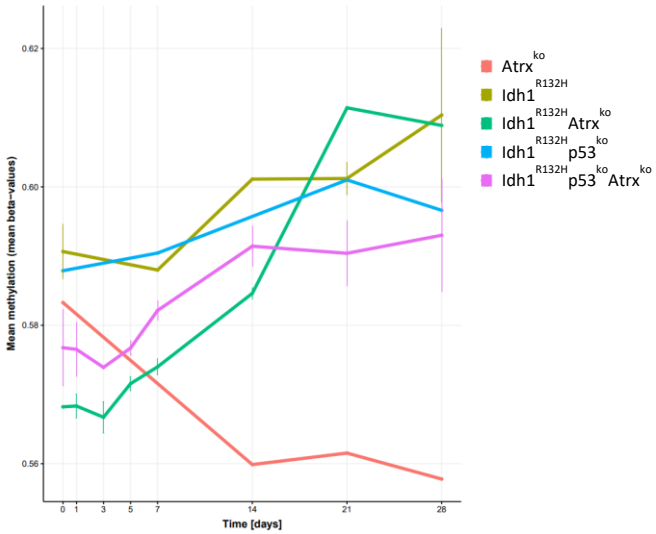

Figure 6: ***Global mean methylation per genotype over time****. Methylation levels measured via Illumina Mouse Methylation BeadChip, converted to beta values with preprocess Noob to perform background subtraction. The global mean beta values were determined for each time point and cell line. Here the mean per genotype (including either one or two cell lines) and day after induction is plotted for* $Idh1^{R132H}$*,* $Idh1^{R132H}p53^{ko}$*,* $Idh1^{R132H}Atrx^{ko}$*,* $Idh1^{R132H}p53^{ko}Atrx^{ko}$ *and* $Atrx^{ko}$ *(planned as negative control). For most genotypes at least 0, 7, 14, 21 days a n=2 different cell lines was performed; for* $Atrx^{ko}$ *only n=1*

One advantage of my well-defined model is the possibility to observe processes during progression. Thus I was able to track the changes in beta value distribution of all CpG sites in different genomic regions of all genotypes. (Irizarry et al., 2009; Sandoval et al., 2011) Thereby islands are defined as genomic areas (longer than 500 bp) with over 55% GC content and CpG ratio of over 0.65. They account for 40% of gene promotors. The flanking region up to 2 kB up- and downstream are shores. Over 75% of these are associated with regions that exhibit a tissue-specific differential methylation. Changes in shore methylation might better correlate with altered gene expression than CpG islands. (Irizarry et al., 2009) The region 2-4 kB is annotated as shelves and the rest of the genome is open sea.

Figure 7 provides an overview of the density plots split in the different regions (columns) and analyzed genotypes (rows). Idh1^{R132H} NSCs reveal a decreasing number of CpGs that have low methylation scores, indicated by low beta-values, over the time lapse of 28 days, particularly seen in the island, NShore and SShore regions. Concurrently the density in highly methylated probes raised in relation to day 0 in the both Shelfs and Shores. In a comparable way Idh1^{R132H}Atrx^{ko}, Idh1^{R132H}p53^{ko} and Idh1^{R132H}p53^{ko}Atrx^{ko} behaved within the observation period. This gradual shift from low to high beta-values can be seen even better when only the 500 most different CpGs are applied to this density plots, exemplarily done for Idh1^{R132H}p53^{ko}Atrx^{ko} (Supplement 2). The development of the hypermethylation phenotype does not stop with 14 days, where the 2-HG levels showed their peak. The d14 data depict more an intermediate stage between wild-type d0 and d28 unrestricted to any genomic region.

Atrx^{ko} was planned to serve as control, since I did not expected any changes in methylation without demethylase inhibitory 2-HG. The most striking result was the rather reversed effect. For the island region the density of low beta-value probes was smaller than at d 28, while especially for the Shelf regions the high methylation drops from day 0 to day 28.

What can be clearly seen in this summarizing figure is the general pattern of the Idh1^{R132H} induced methylation shift towards hypermethylation in corresponding murine cells.

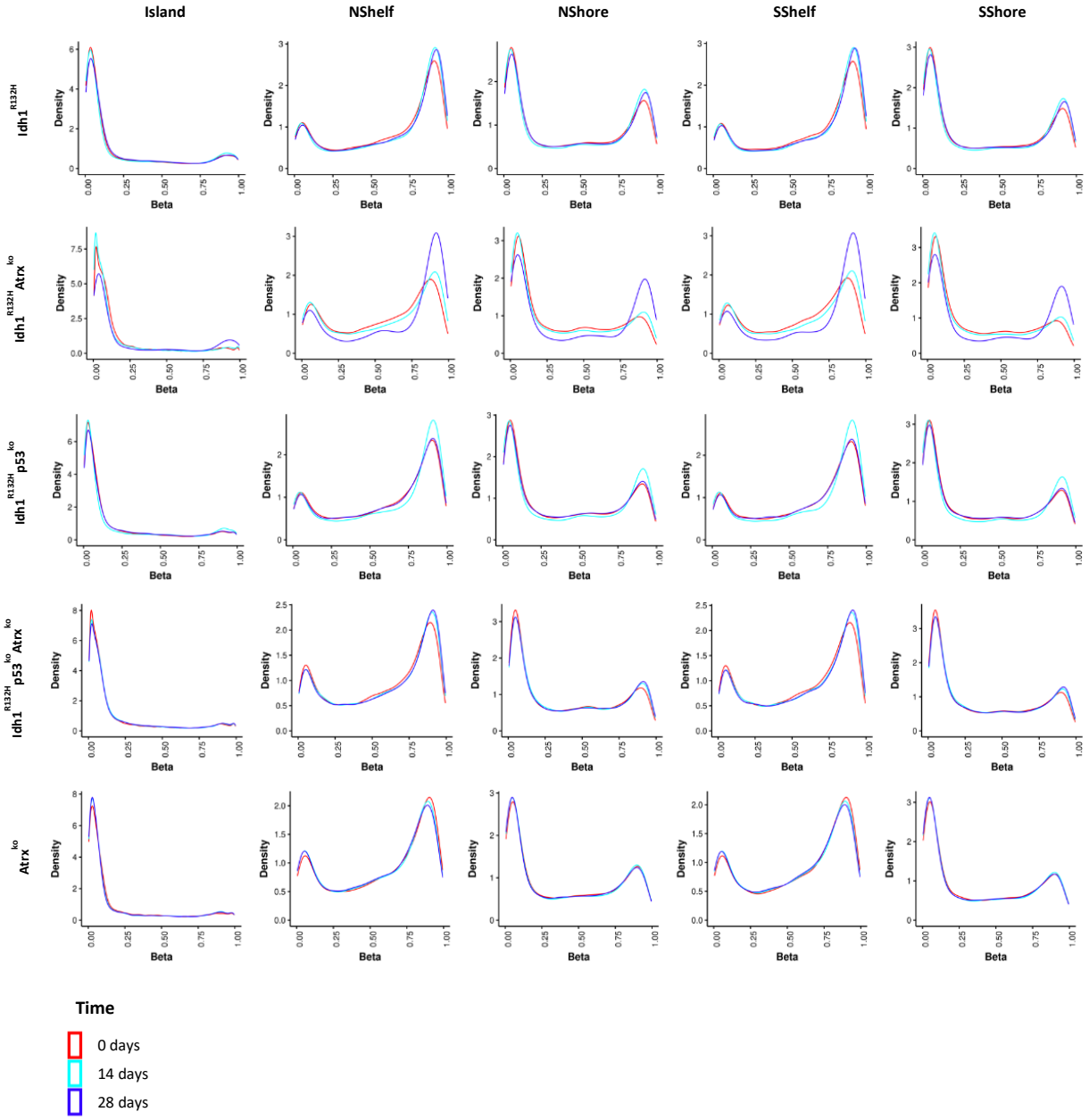

Figure 7: ***DNA methylation level distribution for all murine genotypes over 28 days****. The probe methylation density plot compares the density of probes at each CpG (y-axis) against the methylation beta values (x-axis). The distribution of the mean methylation levels by genomic regions (Island, NShelf, NShore, SShelf, SShore) for d0, d14 and d28 exhibits specific patterns for Idh1^{R132H}, Idh1^{R132H}Atrx^{ko}, Idh1^{R132H}p53^{ko}, Idh1^{R132H}p53^{ko}Atrx^{ko} and Atrx^{ko}. Thereby islands are defined by high CpG motifs. The up to 2 kB flanking region is denoted as shores and 2-4 kB from island as shelves. North marks the 5' end whereas 3' end is labelled as south. The red lines represent distribution of CpG methylation at day 0, light blue at day 14 and blue at day 28 after induction of corresponding genotypes. All mouse chip CpGs were*

To get an impression how these density patterns behave in patients, I compared samples from healthy control hemispheric tissue against IDH-mut A and IDH-mut A (high-grades). The distinction between IDH-mut A and high-grade IDH-mut A is based on methylation classification. But as grading does not play the most important role I here focused on IDH-mut A. The human distribution analysis using all CpGs from 850K data showed density shifts between control hemisphere and the IDH-mut A samples. Comparing control and tumor the number of CpGs with high beta-values at least double in all regions,

except islands (Figure 8). For example for both shore regions the density the right peak of the bimodal distribution has a density of 2 in the control hemisphere and in IDH-mut A CpG density reaches a density over 5. This observations clearly illustrate the known hypermethylation phenotype.

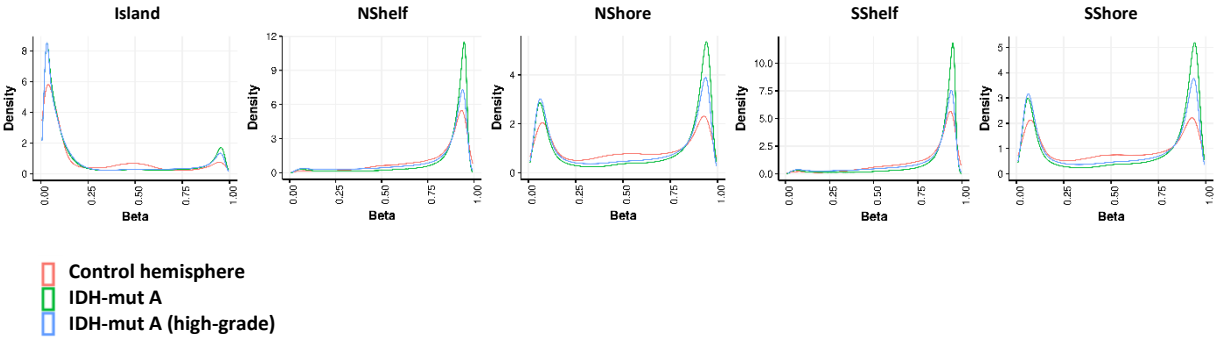

*Figure 8: **DNA methylation pattern for IDH-mut A**. Density plots for the predefined genomic regions (island, shelves and shores) were performed using human hemisphere (red), IDH-mut A (green) and IDH-mut A (high-grade). A representative number of cases for each category was selected based on the methylation classifier score and EPIC data were used to generate the illustrated plots.*

Since I performed the analysis for all as well as the 500 most different CpGs also using the murine data (Figure 7 and Supplement 2) a first comparison was possible. Healthy human hemisphere was chosen to correspond to d0 wild-type cells, because for both tissues no tumor associated alterations are expected. I detected the same trends seen in the human profiles for the murine d28 data (Figure 7) compared to control (d0), meaning tendencies towards higher density of high beta-values.

The results of this elementary methylation analysis part indicate that Idh1 mutation is capable of inducing a global hypermethylation in murine NSCs within 28 days. Comparing the mouse profile with what can be seen in patient data similarities are found. The next chapter moves on to discuss these methylation data in more detail.

3.6.2. G-CIMP in Idh1^{R132H}p53^{ko}Atrx^{ko}

To point out the conformity/consistence between the murine cellular model and human IDH-mut A induced by this hypermethylation, I will focus below on the genetically closest combination the murine model provides. Therefore I analyzed the Idh1^{R132H}p53^{ko}Atrx^{ko} NSCs in more depth.

In human IDH mutant glioma a G-CIMP develops as a result of deficient demethylation. For a manifested G-CIMP not global hypermethylation is considered, but methylation status of specific genes. (Noushmehr et al., 2010) Analysis of my murine model including these genes revealed 82% (32/39) of the as Top 50 defined genes were also differentially methylated in murine Idh1^{R132H}p53^{ko}Atrx^{ko} NSCs (Table 15). (Noushmehr et al., 2010) Not all genes were found on the mouse methylation chip and the found genes were methylated to a varying extent from 1 CpG in 15 CpGs on the chip such as for Ephx2 to 5 CpGs out of 7 probes identified for Lgals3.

*Table 15: **Table of the top 50 G-CIMP genes and their methylation status in Idh1^{R132H}p53^{ko}Atrx^{ko} cells**. The groundwork of this analysis was the Noushmehr paper from 2010 were the G-CIMP was described and the applied gene list of 50 genes (column 1) was published. Due to the limited coverage 39 out of 50 genes were identified (column 2), while 32 of those were identified to be differentially methylated in the Idh1^{R132H}p53^{ko}Atrx^{ko} (here: IPA) comparing d0 versus d14.*

Top 50 genes	# probes on the chip	# CpGs diff. methylated in IPA
Aqp5	6	-
Armc3	12	3
B3Gnt5	8	2
Birc3	6	2
C10Orf107	-	-
C11Orf63	-	-
C7Orf46	-	-
Ca3	-	-
Cbr1	3	2
Ccna1	7	4
Chi3L1	-	-
Chrdl2	12	1
Chst6	-	-
Crygd	4	-
Cthrc1	7	5
Dkfzp586H2123	-	-
Ephx2	15	1
F3	6	-
Fabp5	6	-
Fkbp5	15	5
Flj21963	-	-
Flnc	8	4
Fmod	9	3
Fzd6	5	-
G0S2	2	2
Gjb2	6	1
Itgbl1	28	3
Kiaa0746	-	-
Ldha	11	-
Lect1	9	2
Lgals3	7	5
Lgals8	15	3
Mmp9	12	1
Mosc2	-	-
Nmnat3	14	1
Ociad2	7	5
Pdpn	16	4
Rab36	7	2
Rarres1	5	3
Rarres2	6	2
Rbp1	10	4
Sema3E	18	7
Slc25A20	6	2
Slc39A12	5	1
Spon2	3	-
Tctex1D1	12	1
Tmem22	-	-
Tom1L1	9	2
Trip4	23	5
Ttc12	5	1
50	39	32
		82.05%

In summary all these observations demonstrated that besides the global hypermethylation also the G-CIMP is manifested in my murine Idh1^{R132H}p53^{ko}Atrx^{ko} model similar to the human situation.

3.6.3. Orthologous CpG

With the advanced bioinformatical support of Dr. Damian Stichel (CCU Neuropathology, Heidelberg) I spotted 2 322 orthologous CpGs (associated to 1 740 different genes) that can be found on both the human EPIC chip and the murine methylation chip (Needhamsen et al., 2017). To have a comparative analyses of mouse and human all 2 322 CpGs were illustrated in Figure 9 Each CpG site is represented by a single arrow visualizing the methylation changes between healthy human brain tissue and IDH-mut A (x-axis) and between murine Idh1^{R132H}p53^{ko}Atrx^{ko} NSCs uninduced versus 14 days after induction (y-axis).

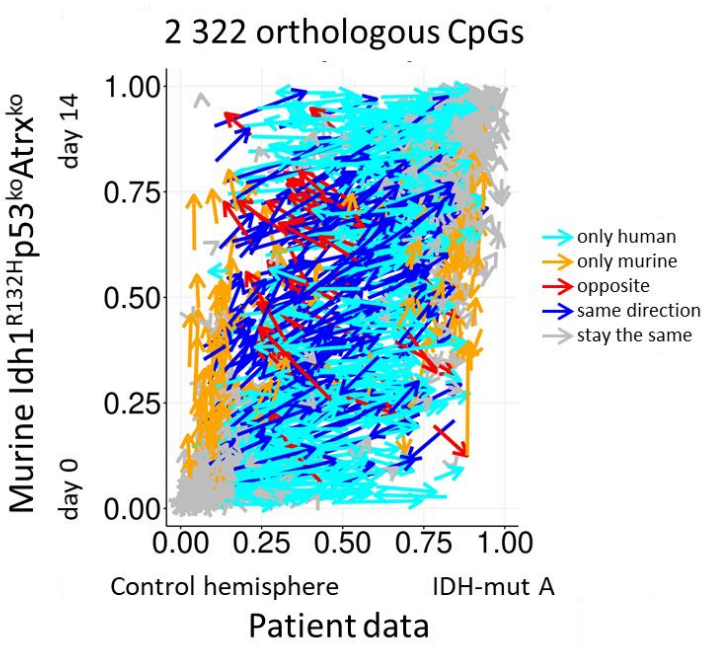

Figure 9: ***Comparison of the 2 322 orthologous CpGs in human and mouse data sets.*** *The CpGs identified as orthologous and present on EPIC and mouse chip were plotted as one arrow. The x-axis represents the human changes in beta-values from healthy control hemispheric tissue (arrow starting point) and IDH-mut A (arrow head). The same function was applied for the murine y-axis. Here methylation status of d0 Idh1^{R132H}p53^{ko}Atrx^{ko} matches with the arrow starting point while the changes after 14 days are depict by the arrow head. Depending on the delta(x) and delta(y) the arrows were categorized into changes only in human (light blue), only in murine (orange), into opposite directions (red), into the same direction (blue) and no changes (grey). Deltas were considered >0.05.*

Thereby I identified 200 CpGs increased their methylation in both, human and mouse. 10 additional CpGs showed up that decreased their methylation in the same direction (Figure 10). The majority of CpGs stayed hypermethylated (751 CpGs) or hypomethylated (547 CpGs) (Figure 11). Figure 12 shows the species specific category of arrows: 594 CpGs that changes only in human samples and 169 only in murine samples.

This approach was used to allow a deeper insight into what processes are involved in the reshaping via methylation. I performed an enrichment analysis for Gene Ontology (GO) terms. The category of highest interest contained the probes moving the same direction. The identified 210 CpGs (blue arrows) can be assigned to 170 genes including multiple CpGs, that are related to one gene and some not annotated CpGs.

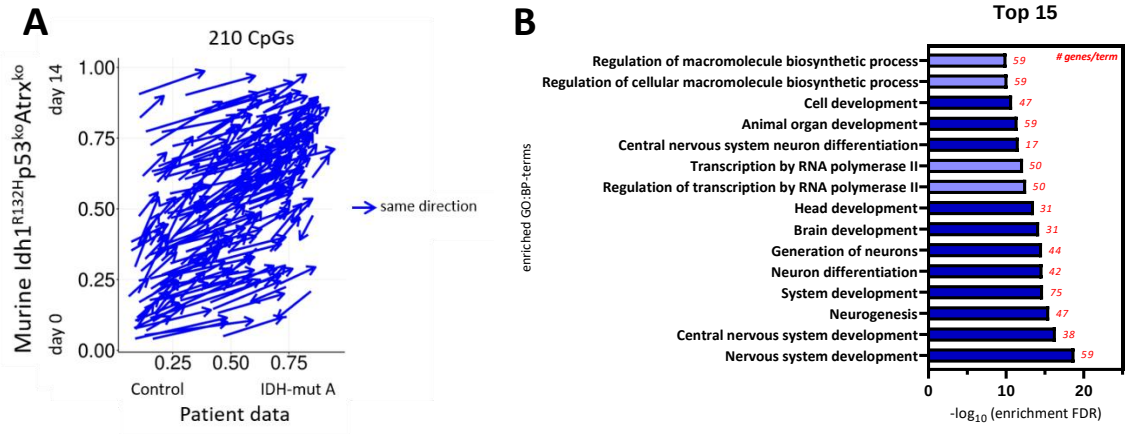

*Figure 10: **Analysis of 210 CpGs moving in the same direction.** For a better overview only the blue arrows are plotted using the same conditions as before (**A**). Within these 210 CpGs 200 show increased methylation in both species, while 10 CpGs are lower methylated in human and mouse. The associated top 15 biological process GO-terms (**B**) are depicted containing information about false discovery rate for enrichment and number of genes in my gene set falling into the respective terms. The bars marked with dark blue are associated with processes of development and differentiation, while the lighter blue with biosynthesis. The analysis was done with the ShinyGOv0.741.*

I analyzed the terms defining biological processes that were enriched in these gene set compared to a randomly generated list of genes (Figure 10 B). Among these 15 top hit, 11 terms were closely related to developmental and differentiation processes, indicating an influence of IDH induced methylation changes on the cell status and maturity. The other 4 terms all belonged to biosynthesis processes playing an important role in adjusting the amount of proteins and thereby regulating the whole cellular metabolism.

Since several of the GO-terms are overlapping regarding the included genes, this implies that additional not less important terms might not appear in this analysis. In order to overcome this problem and to obtain a better overview I did a GO based analysis were my gene set is grouped into functional categories defined by high-level GO terms (Supplement 3). Essential processes such as growth, proliferation, stress response, signaling and immune system process were listed among them. Particularly for later comparisons this not too specific but informative list was important.

Beside the blue arrows moving in the same direction several other arrows stayed either hyper- or hypomethylated (Figure 11) independent of status and species of the sample. GO enrichment analysis of the corresponding 471 genes with permanent low methylation showed 28/30 terms coming under the heading of metabolic processes (GO:0008152). These processes contain anabolism and catabolism, transforming chemical substances. Also macromolecular processes such as protein synthesis are included. Since a basal metabolic activity is essential for cells it seems to be important not to disrupt all of these processes by methylation.

The 650 genes of the high methylated CpGs clustered under different categories. Among this 12/30 belonged to developmental processes (GO: 0032502), 18/30 to metabolic processes (GO:0008152), 20/30 to cellular processes (GO:0009987) and 15/30 to biological regulation (GO: 006500). Some terms can be assigned to more than one category. Constant hypermethylation serves a possibility to regulate processes which here have to be restrained in healthy and mutated cells for a balanced state.

The last group of CpGs I found, showed species specific change (Figure 12). Analyzing the 146 identified genes (belonging to 170 CpGs) only changed in murine samples mainly developmental processes were effected. Whereas for the human specific genes (593 CpGs connected to 481 genes) also reshaping of metabolic processes occurred.

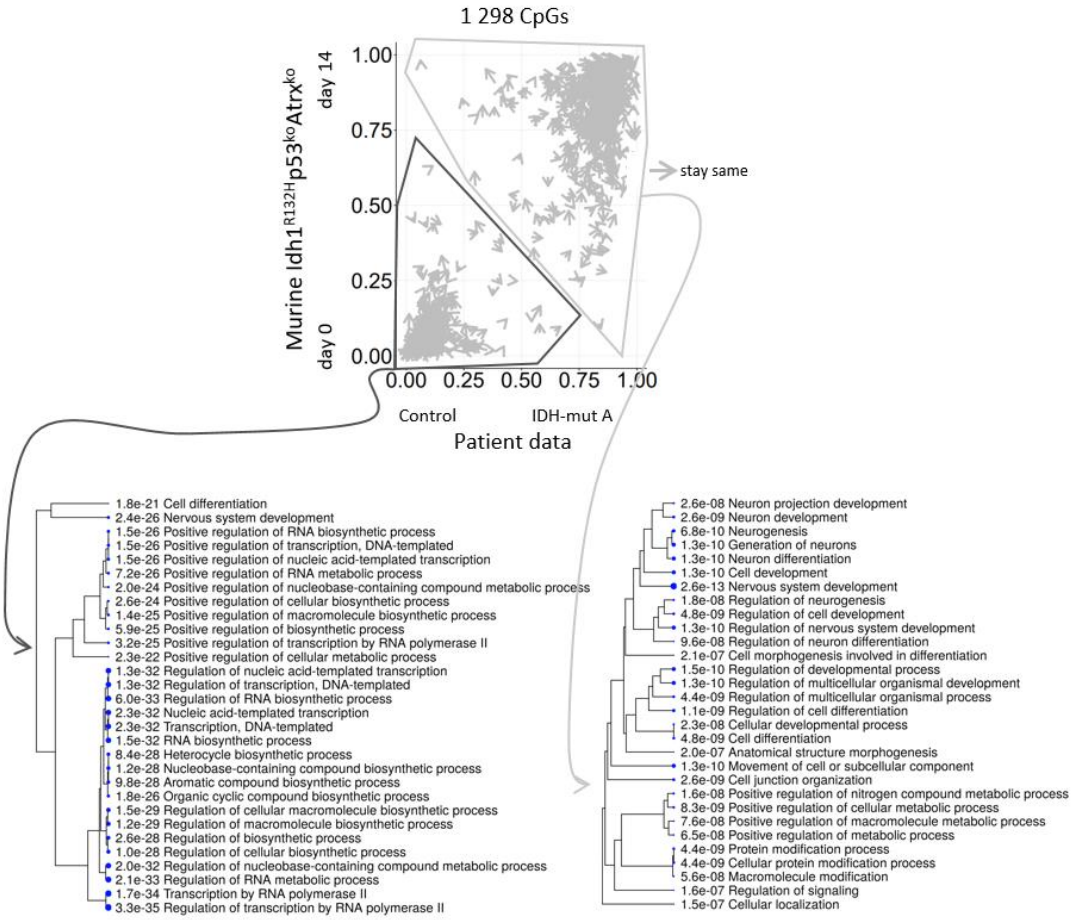

Figure 11: ***Analysis of 1 298 CpGs staying the same.*** *Only the grey arrows are plotted using the same conditions as before. Two groups were defined with CpGs stayed low (lower left) and CpGs stayed high (upper right). The corresponding GO term enrichment analysis is shown below for both groups (done using ShinyGo). The hierarchical clustering tree shows the correlation of pathways, so that pathways with multiple shared genes cluster closer together. The size of the dots represents the p-values.*

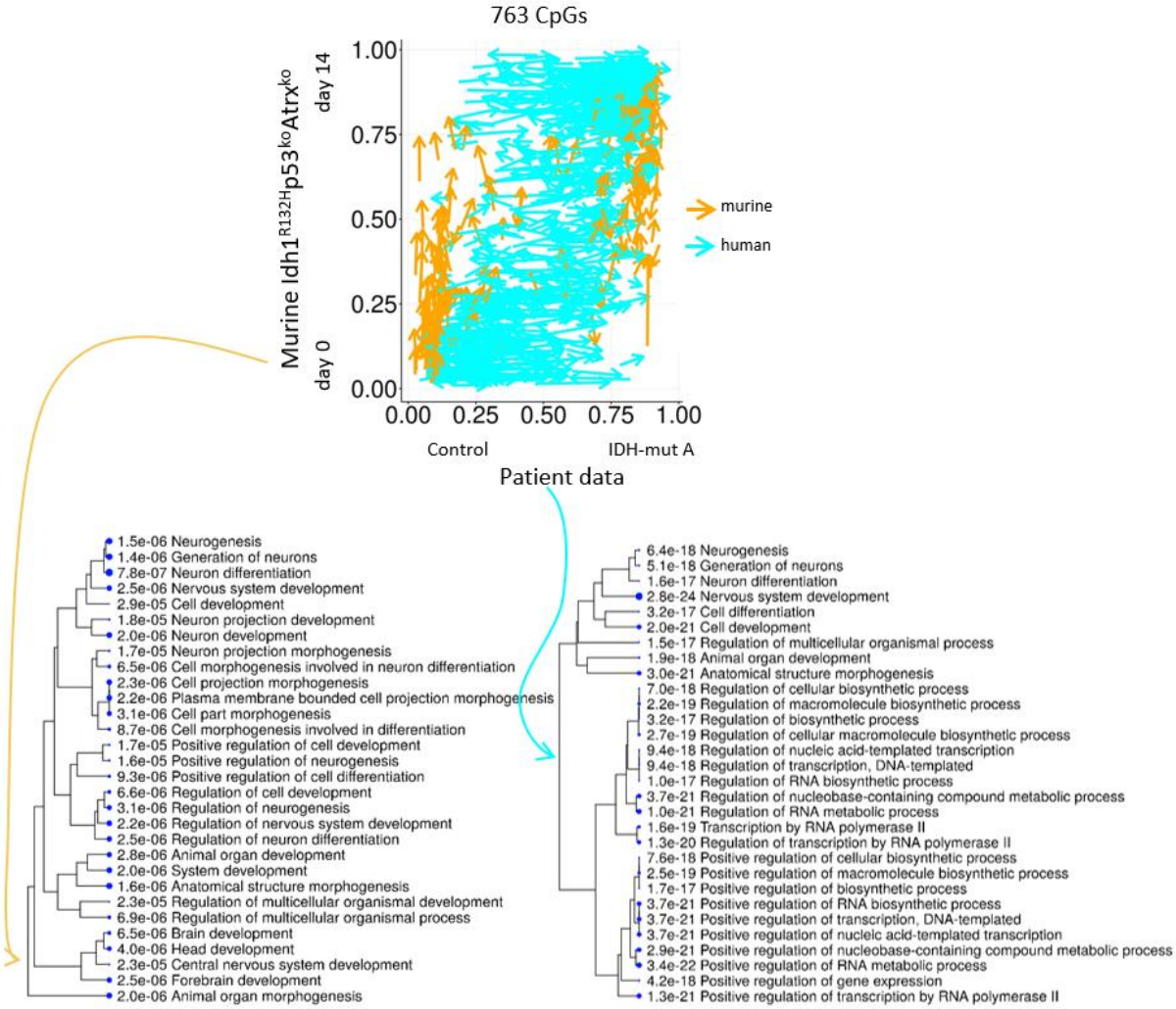

Figure 12: ***Analysis of 763 CpGs changed species specific.*** *CpGs of human (light blue) and murine (orange) dependent CpGs are plotted as done before. The two groups were analyzed for enriched GO terms as described in Figure 11.*

3.6.4. Tumor driving pathways are effected in mouse and human samples

The orthologous CpG analysis gave a first idea how the murine model can mimic the epigenetic landscape of patient samples and related biological processes. Due to the restrictive start numbers I continued with a broader collection of CpGs and focused more on pathways by applying KEGG-analysis.

My methylation data set of Idh1^{R132H}p53^{ko}Atrx^{ko} cells at day 14 contained 65 309 CpGs (23 % of all CpGs on the chip) annotating for 19 565 genes that were differentially methylated over time with a $p<0.05$. For the human samples I ended up with 16 166 CpGs related to 6 013 genes that significantly differ between IDH-mut A and healthy samples. The overlap between mouse and human was a gene set of 4.057 genes.

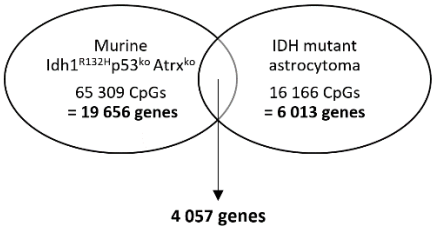

These joint genes showed several pathways enriched in KEGG analysis. The top 30 hits indicate that the three core alterations reshaped the methylome of the cells so that particularly pathways that were important for tumor biology (18/30) are among them. I considered the summarizing hit 'Pathways in Cancer' (p_{adj} = 1.04x10^{-6} and 166 genes; mmu05200) as worth a closer look. The term covers all important signaling pathways (MAPK, Wnt, TGF-b, PI3K, VEGF etc.) leading to cancer hallmarks like apoptosis avoidance, cell proliferation, immortalization, angiogenesis, genomic damage and instability. In total 166/534 genes were differentially methylated in the overlap of human and mouse (Supplement 4). 82.6% of the KEGG-genes present on the mouse chip appeared in the differentially methylated genes of murine Idh1^{R132H}p53^{ko}Atrx^{ko} (441/534), indicating an impact of triple mutation on cancer related pathways in mouse background.

Besides direct cancer-linked pathways, metabolic pathways as well as cell cycle were under the top hits augmenting the processes important for tumorigenicity (Figure 13).

Since I do not know how the hypermethylation of single CpGs impact the expression, I restricted the 4 057 genes again to verify the results. For that purpose I filtered murine gene set by only including those where 50 % of the CpGs depicted differentially methylation. I used the emerging 431 hits to repeat the KEGG analysis. With a 2.5 fold enrichment and a FDR of 2.5x10^{-3} 'Pathways in cancer' appeared again (Supplement 5). The notable shorter list also contained 'Sphingolipid signaling pathway' and 'Focal adhesion'.

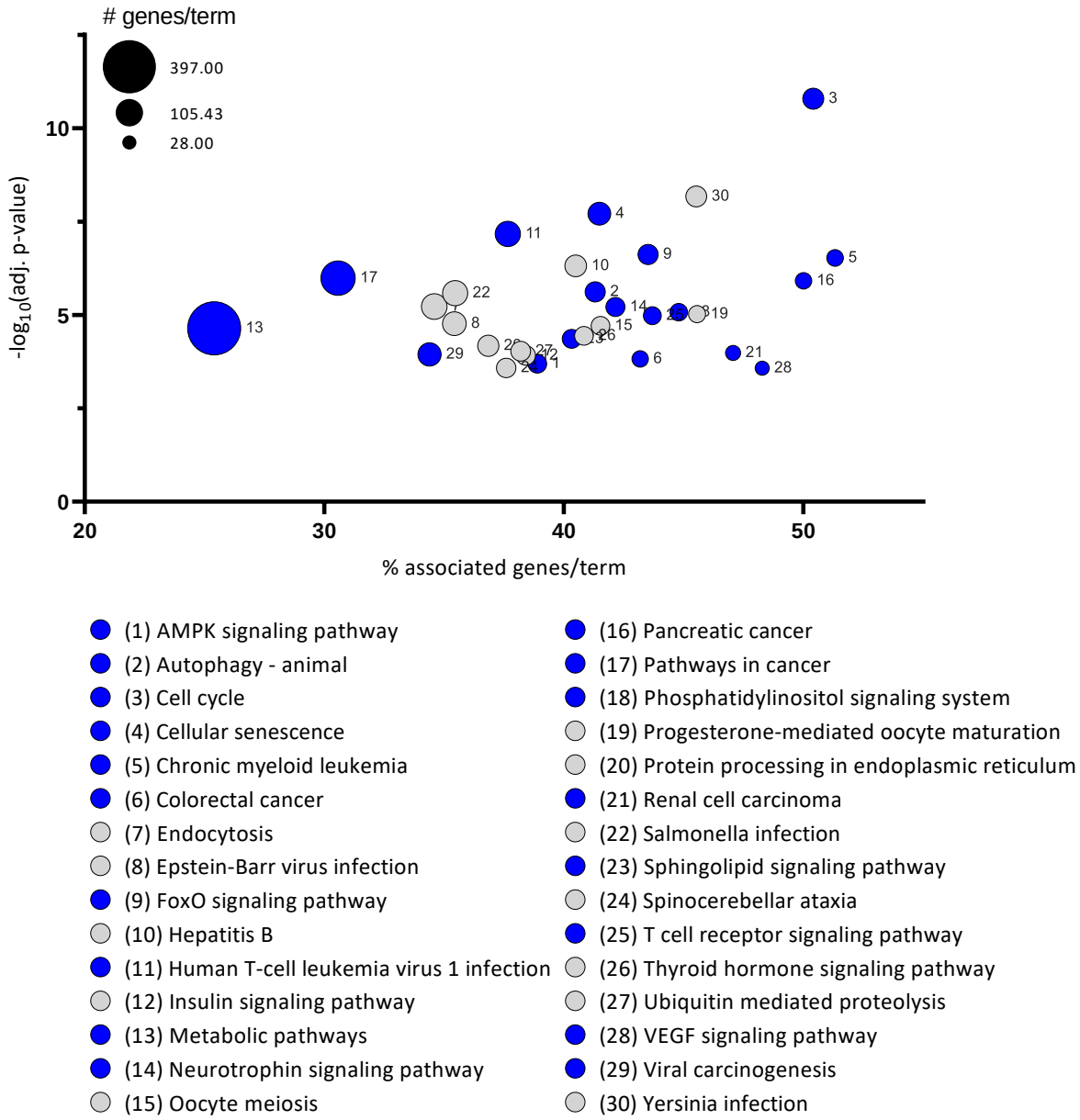

Figure 13: ***KEGG pathway analysis of the differentially methylated genes in the human-mouse overlap.*** *Functional enrichment analysis (done with gprofiler) of genes showing a differential methylation in both species illustrating the top 30 hits. For each term the adjusted p-value and the % of associated genes per term are plotted on the axis, while the size of the dots indicates the number of genes per term. Terms marked in blue are associated to tumorigenicity.*

Taken together, these results suggest that there is an association between the induction of Idh1^{R132H}p53^{ko}Atrx^{ko} and profound effects on the methylome of the murine cells impacting essential processes that are involved in tumor associated behavior. Moreover, the various approaches of comparison between patient situation and mouse model provide evidence for overlapping mechanisms.

3.7. Proteome analysis as connecting verification and

Its known that changes in CpG methylation are associated with inducing gene expression that further can alters protein and metabolite levels and modulate other cellular processes. However, since the proteome of cells can be described as final connection between genotype and phenotype, protein abundances are of special interest to obtain more accurate information about the state of the cell and disturbed processes. (Magzoub et al., 2019)

The recent technological progress offers the possibility to analyze the proteome of cells using highly sensitive mass-spectrometry (MS) machines.

3.7.1. Proteomic changes induced by Idh1^{R132H}p53^{ko}Atrx^{ko}

I started with a phenotypical analysis of the *in vitro* model, went on with showing the impact of the induced alterations on Idh1^{R132H}p53^{ko}Atrx^{ko} on methylome and in the next step I tried to explain the detected changes towards tumorigenic behavior and how methylation might influences also the proteome of IPA cells. Analysis of these data was performed in cooperation with Dennis Friedel and David Vonhören, members of our Department Neuropathology, Heidelberg.

After establishing a sample preparation procedure that fits best for my NSC cultures and resulted reliably in high numbers of detected proteins using the timsTOF Pro, I processed Idh1^{R132H}p53^{ko}Atrx^{ko} samples. In general I thereby detected between 3 500 and 6 000 proteins.

After filtering the detected LFQ abundances the generated heatmap clearly distinguish two groups. The two groups represent the two conditions I used in my experimental setting (Figure 14). For each sample set one condition was induction for 14 d whereas the other was treated with the corresponding solvent so that cells stayed wildtype. The formation of these distinct groups suggests that the expression of my alterations clearly modulate the proteome of the cells. Analyzing the 2 185 proteins found in all samples I detected proteins with higher abundance due to induced alteration as well as proteins that were less abundant compared to the wild-type cells.

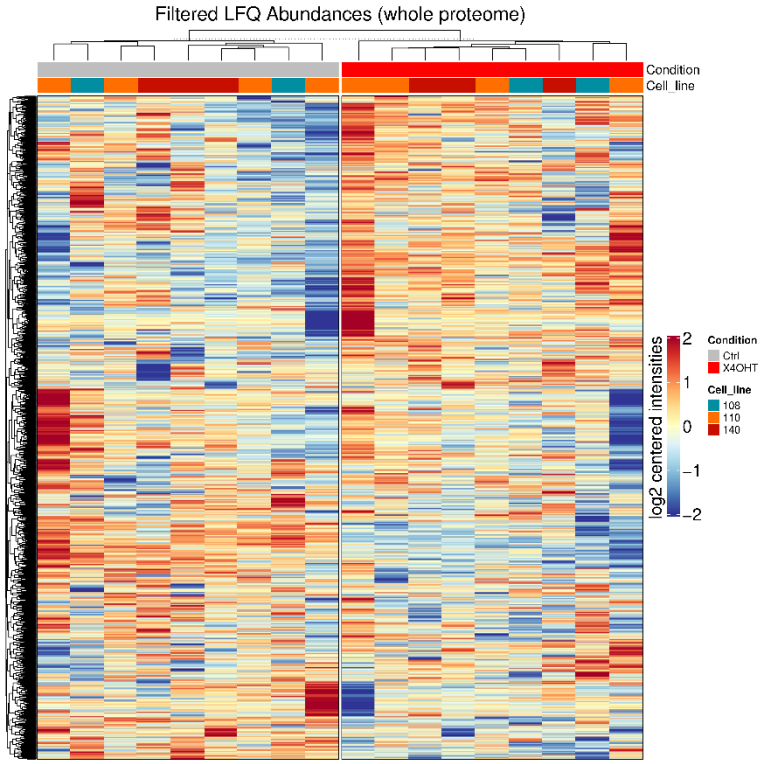

Figure 14: ***Proteomic analysis reveals distinct protein expression patterns****. Heat map of all filtered (missing values <0.9) protein abundances identified by TimsTOF Pro in the proteomic analysis of Idh1^{R132H}p53^{ko}Atrx^{ko} NSCs. The columns of the heat map shows 2-4 biological replicates of three different cell lines (108=cyan, 110=orange, 140=deep red) all carrying conditional Idh1^{R132H}p53^{ko}Atrx^{ko} either induced with 4-OHT (red) or treated with ethanol (grey). Each row represents one particular protein (n=2 185). The color scale illustrates the relative expression level of each protein; red indicating high intensity and blue low intensity.*

After setting the proper cut-offs, 343 out of the 2 185 proteins were significantly different comparing Idh1^{R132H}p53^{ko}Atrx^{ko} against corresponding wildtype NSCs. Within these significant proteins I identified candidates fitting and thereby verifying my phenotypic changes Idh1^{R132H}p53^{ko}Atrx^{ko} showed in the functional assays. The Bax abundances is significantly lower (p_{adj} = 7.17x10^{-6}) in the induced NSCs compared to their controls (Figure 15B, left). Bax is a pro-apoptotic protein. Lower Bax levels thereby correlate with the reduced Caspase activity of Idh1^{R132H}p53^{ko}Atrx^{ko} NSCs, I observed before in apoptosis assays.

The next functional characteristic I identified was increased proliferation. Referring to this the high abundance of Ki-67 has to be highlighted. Ki-67 is a commonly used proliferation marker in tumors, that is significantly increased (p_{adj} = 0.0492) under Idh1^{R132H}p53^{ko}Atrx^{ko} conditions and represent another example to link phenotypic changes and molecular signature induced by induction. Since this high Ki-67 levels is not mouse specific but rather a typical tumor feature, this points to a transferability of my model to the tumor situation.

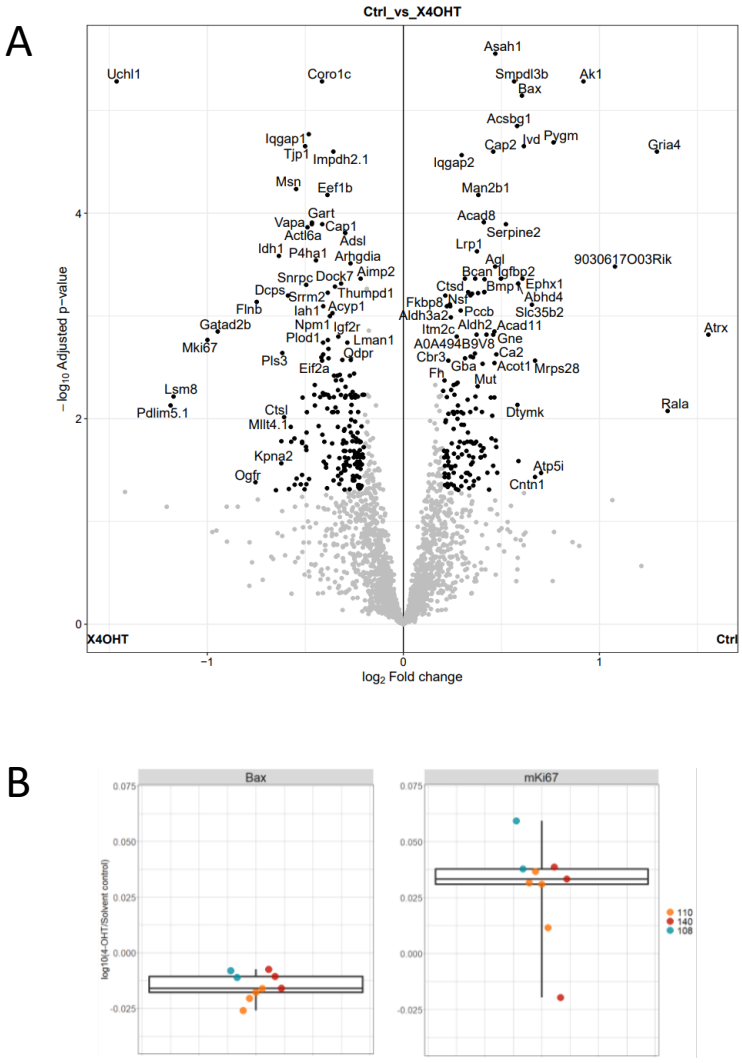

Figure 15: ***Detailed proteomic analysis of Idh1^{R132H}p53^{ko}Atrx^{ko}.*** *(**A**) Differential expression analysis comparing induced versus wild-type control. The volcano plot visualizes all identified proteins by illustrating fold changes (log_2) and adjusted p-values ($-log_{10}$). Significantly increased and decreased hits are shown in black (with $p_{adj.}$<0.05 and fold-change > 20%), all not significant proteins in grey.(**B**) Bax and mKi67 were significantly changed and down- and upregulation is presented as box plot. For each protein the ratio of induced/control for 3 different Idh1^{R132H}p53^{ko}Atrx^{ko} cell lines and 2-4 biological replicates was calculated.*

3.7.2. Pathways enriched in proteomics overlap with methylation results

To get an idea what pathways are enriched on proteome level, I analyzed the correlated biological processes of the 343 significant proteins. For a proper overview at first the genes were grouped by functional categories defined by high-level GO terms. The hit with the most related proteins (94 proteins) is ‘catabolic process’ which indicates an altered metabolism, followed by regulation of biological quality with 89 proteins. Furthermore essential terms associated with developmental processes, signaling and stress response, cell cycle and proliferation as well as regulation of the immune system emerged (Figure 16).

To analyze the high level GO terms was helpful to get an overview since the detailed analysis of the top 30 pathways using GO-term enrichment as well as KEGG analysis was not very informative and meaningful (Supplement 6). For detailed information about impact on citrate cycle for example this detailed analysis can be supportive. In my protein set it was redundant with multiple metabolic processes. Hence metabolism seems to be the major impacted sector concerning proteome changes.

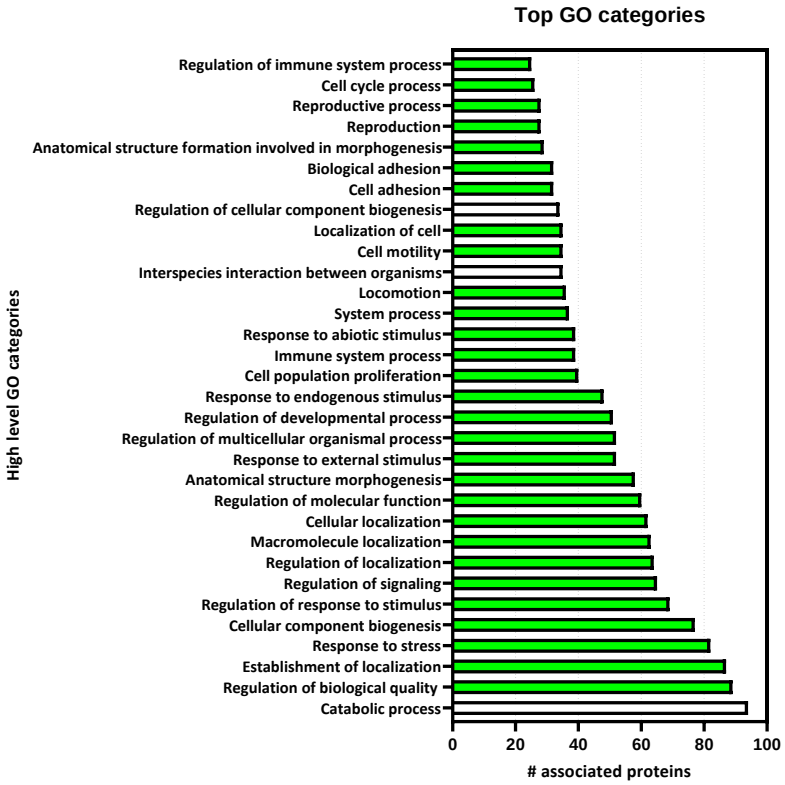

Figure 16: ***High level GO categories of significant changes in Idh1^{R132H}p53^{ko}Atrx^{ko}proteome****. Analysis of the significant proteins modulated after 14d were performed with ShinyGOv0.741. The result shows the categories and the corresponding number of associated proteins. Every term marked with a green bar overlaps with the methylome analysis (Supplement 3).*

After finishing the pathway analysis of the Idh1^{R132H}p53^{ko}Atrx^{ko} NSCs, I wondered how the methylation and proteomic data match. On that account I compared the most significant high level GO categories from both data sets. Except for the proteomic top hit ‘catabolic process’ and two other categories the remaining hits are consistent with what I received from the methylome data only with ranking differences (Supplement 3). However, none of the differentially methylated genes appeared in the list of significant proteins.

Overall these results indicate that the murine NSCs are impacted by induction of Idh1^{R132H}p53^{ko}Atrx^{ko} on several cellular levels. By now I cannot directly translate the changes of methylation status to protein abundance, but can show that essential processes are overlapping that are changed during the cells formation and adaption.

3.8. In vivo animal model

3.8.1. Special need and requirements of *in vivo*

For multiple reasons an *in vivo* approach valorizes the significance of such a model. First of all, I as well as others had problems to keep the Idh1^{R132H} mutation in the cell *in vitro*. The inducible system thereby helped a lot but I was not able to culture cells longer than 4-6 weeks and be sure that a subpopulation of cells had not already lost their mutation. Efforts to prevent this by conditioned medium or co-cultures were not successful (data not shown). As mentioned it is known that the tumor microenvironment especially for IDH-mut A plays a key role: IDH mutation directly influences the extracellular matrix of the surrounding tissue as well as having an inhibitory impact of 2-HG on immune cells was described previously. For that the need of a mouse model is clear. Doing literature research showed us that there are indeed models published (see 1.3.3) but none of them met the requirements an *in vivo* model needed for my comprehensive approach. In the following section I describe how I proceeded.

3.8.2. Pilot experiment

In previous animal experiments (mainly performed by Viktoria Brendel) we noticed how important the choice of a proper host mouse strain is. Problematic with these was the long development time of Idh1 mutated cells that was not compatible with the leaky immune system of the used mouse strain. Furthermore, it is known that different host animals result in distinct tumor growth. For this reason I planned a pilot experiment preparatory to the main experiment. 8 mice strains were compared regarding the tumor uptake rate, histological growth behavior and survival times specific for IDH-mut A tumor cells. The mouse strains differed in their immune status (Figure 17 A) based on several knockouts of genes important for a mature immune system on different background strains. To narrow down my experiments to one immune deficient strain, I implanted patient-derived NCH 551b cells into the 8 different groups. NCH 551b is an acceptable growing glioma stem cell culture generated from a human IDH-mut A 4 that received multiple treatments. This cell line is one of the few cell lines that keeps its IDH^{R132H} mutation during cultivation, albeit in a hemizygous way without the wildtype allele. After intracranially implanting 250.000 cells into the cerebral cortex of the mice, they were monitored by standard MRI, performed by the core facility animal imaging from week 4 on (Figure 17 B). Starting after detectable tumor formation, I in cooperation with Dr. Andreas Korzowski and Justyna Platek (Department of Medical Physics in Radiology, NMR spectroscopy group) worked on the development of advanced approaches. The idea behind this was to have alternative options of 2-HG detection, illustration and quantification using MR spectroscopy.

A

	Mature T-cells	Mature B-cells	NK-cells	Leakiness
BALB/c nude	Absent	Present	Present	High
SCID Beige	Absent	Absent	Deficient	Low
NSG	Absent	Absent	Absent	Very low
NRG	Absent	Absent	Absent	Absent
B6 Rag2	Absent	Absent	Present - high	Absent
BALB/c Rag2 Il2rγc	Absent	Absent	Absent	Absent
BALB/c Rag2	Absent	Absent	Present - high	Absent
B6 Rag2 Il2rγc	Absent	Absent	Absent	Absent

B

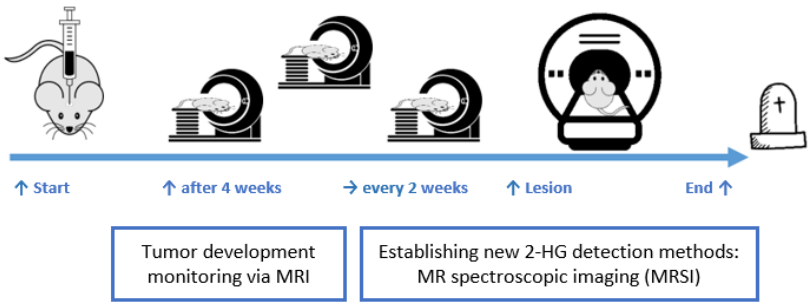

*Figure 17: **Main idea behind the pilot experiment.** The table in (A) presents the used mouse strains with multiple genetic backgrounds as well as different immune suppressive genetic alterations resulting in specific immune cell (T-cell, B-cell, NK-cell) activities. Each mouse underwent the same procedure (B). After implanting NCH 551b tumor formation was monitored by MRI biweekly and with appropriate tumor volume advanced imaging was applied. The experiment was covered by the TVA G-12/20.*

As expected I detected marked differences between the strains. Within the BALB/c nude group 2 out of 4 animals had lesions detected via MRI (Figure 18, row 1). The post-mortem histological analysis showed for both cases an area of solid tumor with infiltrative outgrowth. This strain was considered as kind of control since all past experiments were performed in this animals.

Only one NSG mouse developed tumor before the termination of the experiment after 16 weeks. The histology of this tumor compared to group 1 was predominantly diffuse infiltrative with less solid portions (Figure 18, row 2).

With 4/4 the NRG group had maximal tumor uptake rate with a sharp rising tumor volume for all animals. HE and Idh1^{R132H} staining verified what I already saw on the MRI images, the tumor cells accumulated more on top of the brain, pressed inward and destroyed the normal brain structures such as ventricular system (Figure 18, row 3).

The 2 tumors developed in SCID Beige (group 4) in contrast infiltrated the tissue more diffusely. But for this group I also determined an abnormal anatomical structure in both MRI and staining.

For the B6 Rag2 KO group the MRI results showed no clear enrichment. However the immunohistologic Idh1 staining of mouse V_E02 was positive, particularly in the region of the ventricular system. The HE staining supports this observation. The $Idh1^{R132H}$ positive structure were rich in cells and surrounded by cellular structures indicating ependymal.

The 6^{th} group harboring the same genetic mutations (Rag2 KO) as group 5 but in another background strain (BALB/c) had MRI monitoring with distinct lesion. None of the animals survived week 7 but rather were symptomize and euthanized. In the post-mortem analysis all 4 animals showed positive $Idh1^{R132H}$ stainings. The most striking point hereby was that the positive areas were highly associated with ventricles and from there cells also infiltrated into the brain tissue. This could explain why this group became symptomatic that early.

The last two groups included besides Rag2 KO an additional Interleukin 2 receptor y-chain (Il2ryc) alteration, similar to NSG and NRG animals, but here in a B6 background and BALB/c background. Within Group 7 all animals developed a lesion detected in MRI, compared to the calculated tumor volumes of the other groups, the B6 Rag2 Il2ryc data I received from the core facility were quite low. In contrast the histology showed large $Idh1^{R132H}$ positive areas, with ventricular parts but also an extended infiltrating zone.

Implanting into animals with the same genetic alterations but a BALB/c background (group 8) resulted in 3 MRI detected lesions with again comparable small calculated volumes. The staining results also indicated a tumor formation in these 3 animals.

In addition to this analysis, I performed a 2-HG measurement of one animal, which still showed one more or less healthy hemisphere (Supplement 7). The tumor hemisphere had significantly enhanced 2-HG concentrations of 14.99 mM compared to 3.05 mM measured in the opposite hemisphere.

Overall, these experiment pilot results showed how important the genetic background as well as the immune status of the host strain is in working with IDH-mut tumors. The next step would have been the allograft implantation of the NSC model into the selected immunodeficient host strain.

Results

Tumor growth	MRT image	HE staining	Idh1^{R132H} staining
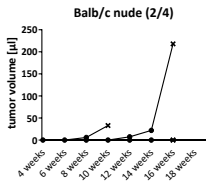	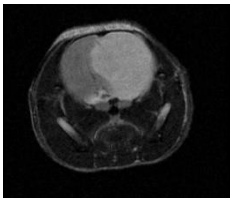	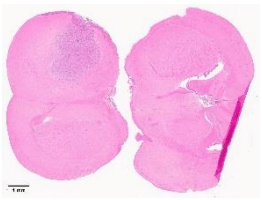	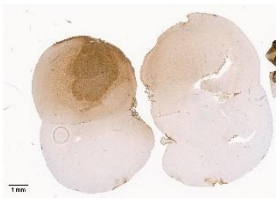
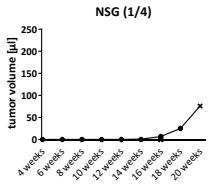	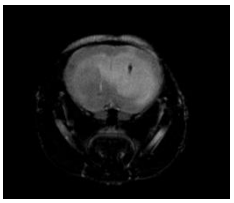	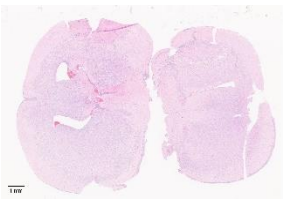	
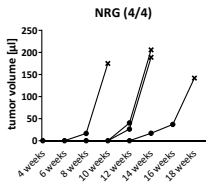	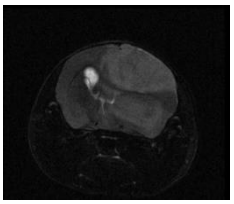	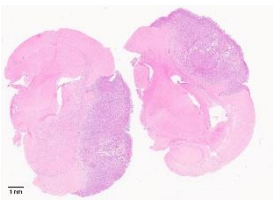	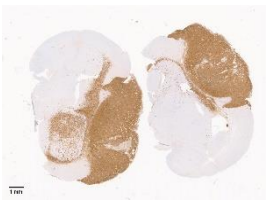
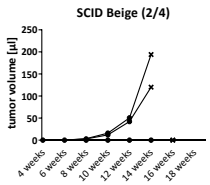	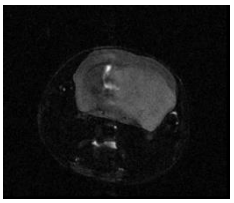	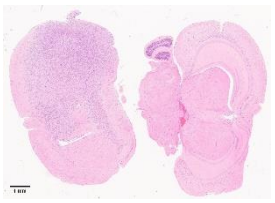	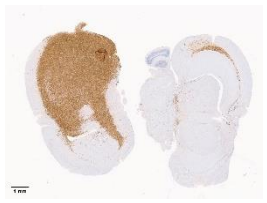
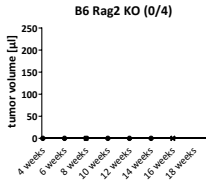	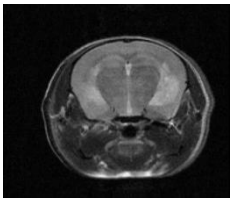	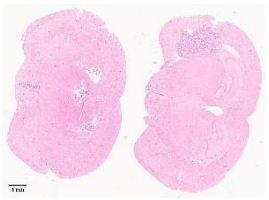	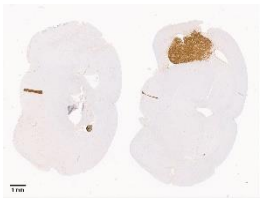
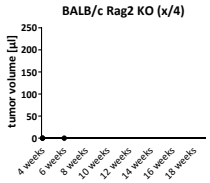	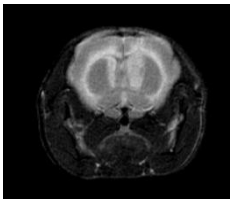		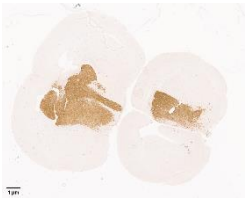
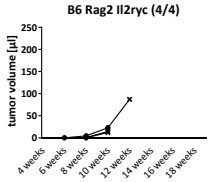	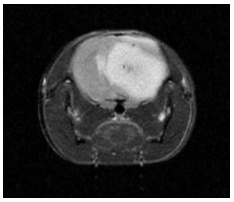	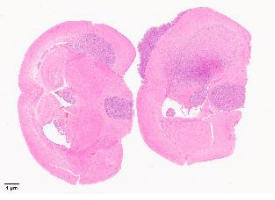	
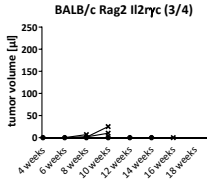	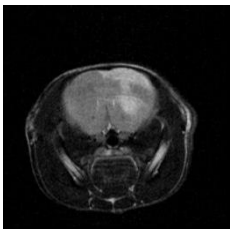	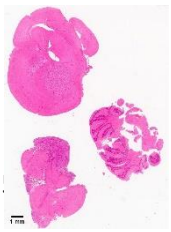	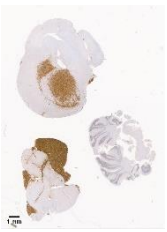

Figure 18 ***Overview of the pilot experiment results****. 8 different mouse strains were selected (rows) to compare uptake rate und growth behavior of patient-derived, IDHmut NCH 511b cells related to varying immune status. The 4 animals per group were monitored via MRI (column 2 showing one example). From this data tumor volume in µl was roughly calculated (column 1). After reaching termination criteria or after 16 weeks post-mortem, histological analyses of all mice were performed applying HE staining and mutation specific Idh1^{R132H} staining (column 3 and 4).*

3.8.3. Main experiment

Major goal of the main experiment was to generate an allograft model. More precisely I was interested in the differences between Idh1^{R132H}p53^{ko} and Idh1^{R132H}p53^{ko}Atrx^{ko} NSCs regarding the tumor rate and histological behavior over time. Due to the lacking tumorigenic potential detected in the *in vitro* data of Idh1^{R132H}Atrx^{ko}, I refrained from including them for implantation.

The comparison between these NSCs injected into immunodeficient mice versus immunocompetent B6 was also planned originally. Due to the coronavirus pandemic, I were not able to perform all experiments, but focused on the immunocompetent part. To generate an allograft with an intact immune system would be the optimal model for further treatment experiments including increasingly important immunotherapies.

The study was structured as follows aiming to monitor the whole tumor formation process: 10 groups including 3 animals as well as a group of 5 animals acting as long term group and 5 reserve animal were injected with either Idh1^{R132H}p53^{ko} or Idh1^{R132H}p53^{ko}Atrx^{ko}. After every month 1 of the 10 groups was removed from the experiment. The cervical lymph nodes, spleen and brain of these animals were harvested. Thereby I was able to have a continuous monitoring over 10 months to investigate how the NSCs behave over time after implantation. The whole process was additionally monitored by regular MRI measurements. 5+1 mice with Idh1^{R132H} alone and p53^{ko} alone served as control groups.

Idh1^{R132H}p53^{ko}

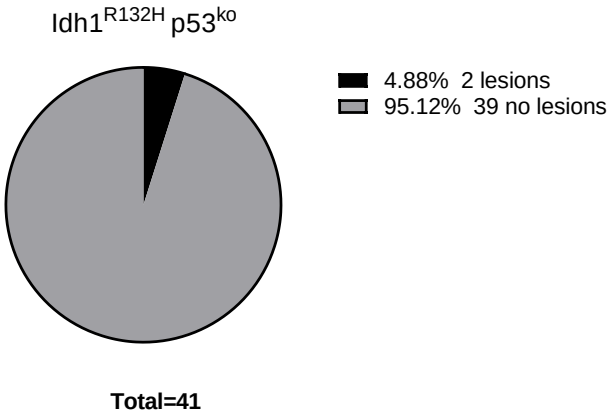

Figure 19: ***Pie chart representing the proportion of detected lesions in B6 Idh1^{R132H}p53^{ko} group****. I performed implantations of Idh1^{R132H}p53^{ko} into 41 animals from which every 4 weeks 3 were euthanized. Over the entire observation period of 10 months, 2 lesions were identified via MRI.*

Within the entire group of 41 animals with implanted Idh1^{R132H}p53^{ko} NSCs a number of 2 mice showed a lesion during the 10-month experiment duration (Figure 19). The animals were monitored biweekly via routinely MRI. The received data did not show evidence of big differences in tumor volume over time (Figure 21, upper plot). For mouse 04_01 first MRI screens were negative while I saw an enrichment in MRI at week 13 (1.8 µl) and 15 (1 µl). Mouse 10_03 had constant levels of tumor volume around 2 µl. The MRI data of both animals show the abnormalities in the right hemisphere at the location where I implanted the cells, indicating the lesion is caused by the injection of cells (Figure 21).

To verify the detected lesion as tumor induced by Idh1 mutated cells the animals were further analyzed post-mortem. Since normal brain tissue is expected to be negative for Idh1^{R132H} expressing cells, I used HE and Idh1^{R132H} staining to identify the lesion. The harvested brains are frontal cut at the site of injection into a rostral and caudal part. Strikingly, neither at this section nor at a later section I was able to detect Idh1^{R132H} positive cells. (Figure 20)

This is an unexpected result, not necessarily indicating that no tumor had grown, but more that my approaches fail to detect it.

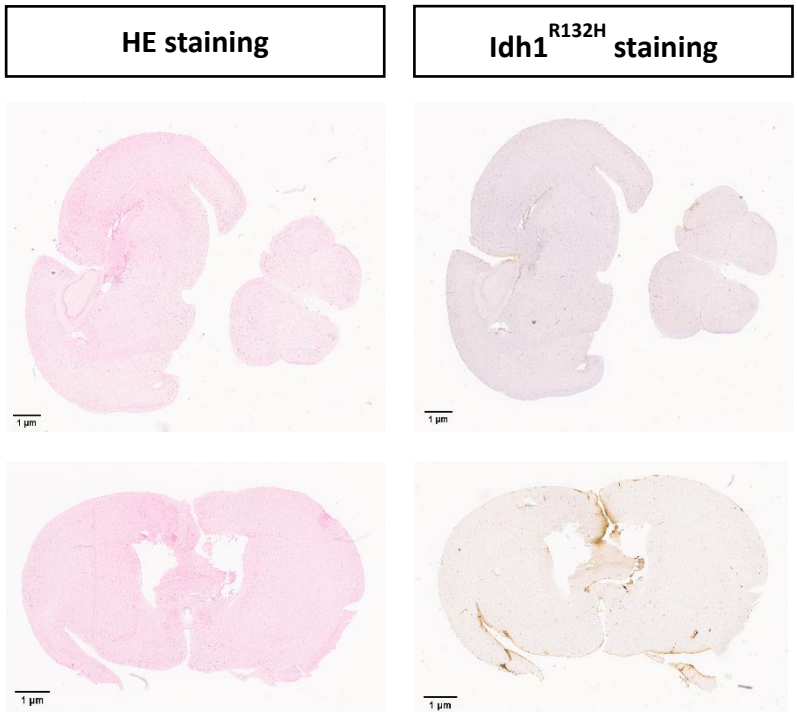

Figure 20: ***Histological analysis of mouse 04_01****. Frontal sections close to the injection site (upper row) and more distant sections (lower row) were HE and Idh1^{R132H} stained.*

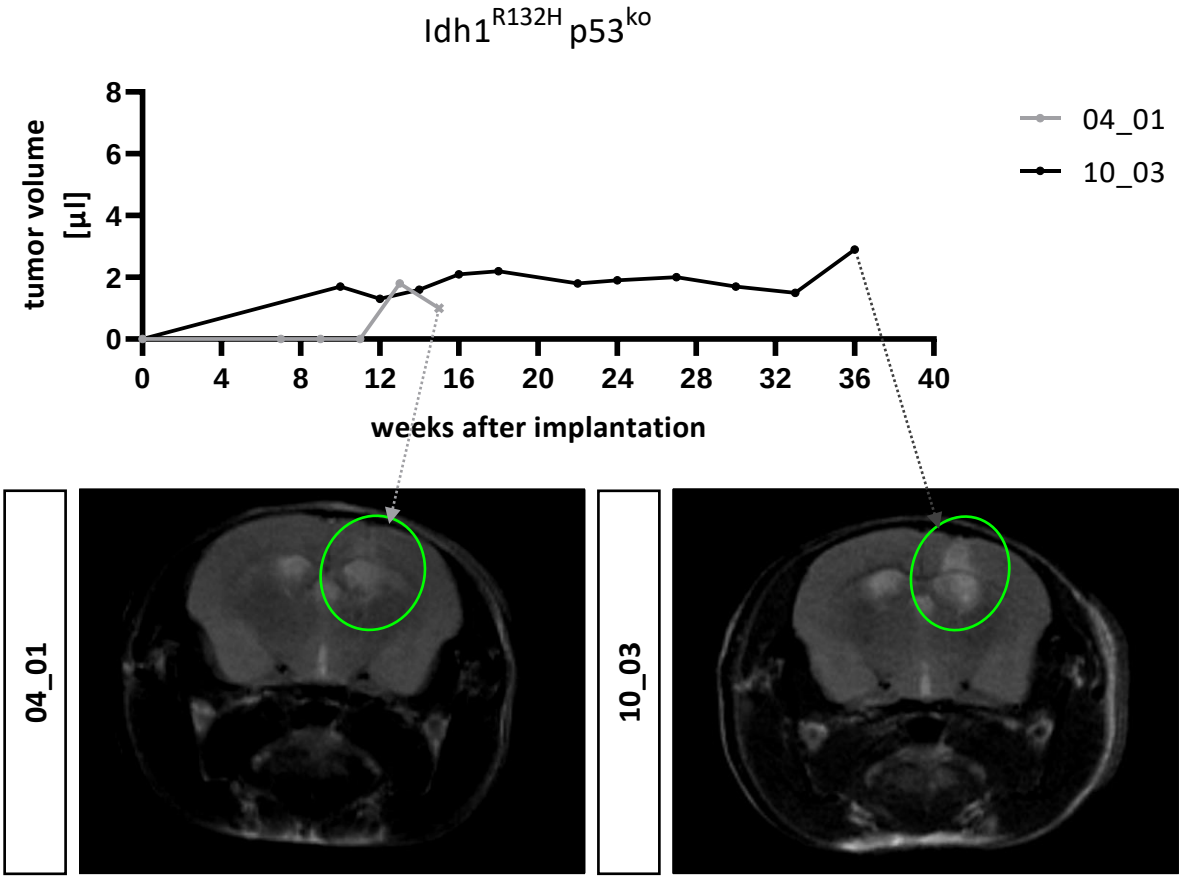

Figure 21: ***Summary MRI results of group Idh1^{R132H}p53^{ko}.*** *Here the detailed course of tumor development based on MRI data is presented. Mice 04_01 and 10_03 were imaged and calculated data were plotted in relation to the weeks after implantation. The latest images for both mice are shown below and lesion (potential tumor formation) is marked (green circle).*

Idh1^{R132H}p53^{ko}Atrx^{ko}

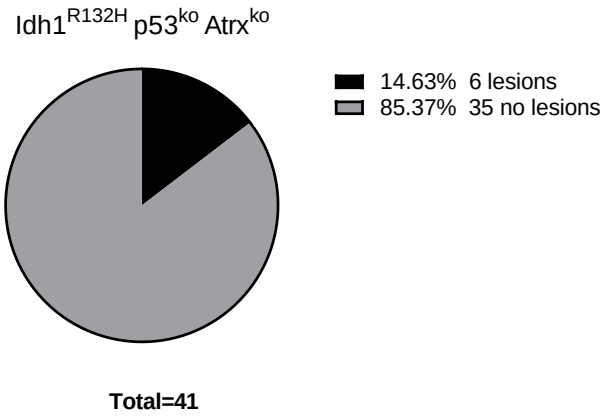

Figure 22: ***Pie chart of the Idh1^{R132H}p53^{ko}Atrx^{ko} group and related lesions****. Out of the 41 B6 mice injected with the triple mutant I obtained 6 lesions monitored by MRI.*

However, the implantation of Idh1^{R132H}p53^{ko}Atrx^{ko} NSCs into B6 mice resulted 14.63 % of the mice a MRI detected lesion. This considerable difference compared to the 4.88 % of the B6 Idh1^{R132H}p53^{ko} group suggests an impact of the additional Atrx^{ko}. Within these 6 animals mouse 10_03 showed the enhanced tumor growth compared to the entire Idh1^{R132H}p53^{ko} group. Figure 23 illustrates the MRI results at the earliest point of time I identified a lesion in this mouse, with a volume of 3.8 µl and the latest point of time in week 39, with a volume of 6.1 µl before the end of the experiment. During this 20 weeks a progression can be seen in both reprehensive sections (Figure 23, MRI images). For the other 5 animals I received data comparable to Idh1^{R132H}p53^{ko} reveals, with tumor volumes around 2 µl.

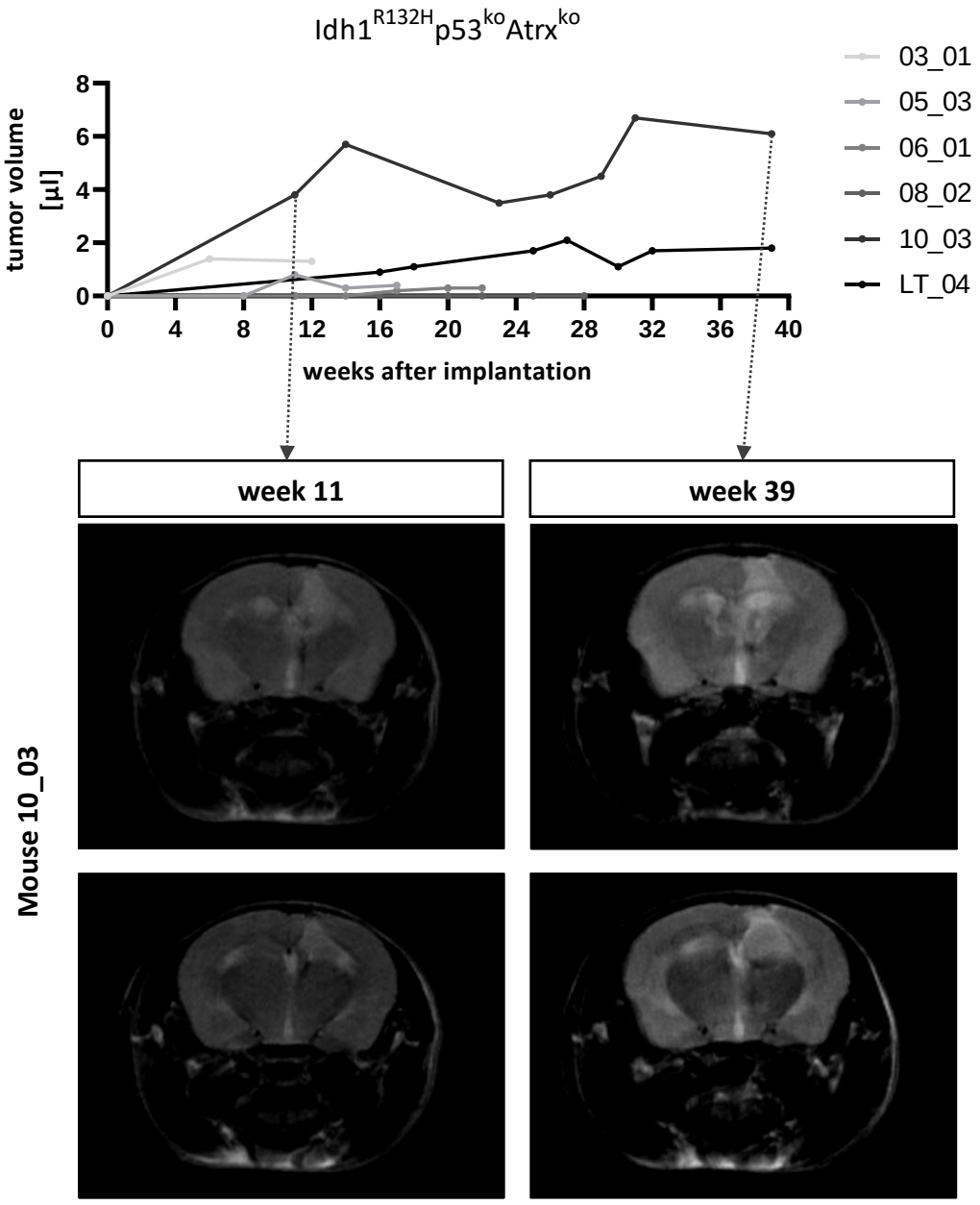

Figure 23: ***MRI summary of B6 Idh1^{R132H}p53^{ko}Atrx^{ko} group.*** *The tumor monitoring showed lesions in 6 mice depicted in the upper plot over the observation time of 10 months. Till some groups were euthanized after corresponding time not all animals were screened for 40 weeks. The data of the mice with major changes is illustrated below. 11 weeks after implantation the lesion was seen the first time, 20 weeks after, MRI images reveal higher tumor volume. Since tumors infiltrate the brain and grow in 3D I decided to show to exemplary sections, the second represents a more posterior area.*

As already mentioned I started a collaboration with Dr. Andreas Korzowski and his students (Department of Medical Physics in Radiology, NMR spectroscopy group) aiming to apply spectroscopy and thereby dissect the tumor more in-depth, particularly the involved oncometabolite 2-HG. In this process the animals were imaged using the 9.4 T MRI, which besides multiple other advantages, gives images with higher quality. We performed one trial with mouse 10_03 and received high resolution data of the 3D structure of the lesion (Figure 24). Hereby we observed a distinct abnormal structure around the injection site, which emerges more detailed in 9.4T MRI (visible as white lesion) and involves clearly an area of several mm.

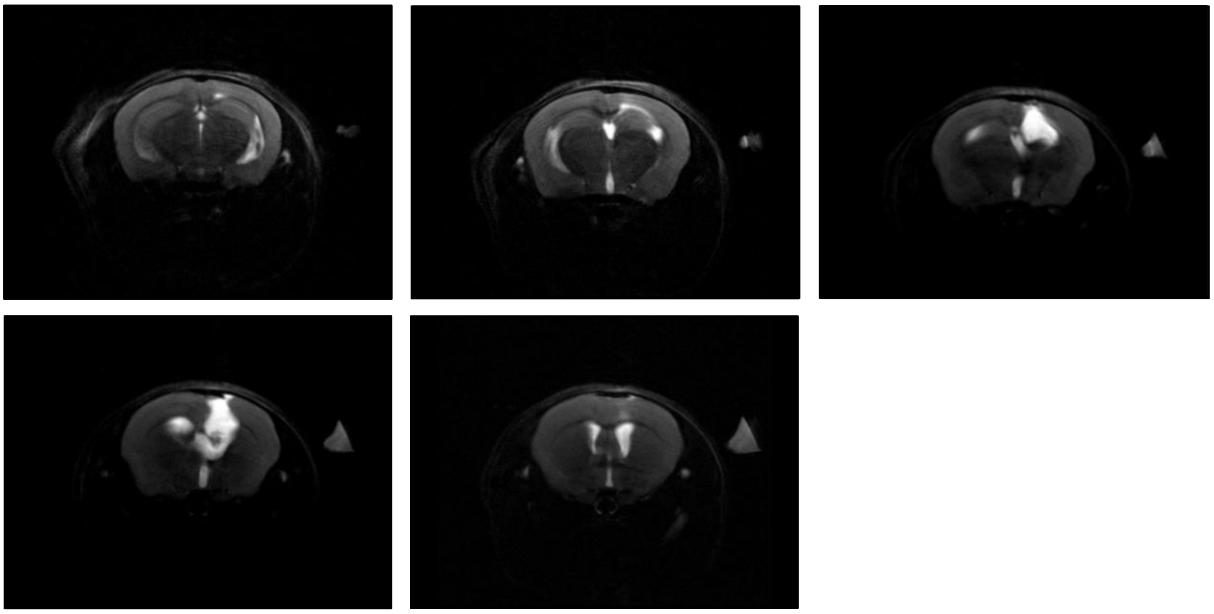

Figure 24: ***High resolution MRI of mouse 10_03****. While advanced analysis done with the 9.4T MRI (Bruker) this serial section (every 1 mm from anterior to posterior) was obtained from mouse 10_03 37 weeks after implantation.*

However, the histological analysis I performed was again counterintuitive. I were not able to identify and verify the lesion by immunohistochemistry.

Figure 25: ***Example of histological analysis of one Idh1^{R132H}p53^{ko}Atrx^{ko} mouse.*** *Here the results of one HE (left) and 2 Idh1^{R132H} stainings are shown. Neither the section close to the injection side (middle), nor a later section (right) depicted positive results.*

Controls

I also included groups of 5+1 animal to have proper controls. Into the first control group I implanted NSC with Idh1^{R132H} alone to check what's reported multiple times, that Idh1^{R132H} is by itself as NSC allograft not tumorigenic enough to develop a lesion. The second control group received p53^{ko} NSCs, considering that the deletion of such a tumor suppressor already induce tumor formation (reported in some studies).

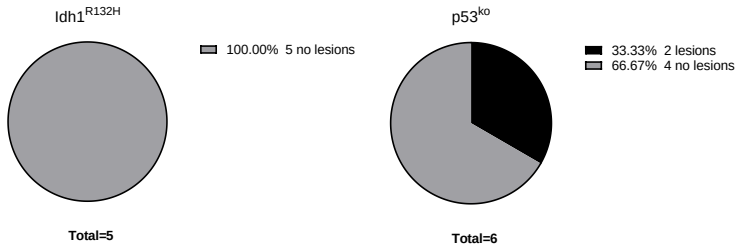

*Figure 26: **Pie chart of the control groups**. Control groups included 5+1 animal injected with Idh1^{R132H} or p53^{ko} NSCs. In the Idh1^{R132H} one animal died during surgery.*

The control groups had a tumor rate of 0/5 for Idh1^{R132H} confirming my expectations and 2/6 for p53^{ko} (Figure 26). Having a look at the calculated tumor volume received from the MRI screen, the two animals constantly stayed at low levels, not higher than 1.6 µl (Figure 27). To check how reliable the measurements are I received from the animal imaging core facility are, the MRI data with the highest tumor volume are presented (Figure 27). These results therefore need to be interpreted with caution.

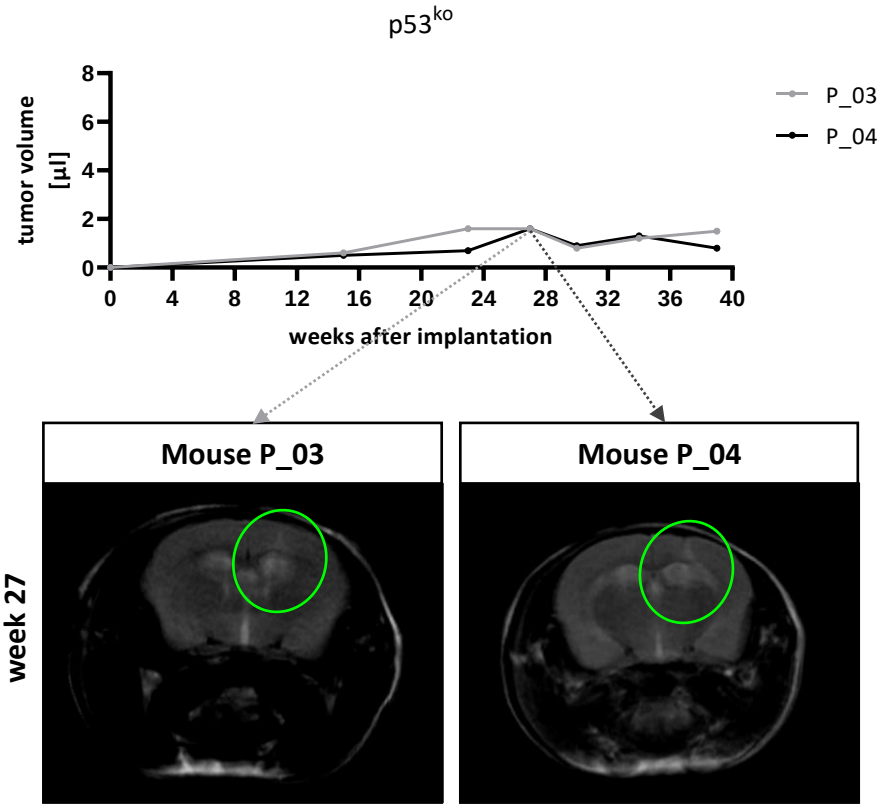

Figure 27: **Summary of the control groups**. 2 animals of the p53ko group had lesions with steady tumor volumes over time

The MRI gave no evidence for tumor formation in mice with Idh1^{R132H} NSCs, to examine if I nevertheless detect Idh1^{R132H} expressing cells, the animals were post-mortem additionally histological processed. At that no positive cells were observed in the stained mouse sections.

3.8.4. 2-HG spectrometry

As already mentioned, I worked together with spectrometry experts to establish an advanced non-invasive method for 2-HG localization and quantification. Despite multiple complications and throwbacks Dr. Andreas Korzowski and Justyna Platek managed to set up an experimental pipeline to obtain first preliminary results (Supplement 9). With this we were now able to compare the spectra from the tumor with the heathly contralateral hemisphere. With data of high quality the single metabolites can be measured including 2-HG. The spatial resolution, reliability and comparability within the tumor and the close-by infiltration zone are limiting factors that need to be improved. Nevertheless this achievement opens up new possibilities for future experiments.

4. Discussion

Until today the big challenge in the field of IDH-mut glioma is the establishment of a highly biologically relevant, powerful preclinical model to gain more insights into basic biology and do relevant translational research. To solve this I developed a genetically engineered murine NSC based model with several advantages I validated, characterized and investigated in depth during this project.

4.1. Design of the model

As described at the beginning a for me convincing model has to fulfill multiple requirements. In the following the choice for or against specific conditions and parameters is discussed.

Genetical composition

One demand on my model is having a genetic heterozygous IDH mutation, to mimic the real situation found IDH-mut glioma. This particular genetic occurrence found in IDH-mut A cells leads to wildtype IDH work collaboratively with the mutant IDH enzyme.

That's one of the reasons I decided against patient-derived cultures, since several reports show a gradual loss of the wild-type allele in IDH1. (Amankulor et al., 2017; Luchman et al., 2013; Núñez et al., 2019; Piaskowski et al., 2011; Ruiz-Rodado et al., 2020) Additionally it is shown that commonly tumors from glioma patients with a more malignant behavior and additional genetic abnormalities are necessary to get cells that can be sustained *in vitro*. (Mazor et al., 2017; Wakimoto et al., 2014b) Therefore patient-derived cell lines are not useful to model typical low grade IDH-mut A development and progression in a defined genetic background.

However the overexpression of mutant IDH, as often used, neither mimics the physiological situation of patients nor results in completely comparable effects in *in vitro* experiments. (Amankulor et al., 2017; Huang, 2019; Modrek et al., 2017; Núñez et al., 2019; Philip et al., 2018; Ruiz-Rodado et al., 2020) Overexpression might be used to investigate enzymatic impact and effects on the metabolism, but can not be considered as a tumor model. (Garrett et al., 2018)

Another critical point I decided to avoid, is the use of alterations that are not naturally occurring in IDH-mut A such as altered Pten or PDGF expression. (Amankulor et al., 2017; Núñez et al., 2019; Ruiz-Rodado et al., 2020) These mutations are associated with very aggressive progression, relapses or even IDH1 wild-type GBMs. Hence for me it seems not to be a reasonable choice, since I want to mimicking IDH-mut A initiation and formation and investigate the native impact on the genetic alterations on molecular and cellular biology. Everything that is stronger than the Idh1 effect and could overwrite it, should therefore be excluded.

So that I ended up developing a genetically engineered mouse model harboring only my three characterizing core genetic mutations: heterozygous Idh^{R132H}, homozygous $p53^{ko}$ and homozygous $Atrx^{ko}$ integrated into a CreERT2 system. The idea of endogenous heterozygous Cre-based knock-in of $Idh1^{R132H}$ can also be found in other studies. (Bardella et al., 2016; Sasaki et al., 2012) (Sasaki M 2012 Bardella 2016).

However only few currently available models used besides the early event of $Idh1^{R132H}$ both co-occuring mutations, often only shp53 is added. One murine study, probably coming closest to my model, describes the application/implementation of shRNAs against p53 and Atrx albeit in the background of overexpressing $Idh1^{R132H}$ with additional NRAS or with altered Cdkn2a, Pten, PDGFB. (Núñez et al., 2019) A second study resemble my idea, is performed in human NSCs. Only shP53 and shATRX additionally to IDH1R132H overexpression are incorporated. (Modrek et al., 2017)

One major advantage of the used CreERT2 system is the opportunity to temporal and spatial control the recombination which helps to model the initiation and monitor the first changes induced by the alterations and their combinations starting directly after recombination. Additionally with this temporal control tool I can ensure a heterozygosity by fresh recombination of wild-type cultures. Albeit the 2-HG data reveal that my cultures over time lose the 2-HG producing $Idh1^{R132H}$, what also has been proven in Viktoria Fischer's project. Although that's a limitation it even so represents the human *in vitro* situation.

Cell of origin

Historically the origin of astrocytoma was presumed to be a mature astrocyte that undergoes dedifferentiation processes, mainly due to the morphological characteristics. Nowadays the hypothesis is that human glioma have their origins in the subventricular zone (SVZ), a niche in the adult brain accounts for high numbers of NSCs. (Alcantara Llaguno et al., 2009; Sanai et al., 2005; Sanai et al., 2004)

NSCs are immature cells with the lifetime capacity of self-renewal, multipotency and proliferation. Due to evidences like the overlap of high expressed NSC markers in glioma, these cell population became a high-level candidate for the cell of origin. (Singh et al., 2004)

Several studies showed , that the mutant IDH1 expressed in the SVZ of mice promote a tumor supporting characteristics. (Bardella et al., 2016; Pirozzi et al., 2017; Sasaki et al., 2012) Hence I preferred the more immature NSCs over differentiated astrocytes, which are also used in multiple projects. Besides it keeps me multiple opportunities open for future investigations including research of differentiation and cell-type impact and a variety of *in vivo* approaches.

4.2. *In vitro* characterization and investigation

4.2.1. Phenotypic changes

After successful generation and validation of my model on multiple levels (Figure 2), I studied the *in vitro* model in detail starting with phenotypical analysis over methylation to proteomic alterations.

The key findings of my growth and cell death assays are (1) Idh1^{R132H} alone is not beneficial for NSCs. The expression of mutant Idh1 results in higher apoptotic activity compared to the other combinations as well as clearly lower viable cells, which corroborates the known disadvantageous, cytotoxic effect of 2-HG.

Therefore my model reflects what has been seen in both experimental settings, *in vitro* and *in vivo.*

2-HG is reported to induce apoptosis in glioma cells as well as in human and murine NSCs.(Cui et al., 2016; Rosiak et al., 2016; Zhang et al., 2019) One explanation here was higher sensitivity to ER stress and disrupted signaling pathways. (Zhang et al., 2019) In contrary to my data and multiple others, one publication propagate that IDH1 mutation drives tumorigenesis by loss of JNK-mediated apoptosis. (Jiang et al., 2017) This makes once again clear, that the choice of a suitable host cell type, which might not be a mouse embryonic fibroblast, as used in this study, and a general relevant model design, overexpressing IDH1 R132Q is not naturally occurring, is important.

On the other hand the *in vitro* expression of IDH1 in established human glioma cell lines lead to a decreased proliferation rate corroborating my data generated in murine NSCs. (Bralten et al., 2011; Cui et al., 2016) Possible explanation for that are described processes like inactivation of mTOR , downregulation of Wnt/β-catenin signaling and dysregulation of YAP and Notch pathways. (Cui et al., 2016; Fu et al., 2015; Wei et al., 2018) . Another study combines the *in vitro* and *in vivo* analysis of murine NSCs and confirms also there reduced proliferation. (Pirozzi et al., 2017)

In summary my observations broadly support the work of other studies, indicating that Idh1^{R132H} disturbing multiple signaling pathways and thereby reducing proliferation capacity *in vitro*.

The second major finding while *in vitro* characterization was the altered behavior when adding p53^{ko} and Atrx^{ko}. Idh1^{R132H}p53^{ko} and Idh1^{R132H}p53^{ko}Atrx^{ko} showed diminished levels of apoptosis plus increased viability (Figure 3and Figure 4)

Since no IDH-mut glioma occur without additional genetic aberrations they might be important to change the adverse impact of the presumed first mutation. Exposing cells to general oncogenic drivers can activate the p53 pathway and provoke cell-cycle arrest or senescence. (Serrano et al., 1997) Further it is seen that the expression of mutant Idh1 in NSCs cause changes cell cycle and p53 signaling implicating an important role of p53. (Pirozzi et al., 2017) The deletion of this tumor suppressor then

could be necessary to compensate the negative part of the Idh1^{R132H} effect on cell growth. All in literature described models were mutant IDH1 expression is associated with enhanced proliferation had a disruption of p53 signaling at one point, one example in human astrocytes immortalized via HPV 16 E6 which inactivates p53. (Koivunen et al., 2012) Whereas the before described glioma cell line with slower growth all had intact p53.

Cancer cells need to avoid cell cycle arrest and apoptosis, that might be the functional explanation why IDH-mut A show TP53 alterations, why animal models need more than Idh1^{R132H} expression alone to develop tumors and my Idh1^{R132H}p53^{ko} and Idh1^{R132H}p53^{ko}Atrx^{ko} revealed a more tumorigenic phenotype.

Nevertheless investigating proliferation capacity I detected a higher viability in Idh1^{R132H}p53^{ko}Atrx^{ko} versus Idh1^{R132H}p53^{ko} over time while having comparable apoptosis levels, meaning Atrx^{ko} shows synergistic effects on top of Idh1^{R132H}p53^{ko}. However Idh1^{R132H}Atrx^{ko} not showed any beneficial changes in behavior. (Figure 3 and 4)

There is one publication using a model system based on human NSCs, where step by step the three alterations can be added by overexpression and shRNAs. (Modrek et al., 2017) Some results of their experiments exactly reveal what my murine system shows. Idh1^{R132H} and Idh1^{R132H}Atrx^{ko} grew slower and had increased cell death signal matching what I observed. They identify the rescue in Idh1^{R132H}p53^{ko} and Idh1^{R132H}p53^{ko}Atrx^{ko} but no differences between both regarding growth or cell death. This might be explained by the unnatural mutant IDH1 overexpression approach causing a not suitable environment as well as the reduction of ATRX mRNA levels only to 50%. Interestingly they detected in Idh1^{R132H}p53^{ko}Atrx^{ko} evidences of ALT development and genomic instability by identifying higher chromosomal fragment numbers.

The hallmark of immortalization which the tumor in the case of IDH-mut A might reach by ATRX loss and resulting ALT seems to depend also on mutant IDH1 expression and disrupted p53 pathway. (Mukherjee et al., 2018).

It could therefore be assumed that Idh1^{R132H}p53^{ko} seems to provide the basis on which the loss of Atrx can additionally alter the cell into a more aggressive phenotype.

4.2.2. Methylation changes

Global hypermethylation and G-CIMP

The inhibition of DNA demethylases cause global hypermethylation in IDH-mut A, an essential characteristic a relevant model system has to share.

As required, my *in vitro* model showed a global hypermethylation when examining the methylation status of over 285 000 CpGs with the novel Illumina mouse methylation chip. Since this easy and low-cost method was in the past only possible for human samples, most previous mouse models had only the possibility to indirectly prove this phenotype. They made use of 5hmC and 5mC level which allow a mediated conclusion to the global methylation status of the cells. Methods as immunohistochemistry, dot plot or HPLC were therefor used to demonstrate decreased 5hmC or elevated 5 mC levels indicating a hypermethylation already in several murine studies. (Amankulor et al., 2017; Bardella et al., 2016; Sasaki et al., 2012) One study profiled the DNA methylome of mouse gliomas by methyl-seq. (Philip et al., 2018) Their *in vivo* hypermethylation data go in line with my *in vitro* mouse data.

The first approach that connected the IDH1 mutation and the development of the G-CIMP was published 2012. (Turcan et al., 2012) Besides the proof in patient samples, they used human immortalized astrocytes with an overexpression of mutant IDH1. This experiment resulted in around 45 000 differentially methylated CpGs after an extremely long time of passaging (P 40-50). For unknown reasons a G-CIMP signature of 17 new identified genes was established without a correlation to the original G-CIMP publication. (Noushmehr et al., 2010)

However, my model develops its hypermethylation gradually already within 28 days. The novel chip technology allowed us to demonstrate this modulation of the methylome in relation to the time $Idh1^{R132H}$ is expressed. While the developing time was faster my murine NSCs harbored a comparable amount of differentially methylated CpGs (65 309 CpGs) as the human model. (Turcan et al., 2012) One possible explanation for this might be the endogenous, heterozygous $Idh1^{R132H}$ expression as well as better modeling of the original cell type. Inducing extensive changes in mature cells such as astrocytes might be more difficult than in a more plastic NSC.

Since the definition of G-CIMP positive is still ambiguous and literature-dependent, I used the top 50 gene candidates from the original paper to identify a G-CIMP. (Noushmehr et al., 2010) The overlap of 82 % of the analyzed genes supports the successful development of the characteristic phenotype in my model. These findings may be somewhat limited. CIMP classically is defined by hypermethylation of CpG islands, while my analysis included all CpGs due to shortened number of island CpGs. Nevertheless especially the data in Supplement 2 clearly support the hypermethylation for the island

region. Moreover methylation data are often added by gene expression data, which I do not have for my model.

Comparison mouse and human

To illustrate biological relevance and transferability of the mouse model I aimed to compare the murine data with the patients' situation. But what we learned already after a short period of time was that this is not too simple. Approach to simply map the mouse methylation data into the human TSNE based on EPIC data and used for tumor classification failed. Hence the orthologous CpG and overlapping gene approach followed.

The major topic emerging during the orthologous CpG analysis was differentiation and developmental processes. The importance of these can be confirmed by multiple research of both human and mouse data consistent in various analyzed methods (ChIPseq, RNAseq and other gene expression data). (Amankulor et al., 2017; Lu et al., 2012; Modrek et al., 2017; Núñez et al., 2019; Pirozzi et al., 2017) The enrichment for processes related to differentiation and development suggest a remodeling function of mutant IDH, that is essential to mold the perfect composition of a cell of origin.

Furthermore the species overlapping KEGG analysis gave indications for an enrichment of pathways associated with cancer. Till this hit remained after applying stricter filters, I considered it as convincing. These pathways contain also processes like apoptosis and proliferation, which I already validated in the functional analysis part of my study and was confirmed by multiple other IDH-mut studies. But also for example Wnt signaling and sphingolipid signaling were suggested to be modified as a result of $Idh1^{R132H}p53^{ko}Atrx^{ko}$ in my data support evidence from previous murine and patient observations. (Bardella et al., 2016; Cui et al., 2016; Dowdy et al., 2020)

The immune-related topic, emerging during my analysis, matches the current trend in the field of IDH-mut A. 2-HG seems to be also an 'immunometabolite' which influences the microenvironment as well as the tumor cell and its response to those stimuli. (Du and Hu, 2021b)

All this findings support the reliability of my generated model system to mimic human situation and thereby provides the opportunity for coming deeper analysis.

Despite these promising results, questions remain including a possible $Idh1^{R132H}$ induced methylation pattern and how the cell status influences this whole process. And since I have seeing that $Atrx^{ko}$ has some exclusive effects on the methylome (Supplement 8) the chromatin assembly might be involved in this in an unidentified way. Further research in this topic could provide also evidences about the identified synergistic role seen in proliferation.

However, it is important to bear in mind, that my findings received from methylation data are not directly correlated to actually modified mechanisms or processes, since it is not yet fully understood

how methylation status of single CpG impacts gene expression and biological processes. Furthermore the annotation of the mouse chip offers room for improvement.

4.2.3. The Idh1^{R132H}p53^{ko}Atrx^{ko} proteome

The cell's proteome is what most effective influences the entire cellular processes. Hence the impact of inducing genetic alterations on the protein abundances was of great interest. Here I focused on the analysis of the genotype that is closest to the patients' genetics and showed the most relevant changes in behavior: Idh1^{R132H}p53^{ko}Atrx^{ko}. What clearly was seen is a distinct pattern of modulation in the proteome of IPA cells. This changes were so substantial that two defined clusters could be identified, separating Idh1^{R132H}p53^{ko}Atrx^{ko} cells from wild-type cells. Besides the abundance pattern the groups differ in over 300 significant altered proteins. Within these important candidates emerged.

Bax as protein falling into the category of pro-apoptotic members had a remarkably low abundance within all IPA samples. As response to stress, Bax translocate to the mitochondria membrane and by pore formation lead to the release of cytochrome c which activates caspase 9 activity resulting in high activity levels of caspase 3/7. (Martinou et al., 2000) Compromising, the reduced protein levels of Bax identified in Idh1^{R132H}p53^{ko}Atrx^{ko} could play a part in contributing to the low caspase 3/7 activity leading to decreased apoptosis and facilitating the elevated numbers of viable cells.

Ki-67 is a proliferation marker used in diagnostic and grading of tumors. The observed upregulation in the Idh1^{R132H}p53^{ko}Atrx^{ko} group molecularly confirms the enhanced proliferative capacity of this genotype identified in my first analysis. Moreover it supports the transition from normal NSCs into more tumorigenic cells by fulfilling several hallmarks of cancer.

The third interesting observation in these proteomics data set was the high abundance of Idh1. Within this analysis I cannot distinguish between mutant and wild-type Idh1. Nevertheless an upregulation might be explained by an only heterozygous occurrence of wild-type Idh1 which is essential to produce NAPDH and a-KG. (Bleeker et al., 2010) NADPH and a-KG are necessary for multiple essential cellular processes such as fatty acid synthesis, macromolecule synthesis and regulation of redox balance. Hence it is known that, the expression of mutant IDH1 leads to metabolic imbalance. (Waitkus et al., 2016) Furthermore tumor cells are metabolic highly active and even in IDH wild-type GBMs an upregulation of wild-type IDH1 can be seen leading to metabolic reprogramming to support enhanced tumor progression. (Calvert et al., 2017) Analyzing the TCGA data set regarding mRNA level of IDH1 the result corroborate these findings for IDH-mut A and IDH wild-type GBMs, further suggesting an increase for IDH-mut A high-grade compared to IDH-mut A or IDH-mut oligodendroglioma. (TCGA Research Network: https://www.cancer.gov/tcga)

After focusing on specific candidate proteins supporting the observed behavioral shifts, I analyzed the proteomic data of my murine IDH-mut A model on a broader level. The results demonstrated that I likewise can achieve described modifications of biological pathways in my murine $Idh1^{R132H}p53^{ko}Atrx^{ko}$ NSC model.

Major aim hereby was to check the murine proteome against the real patient situation. A recent study compared the proteomic changes between a set of IDHmut A, IDHmut oligodendroglioma and IDH wild-type GBMs. (Dekker et al., 2020). This data set indeed provides a relevant cohort for comparison. But by being limited to tumor samples, it lacks normal tissue as counterpart of my wild-type cells.

The overlap between my murine NSCs and the human patient samples was higher than expected. The major findings in their human data concentrated mainly on metabolic effects. They describe aerobic glycolysis and glutaminolysis as one of the top regulated hits, identified also on RNA level before. These are processes known to be altered several cancers as well as play an important role in IDHmut glioma. (Lenting et al., 2019; Yang et al., 2017) Furthermore the human IDH-mut glioma revealed alterations in enzymes that convert valine, leucine, isoleucine and proline into glutamate as well as TCA-cycle enzymes. These findings are consistent with data , determined with different methods then proteomics investigating IDH mutation. (Grassian et al., 2014a; Strickland and Stoll, 2017) It has to be mentioned that they did not distinguished between astrocytoma and oligodendroglioma within the analysis, but rather checked IDH wild-type versus mutant.

Nevertheless I obtained a similar pathway enrichment pattern especially focusing on my top 30 KEGG terms, but even so within the GO-terms (Supplement 6). Citrate cycle, amino acid catabolism (valine, leucine, isoleucine degradation), pyruvate metabolism, glycolysis, fatty acid degradation, so in general most of the in my proteomic data enriched terms closely fit to the human data set. Also the upregulation of Idh1 goes in line with this metabolic-associated findings complemented by altered protein abundances of multiple Aldhs (Aldh7a1, Aldh2, Aldh3a2), Abat, Aco2, Hk2, Ldhb etc.

Likewise, the metabolic changes including TCA cycle processes was confirmed in a IDH1 mutant mouse model. (Ruiz-Rodado et al., 2020) This metabolomics based approach described the comprehensive term of central carbon metabolism as reprogrammed in IDH1mut tumors of mice. With an enrichment of 6,7 fold my proteomic data also reflect the modulation of this major term.

Altogether IDH-mut A typical alterations seem to contribute to an adaption of cells' metabolic processes including the import and processing of glutamate, lactate and other essential substrates to reduce the cellular stress induced by the mutations as well as modified cancer associated pathways influencing this metabolic complex.

The results of my data set depict another term to be modified that caught my interest: proteoglycans in cancer. This includes proteoglycans and their interplay with tumor microenvironment as well as signaling that downstream effects tumor growth, invasion, adhesion and angiogenesis. Since proteoglycans seems to play an important role in brain tumors and the murine Idh1^{R132H}p53^{ko}Atrx^{ko} NSCs already show changes *in vitro*, this should be bear in mind for *in vivo* analysis (Siebzehnrubl, 2021; Yan and Wang, 2020)

Overall the proteomic investigations showed that Idh1^{R132H}p53^{ko}Atrx^{ko} mainly contribute to modulate the cellular proteome in such a way that tumor associated pathways and metabolic processes are enriched to provide the suitable molecular environment to get tumorigenic. Since this part was limited to Idh1^{R132H}p53^{ko}Atrx^{ko}, it was not possible to determine which regulation belongs to which alteration or if there are synergistic effects only occurring with certain combinations.

4.2.4. Overlaps between methylome and proteome changes

Despite its exploratory nature, this study offers some insight into Idh1^{R132H}p53^{ko}Atrx^{ko} induced changes effecting the cellular system. As mentioned investigating methylation alone is already challenging and every hind has to be validated on additional levels. What was encouraging to identify, is the high overlap between the two approaches within my comprehensive analysis. This supports that even though I did not identified exactly the same candidates at all levels, the mechanisms modulated by Idh1^{R132H}p53^{ko}Atrx^{ko} are at a higher level congruent.

However, one aspect appeared in the data analysis of both, methylome and proteome: the sphingolipid metabolism. Sphingolipids are lipids with functions in regulating proliferation but also drug response. Lipids in general are known to be effected by the mutations of IDH matching to what not only the epigenetic but also the proteomic results indicates about this specific class.

The interesting overlap here was found in a human study suggesting an IDH-mut specific sensitivity and vulnerability targeting the sphingolipid pathway. (Dowdy et al., 2020)

4.3. Prospects of the *in vitro* system

The aim of the present *in vitro* research was to examine if and how Idh1^{R132H}, p53^{ko}and Atrx^{ko} have the capacity to profoundly alter my murine model system. In this work I was able to tackle major questions and problems and find multiple answers. Nevertheless several topics still remain open and new issues raised by this study. For this my established model should provide an improved basis.

Further research should be undertaken to explore the accurate role of Atrx. Most studies in the field have only focused on its contribution to ALT. But what my methylation data clearly reveal is a hypomethylation of specific CpGs under Atrx^{ko} conditions. Moreover the added Atrx^{ko} in an I Idh1^{R132H}p53^{ko} background affect the rate of proliferation, indicating an notable impact of this

combination on biological processes. My data support evidence from other studies identifying Atrx as contributor to an astrocytoma associated phenotype. (Danussi et al., 2018)

The next logical steps to approach this research questions would be to examine with ATAC seq how chromatin accessibility is changes under $Atrx^{ko}$ with or without $Idh1^{R132H}$ influence, as well as what influence the cellular context plays since $Atrx^{ko}$ is only identified in astrocytoma. At that my NSCs and their potential do differentiate into multiple cell types are of advantage.

For that purpose and to detect more insights the proper analysis of all genotypes could produce revealing results. With this the effects particularly on protein level induced by $Idh1^{R132H}$ alone, $Idh1^{R132H}p53^{ko}$ and $Idh1^{R132H}Atrx^{ko}$ and probably also $Atrx^{ko}$ alone could identify the interplay between the core alterations better. Also going into even more depth for the methylation analysis might be supportive.

In a next step the translation to the patient has to be done again. Therefore a reliable cohort of human samples with a clear defined mutation pattern the corresponding methylation data and protemic data would be necessary before a solid comparison can be performed.

With all this done and further investigation this model offers the perfect foundation to target identified pathways or weak spots testing treatment response or adding additional modification with CRISPR/Cas for example. Applying broad drug screens could in addition detect vulnerabilities and provides the possibility to trace certain responses or resistances back to specific genotypes. Candidates of interest are PARP inhibitors, Bcl-xL inhibitors, demethylation agents (e.g. decitabine) or other epigenetic modulator, drugs targeting the sphingolipid pathway, synergistic effects with 2-HG inhibitors and so forth. All of them were recently either identified in experimental settings or in other IDH-mut tumor entities such as AML. (Dowdy et al., 2020; Park and Turcan, 2019; Venugopal et al., 2021)

The most important limitation of this part of my study lies in the fact that the tumor microenvironment cannot be included. The next chapter, therefore, moves on to discuss the *in vivo* achievements.

4.4. *In vivo* experiments

Due to several variable limitations of my established in vitro system ranging from loss of heterozygosity to lacking microenvironment my final step was the generation of an *in vivo* model.

4.4.1. Pilot experiment

As described, in previous experiments we discovered difficulties with the mouse strain used by default, BALB/c nude. The animals carry the homozygous Foxn1^{nu} mutation resulting in failed thymic development. (Flanagan, 1966; Pantelouris, 1968) However, they are able to develop normal T cell precursors, and over time produce mature T cells. (McClellan et al., 2017)

IDH-mut A are tumors not growing as fast as IDH wild-type GBMs for example. As a result I expect also in mice a slower growth and need an all along immunological stable setting. Hence BALB/c nude were not the mouse strain to pick for implantations. Because it is well-known that tumor uptake and growth rate correlate with the selected strain, a pilot experiment was essential to ensure the optimal solution. (Doetschman, 2009; Rivera and Tessarollo, 2008) I ended up with 8 different groups including different backgrounds (BALB/c, C57BL/6, CB17 or NOD) and multiple target genes (Rag1/2, Prkdc, Il2rg) leading to different functionality of the immune system.

The NCH 551b as hemizygous IDH1-mut patient-derived cell line not perfectly matches our requirements but was a reasonable compromise to easily screen several groups while not wasting too much time waiting for tumor development. These cells are already established models in our lab with average tumor developing times of 90 days and proper 2-HG production. I assume that I can draw reliably inferences from the growth behavior of NCH 551b regarding the transfer to the main experiment applying murine NSCs.

Confirming my expectations I saw differences between the groups including tumor uptake rate, growth speed and histological behavior. These relation may partly be explained by the absent NK cell activity in all strains with Rag deletion.

One critical point are the absolute values of tumor volume plotted in Figure 18. As the histological staining demonstrate there are discrepancies between MRI and murine brain. For some cases tumors were not detected as such, for others the IDH1 R132H positive area seems to be comparable large while the tumor volume indicates differences. There might be a bias in analysis since it was performed by varying members of the animal imaging core facility. Cross-checking it supports two solutions. In the first place I counted more on the general tumor development and histology data and avoid comparing tumor volume as deciding factor. For the future I would rather recommend using a more unbiased and better comparable approach also applied on human data such as semi-automated tool to segment MRI images.

A factor also not to be neglected is the comparability. Considering that I generated my murine NSCs from B6 mice and also the host strain for the immunocompetent group are wild-type B6, so that animals with this background represent interesting candidates.

Another significant aspect is the histological behavior of the tumor cells in the tissue context. Whereas IDH-mut A are characterized by diffuse growth infiltrating the existing parenchyma (Wesseling et al., 2011) I demand a comparable, not well-circumscribed growth behavior from a relevant *in vivo* model. This was not or only sparsely the case for NRGs and B6 Rag2 KO groups but clearly seen in NSG, and B6 Rag2 Il2ryc. Of course also the varying tumor uptake rate is essential. Regarding this, groups such as NRG and B6 Rag2 Il2ryc showing in 100 % of the animals tumor development, should be favored.

The pilot experiment was designed to determine a fitting host strain and to avoid previous backstrokes. Taken together the differing data obtained hereby make clear that this was important.

4.4.2. Main experiment in immunocompetent mice, setbacks and prospective solutions

The initial plan was to in parallel implant Idh1^{R132H}p53^{ko} and Idh1^{R132H}p53^{ko}Atrx^{ko} into immunodeficient and immunocompetent mice to have best conditions for a direct comparison. However, due to restricted cage capacities I had to split everything up.

As expected in described several times Idh1^{R132H} were also in the background of murine NSCs not sufficient to initiate tumor formation. (Amankulor et al., 2017; Bardella et al., 2016; Sasaki et al., 2012) In contrast to earlier findings, however, no evidence of abnormal brain structure were detected. This discrepancy could be attributed to the experiment length and method to get Idh1^{R132H} into the brain. In my case cells were probably not proliferative enough to find a niche and as indicated by my *in vitro* data were overgrown or degraded by the host.

The second control group got injected with p53^{ko} NSCs. At first appearance the tumor rate in this group was quiet high. This data must be interpreted with caution, because the MRI images indeed indicate something, but this lesion was neither distinct nor was growing over the time of 10 months compared to at least clearly seen in one animal of the Idh1^{R132H}p53^{ko}Atrx^{ko} group (10_03) (Figure 24).

The comparison of the two big groups I implanted, Idh1^{R132H}p53^{ko} and Idh1^{R132H}p53^{ko}Atrx^{ko} , revealed differences in the number of animals with lesions detected via MRI screen. Since beside my experiment there is no animal model purely using Idh1^{R132H}p53^{ko}Atrx^{ko} in an immunocompetent background, so that proper references to other studies concerning this comparison do not exist. As mentioned all other models make use of unnatural tumor drivers including Pten, Pdgfa or NRAS. One model used

triple alteration, as I did, albeit with an overexpression of IDH1^{R132H} and shRNAs against P53 and ATRX in human NSCs and performed xenografts with this. (Modrek et al., 2017) Their *in vivo* key finding was the imitating of IDH-mut A typical diffuse invasive behavior seen only in the three alterations not in IDH1 P53 combination or IDH1 alone. With this, another possible function of Atrx might be identified. These observations, however, do not match the described inhibited cell migration in another study. (Cai et al., 2015) Since the publication of 2015 used a primary GBM cell line this inconsistency might indicate a cell type dependent role of ATRX. However, it would be worth examining the migration behavior of my murine NSC model *in vitro* to determine differences with and without Atrx.

Another option would be to compare the diffuse invasive nature of injected NSCS between my two groups. But therefore a solution for the rather disappointing histological analysis has to be elaborated (Figure 24). In the near future a thoroughly, time consuming search for the tumor in the important animals will follow. However, there is no perfect option since applying the cells to a dye before future implantation (as often done in short term experiments) will not be detectable after 10 months anymore. The only other possibility would be the co-expression of a fluorescent protein. However, fluorescent proteins have reported impact on the immune system and response, what might limit the validity of the study.

Since I assume clearly higher amount of animals bearing a tumor with considerably higher tumor volume when implanting the murine NSC into immunodeficient mice, I presume a improvement of this issue for the subsequent experiments. Within this part the possibility might arise to receive samples witch proper quality and enough material to compare diffuse infiltration as well as check for epigenetic modulation, further genetic alteration and proteomic data. I would expect even bigger differences in the analysis of these data sets comparing *in vivo* Idh1^{R132H}p53^{ko} against Idh1^{R132H}p53^{ko}Atrx^{ko} than seen *in vitro*.

Another topic I also wanted to approach within my *in vivo* part, was to initiate the establishment of methods to non-invasively identify and measure 2-HG. For that my cooperating physics developed a preliminary pipeline that provides a way to measure metabolites including 2-HG based on spectra changes. Their data (Supplement 9) supported that my MRI detected lesions are at least Idh1^{R132H} positive not losing their mutation as described for *in vitro* cultivation. A 2-HG quantification could assess concentration distributions within the brain as well as predict and monitor response to drugs such as a 2-HG inhibitor or immunotherapy while excluding pseudo progression. A different approach based on an innovative publication aiming for the same was also already considered. (Salamanca-Cardona et al., 2017)

The role of the immune system in the whole complex of IDH-mut A rises in importance but is still not fully explored. For that reason I harvested in addition to the brain also the cervical lymphnodes and

the spleen of my immunocompetent mice to collect samples that in further analysis can be used to screen for example for T-cells with tumor-specific receptors as response to Idh1^{R132H} exposure in the brain.

In conclusion my results were not fully encouraging particularly concerning the setback of verifying the tumor histologically and thereby missing the opportunity of further investigations including methylation or proteomics such as done for the in vitro part. Nevertheless I considered A functional immunocompetent allograft mimicking IDH-mut A was lacking in the field, but with further improvements to overcome identified obstacles I formed with this work a basis for testing and developing also immune-related therapies or combination treatments.

4.5. Conclusion and perspective

This project was undertaken to first design a comprehensive IDH-mut A mouse model and afterwards validate, investigate and evaluate the biological processes being affected by the three core tumor alterations, Idh1^{R132H}p53^{ko}Atrx^{ko} .

I established a murine genetically engineered NSC based model system that satisfied all my rigorous defined requirements, offering *in vitro* and *in vivo* options. During the *in vitro* part I could show that the cells harboring Idh1^{R132H}p53^{ko}Atrx^{ko} mimic essential properties of tumorigenic cells particularly IDH-mut A. This includes cell death prevention and enhanced proliferation, as cancer hallmarks, as well as establishing global DNA hypermethylation, specific for IDH-mut A. My experiments clearly supported that Idh1^{R132H} mutation by itself has no tumorigenic potential on a cellular level, but rather necessarily depends on the co-occurrence with an alteration that's capable of compensate the harmful 2-HG effects. In my case this was assumed by p53. The data targeting the question what role Atrx^{ko} plays indicated an additional and beneficial impact of the third alteration, not only seen *in vitro* but also *in vivo*. Nevertheless there are still many unanswered questions about the function of Atrx^{ko} in the Idh1^{R132H}p53^{ko} background and further work required to clarify that.

Besides the identified induction of hypermethylation developing over time the mouse chip offered an innovative approach to investigate the impact of this onto the cell in depth. Besides some promising results including biological processes and mechanisms being impacted by Idh1^{R132H}, the data provide multiple options for future investigations with the need to dive deeper into the bioinformatics of methylation data. The same holds true for the proteome part. The analysis of Idh1^{R132H}p53^{ko}Atrx^{ko} revealed what is modulated with all three core alterations, but to identify causal connections linking these three and to spot synergistic effects a split approach will be essential. Nevertheless my murine *in vitro* model revealed multiple aspects mimicking human IDH-mut A.

One future highlight that can be achieved with the current setting will be to find correlations between methylation and proteomics data, that would allow to predict how methylation modulates the proteome and to finally to compare everything with the clinical data. So that these findings can have significant implications for the understanding of how every single alteration effects the cell, on which level and why certain combinations are necessary to become a tumor cell. With this the model provides a basis for identifying key points important for formation as well as weak points specific for this cells.

With this *in vitro* achievements the required next step was the challenging *in vivo* modeling to provide an opportunity that can approach all the microenvironmental questions. First I figured out, what would be the immunodeficient host strain that fits best for my approach. Thereafter implantation of Idh1^{R132H}p53^{ko} and Idh1^{R132H}p53^{ko}Atrx^{ko} NSCs into immunocompetent mice followed, resulting in a

higher tumor rate for Idh1^{R132H}p53^{ko}Atrx^{ko}. Nevertheless the area including the lesion was not possible to determine post-mortem within the mouse brain with histological and immunohistochemical methods. Albeit the advanced spectrometric measurements indicate evidence of intra-lesional 2-HG. Improving this method will offer a non-invasive approach to detect Idh-mut cells and will provide valuable insights into the behavior of 2-HG. Particularly in the context of an intact immune system and possible treatment experiments including 2-HG inhibitor or vaccination it would create added value.

But necessarily first the allografting into the identified immunodeficient strain is needed to compare which impact the immune system plays in this sophisticated complex. What I would expect is a distinct higher number of tumor-bearing mice.

To avoid the surgical intervention everything is already prepared to establish the CreERT2 based recombination via a single dose of 4-OHT. Therefore a crossbreeding to have a promoter controlling CreERT2 different from Rosa was necessary. Reasonable possibilities are for example Tlx, associated to NSCs, or Gfap, highly expressed in the astrocyte-lineage. But considerably more will be needed to identify the proper experimental settings and conditions (including right mouse age at treatment, number of cells positive for recombination etc.). Nevertheless this model of Idh1^{R132H}p53^{ko}Atrx^{ko} inducible in every wanted cell to every wanted time point could contribute to address multiple unanswered current issues in the field of IDH-mut A, where patients at long last could benefit from.

With this work I successfully established a comprehensive in vivo and in vitro murine model of IDH-mut A with proven biological relevance that provides a reliable basis for future application necessary to improve research that’s clinical relevant. As with all I detected certain limitations and a significant amount of work has to been done in the future, but the complementary parts of in vivo and in vitro could offer a solution for the majority of issues.

5. References

Alcantara Llaguno, S., Chen, J., Kwon, C.-H., Jackson, E.L., Li, Y., Burns, D.K., Alvarez-Buylla, A., and Parada, L.F. (2009). Malignant Astrocytomas Originate from Neural Stem/Progenitor Cells in a Somatic Tumor Suppressor Mouse Model. Cancer Cell *15*, 45-56.

Álvarez-Aznar, A., Martínez-Corral, I., Daubel, N., Betsholtz, C., Mäkinen, T., and Gaengel, K. (2020). Tamoxifen-independent recombination of reporter genes limits lineage tracing and mosaic analysis using CreERT2 lines. Transgenic Research *29*, 53-68.

Amankulor, N.M., Kim, Y., Arora, S., Kargl, J., Szulzewsky, F., Hanke, M., Margineantu, D.H., Rao, A., Bolouri, H., Delrow, J.*, et al.* (2017). Mutant IDH1 regulates the tumor-associated immune system in gliomas. Genes Dev *31*, 774-786.

Amary, M.F., Bacsi, K., Maggiani, F., Damato, S., Halai, D., Berisha, F., Pollock, R., O'Donnell, P., Grigoriadis, A., Diss, T.*, et al.* (2011). IDH1 and IDH2 mutations are frequent events in central chondrosarcoma and central and periosteal chondromas but not in other mesenchymal tumours. J Pathol *224*, 334-343.

Amorim, J.P., Santos, G., Vinagre, J., and Soares, P. (2016). The Role of ATRX in the Alternative Lengthening of Telomeres (ALT) Phenotype. Genes (Basel) *7*, 66.

Argentaro, A., Yang, J.C., Chapman, L., Kowalczyk, M.S., Gibbons, R.J., Higgs, D.R., Neuhaus, D., and Rhodes, D. (2007). Structural consequences of disease-causing mutations in the ATRX-DNMT3-DNMT3L (ADD) domain of the chromatin-associated protein ATRX. Proc Natl Acad Sci U S A *104*, 11939-11944.

Aubrey, B.J., Strasser, A., and Kelly, G.L. (2016). Tumor-Suppressor Functions of the TP53 Pathway. Cold Spring Harb Perspect Med *6*.

Balss, J., Pusch, S., Beck, A.C., Herold-Mende, C., Krämer, A., Thiede, C., Buckel, W., Langhans, C.D., Okun, J.G., and von Deimling, A. (2012). Enzymatic assay for quantitative analysis of (D)-2-hydroxyglutarate. Acta Neuropathol *124*, 883-891.

Bardella, C., Al-Dalahmah, O., Krell, D., Brazauskas, P., Al-Qahtani, K., Tomkova, M., Adam, J., Serres, S., Lockstone, H., Freeman-Mills, L.*, et al.* (2016). Expression of Idh1(R132H) in the Murine Subventricular Zone Stem Cell Niche Recapitulates Features of Early Gliomagenesis. Cancer Cell *30*, 578-594.

Bleeker, F.E., Atai, N.A., Lamba, S., Jonker, A., Rijkeboer, D., Bosch, K.S., Tigchelaar, W., Troost, D., Vandertop, W.P., Bardelli, A.*, et al.* (2010). The prognostic IDH1(R132) mutation is associated with reduced NADP+-dependent IDH activity in glioblastoma. Acta neuropathologica *119*, 487-494.

Borger, D.R., Tanabe, K.K., Fan, K.C., Lopez, H.U., Fantin, V.R., Straley, K.S., Schenkein, D.P., Hezel, A.F., Ancukiewicz, M., Liebman, H.M.*, et al.* (2012). Frequent mutation of isocitrate dehydrogenase (IDH)1 and IDH2 in cholangiocarcinoma identified through broad-based tumor genotyping. Oncologist *17*, 72-79.

Brady, C.A., Jiang, D., Mello, S.S., Johnson, T.M., Jarvis, L.A., Kozak, M.M., Kenzelmann Broz, D., Basak, S., Park, E.J., McLaughlin, M.E.*, et al.* (2011). Distinct p53 transcriptional programs dictate acute DNA-damage responses and tumor suppression. Cell *145*, 571-583.

Bralten, L.B.C., Kloosterhof, N.K., Balvers, R., Sacchetti, A., Lapre, L., Lamfers, M., Leenstra, S., de Jonge, H., Kros, J.M., Jansen, E.E.W.*, et al.* (2011). IDH1 R132H decreases proliferation of glioma cell lines in vitro and in vivo. Annals of Neurology *69*, 455-463.

Brewer, G.J., Torricelli, J.R., Evege, E.K., and Price, P.J. (1993). Optimized survival of hippocampal neurons in B27-supplemented Neurobasal, a new serum-free medium combination. J Neurosci Res *35*, 567-576.

Bunse, L., Pusch, S., Bunse, T., Sahm, F., Sanghvi, K., Friedrich, M., Alansary, D., Sonner, J.K., Green, E., Deumelandt, K.*, et al.* (2018). Suppression of antitumor T cell immunity by the oncometabolite (R)-2-hydroxyglutarate. Nat Med *24*, 1192-1203.

Cai, J., Chen, J., Zhang, W., Yang, P., Zhang, C., Li, M., Yao, K., Wang, H., Li, Q., Jiang, C.*, et al.* (2015). Loss of ATRX, associated with DNA methylation pattern of chromosome end, impacted biological behaviors of astrocytic tumors. Oncotarget *6*.

Calvert, A.E., Chalastanis, A., Wu, Y., Hurley, L.A., Kouri, F.M., Bi, Y., Kachman, M., May, J.L., Bartom, E., Hua, Y.*, et al.* (2017). Cancer-Associated IDH1 Promotes Growth and Resistance to Targeted Therapies in the Absence of Mutation. Cell reports *19*, 1858-1873.

Cancer Genome Atlas Research, N., Brat, D.J., Verhaak, R.G.W., Aldape, K.D., Yung, W.K.A., Salama, S.R., Cooper, L.A.D., Rheinbay, E., Miller, C.R., Vitucci, M.*, et al.* (2015). Comprehensive, Integrative Genomic Analysis of Diffuse Lower-Grade Gliomas. N Engl J Med *372*, 2481-2498.

Capper, D., Jones, D.T.W., Sill, M., Hovestadt, V., Schrimpf, D., Sturm, D., Koelsche, C., Sahm, F., Chavez, L., Reuss, D.E.*, et al.* (2018). DNA methylation-based classification of central nervous system tumours. Nature *555*, 469-474.

Cesare, A.J., and Reddel, R.R. (2010). Alternative lengthening of telomeres: models, mechanisms and implications. Nature Reviews Genetics *11*, 319-330.

Cheung, N.-K.V., Zhang, J., Lu, C., Parker, M., Bahrami, A., Tickoo, S.K., Heguy, A., Pappo, A.S., Federico, S., Dalton, J.*, et al.* (2012). Association of Age at Diagnosis and Genetic Mutations in Patients With Neuroblastoma. JAMA *307*, 1062-1071.

Chinwalla, A.T., Cook, L.L., Delehaunty, K.D., Fewell, G.A., Fulton, L.A., Fulton, R.S., Graves, T.A., Hillier, L.W., Mardis, E.R., McPherson, J.D.*, et al.* (2002). Initial sequencing and comparative analysis of the mouse genome. Nature *420*, 520-562.

Chowdhury, R., Yeoh, K.K., Tian, Y.M., Hillringhaus, L., Bagg, E.A., Rose, N.R., Leung, I.K., Li, X.S., Woon, E.C., Yang, M.*, et al.* (2011). The oncometabolite 2-hydroxyglutarate inhibits histone lysine demethylases. EMBO Rep *12*, 463-469.

Clynes, D., Jelinska, C., Xella, B., Ayyub, H., Taylor, S., Mitson, M., Bachrati, C.Z., Higgs, D.R., and Gibbons, R.J. (2014). ATRX Dysfunction Induces Replication Defects in Primary Mouse Cells. PLOS ONE *9*, e92915.

Cui, D., Ren, J., Shi, J., Feng, L., Wang, K., Zeng, T., Jin, Y., and Gao, L. (2016). R132H mutation in IDH1 gene reduces proliferation, cell survival and invasion of human glioma by downregulating Wnt/β-catenin signaling. The International Journal of Biochemistry & Cell Biology *73*, 72-81.

D'Oto, A., Tian, Q.-W., Davidoff, A.M., and Yang, J. (2016). Histone demethylases and their roles in cancer epigenetics. J Med Oncol Ther *1*, 34-40.

Dang, L., White, D.W., Gross, S., Bennett, B.D., Bittinger, M.A., Driggers, E.M., Fantin, V.R., Jang, H.G., Jin, S., Keenan, M.C.*, et al.* (2010). Cancer-associated IDH1 mutations produce 2-hydroxyglutarate. Nature *465*, 966.

Danussi, C., Bose, P., Parthasarathy, P.T., Silberman, P.C., Van Arnam, J.S., Vitucci, M., Tang, O.Y., Heguy, A., Wang, Y., Chan, T.A.*, et al.* (2018). Atrx inactivation drives disease-defining phenotypes in glioma cells of origin through global epigenomic remodeling. Nature Communications *9*, 1057.

Dao Trong, P., Rösch, S., Mairbäurl, H., Pusch, S., Unterberg, A., Herold-Mende, C., and Warta, R. (2018). Identification of a Prognostic Hypoxia-Associated Gene Set in IDH-Mutant Glioma. Int J Mol Sci *19*.

Dekker, L.J.M., Wu, S., Jurriëns, C., Mustafa, D.A.N., Grevers, F., Burgers, P.C., Sillevis Smitt, P.A.E., Kros, J.M., and Luider, T.M. (2020). Metabolic changes related to the IDH1 mutation in gliomas preserve TCA-cycle activity: An investigation at the protein level. The FASEB Journal *34*, 3646-3657.

Dhillon, S. (2018). Ivosidenib: First Global Approval. Drugs *78*, 1509-1516.

Dinardo, C.D., Stein, A.S., Stein, E.M., Fathi, A.T., Schuh, A.C., Fernández, P.M., Odenike, O., Kantarjian, H.M., Stone, R.M., Collins, R.*, et al.* (2018a). Mutant IDH (mIDH) inhibitors, ivosidenib or enasidenib, with azacitidine (AZA) in patients with acute myeloid leukemia (AML). Journal of Clinical Oncology *36*, 7042-7042.

DiNardo, C.D., Stein, E.M., de Botton, S., Roboz, G.J., Altman, J.K., Mims, A.S., Swords, R., Collins, R.H., Mannis, G.N., Pollyea, D.A.*, et al.* (2018b). Durable Remissions with Ivosidenib in IDH1-Mutated Relapsed or Refractory AML. New England Journal of Medicine *378*, 2386-2398.

Doetschman, T. (2009). Influence of genetic background on genetically engineered mouse phenotypes. Methods Mol Biol *530*, 423-433.

Dowdy, T., Zhang, L., Celiku, O., Movva, S., Lita, A., Ruiz-Rodado, V., Gilbert, M.R., and Larion, M. (2020). Sphingolipid Pathway as a Source of Vulnerability in IDH1(mut) Glioma. Cancers (Basel) *12*.

Du, X., and Hu, H. (2021a). The Roles of 2-Hydroxyglutarate. Frontiers in Cell and Developmental Biology *9*.

Du, X., and Hu, H. (2021b). The Roles of 2-Hydroxyglutarate. Front Cell Dev Biol *9*, 651317.

el-Deiry, W.S., Kern, S.E., Pietenpol, J.A., Kinzler, K.W., and Vogelstein, B. (1992). Definition of a consensus binding site for p53. Nat Genet *1*, 45-49.

Farshidfar, F., Zheng, S., Gingras, M.C., Newton, Y., Shih, J., Robertson, A.G., Hinoue, T., Hoadley, K.A., Gibb, E.A., Roszik, J.*, et al.* (2017). Integrative Genomic Analysis of Cholangiocarcinoma Identifies Distinct IDH-Mutant Molecular Profiles. Cell Rep *18*, 2780-2794.

Feil, R., Brocard, J., Mascrez, B., LeMeur, M., Metzger, D., and Chambon, P. (1996). Ligand-activated site-specific recombination in mice. Proceedings of the National Academy of Sciences of the United States of America *93*, 10887-10890.

Feil, R., Wagner, J., Metzger, D., and Chambon, P. (1997). Regulation of Cre recombinase activity by mutated estrogen receptor ligand-binding domains. Biochem Biophys Res Commun *237*, 752-757.

Figueroa, M.E., Abdel-Wahab, O., Lu, C., Ward, P.S., Patel, J., Shih, A., Li, Y., Bhagwat, N., Vasanthakumar, A., Fernandez, H.F.*, et al.* (2010). Leukemic IDH1 and IDH2 Mutations Result in a Hypermethylation Phenotype, Disrupt TET2 Function, and Impair Hematopoietic Differentiation. Cancer Cell *18*, 553-567.

Flanagan, S.P. (1966). 'Nude', a new hairless gene with pleiotropic effects in the mouse. Genet Res *8*, 295-309.

Flavahan, W.A., Drier, Y., Liau, B.B., Gillespie, S.M., Venteicher, A.S., Stemmer-Rachamimov, A.O., Suvà, M.L., and Bernstein, B.E. (2016). Insulator dysfunction and oncogene activation in IDH mutant gliomas. Nature *529*, 110-114.

Fonseca, M.I., Chu, S.H., Hernandez, M.X., Fang, M.J., Modarresi, L., Selvan, P., MacGregor, G.R., and Tenner, A.J. (2017). Cell-specific deletion of C1qa identifies microglia as the dominant source of C1q in mouse brain. J Neuroinflammation *14*, 48.

Friedrich, M., Sankowski, R., Bunse, L., Kilian, M., Green, E., Ramallo Guevara, C., Pusch, S., Poschet, G., Sanghvi, K., Hahn, M.*, et al.* (2021). Tryptophan metabolism drives dynamic immunosuppressive myeloid states in IDH-mutant gliomas. Nature Cancer *2*, 723-740.

Fu, X., Chin, Randall M., Vergnes, L., Hwang, H., Deng, G., Xing, Y., Pai, Melody Y., Li, S., Ta, L., Fazlollahi, F.*, et al.* (2015). 2-Hydroxyglutarate Inhibits ATP Synthase and mTOR Signaling. Cell Metabolism *22*, 508-515.

Gabizon, R., Brandt, T., Sukenik, S., Lahav, N., Lebendiker, M., Shalev, D.E., Veprintsev, D., and Friedler, A. (2012). Specific recognition of p53 tetramers by peptides derived from p53 interacting proteins. PLoS One *7*, e38060.

Garrett, M., Sperry, J., Braas, D., Yan, W., Le, T.M., Mottahedeh, J., Ludwig, K., Eskin, A., Qin, Y., Levy, R., *et al.* (2018). Metabolic characterization of isocitrate dehydrogenase (IDH) mutant and IDH wildtype gliomaspheres uncovers cell type-specific vulnerabilities. Cancer & Metabolism *6*, 4.

Garrick, D., Samara, V., McDowell, T.L., Smith, A.J., Dobbie, L., Higgs, D.R., and Gibbons, R.J. (2004). A conserved truncated isoform of the ATR-X syndrome protein lacking the SWI/SNF-homology domain. Gene *326*, 23-34.

Ge, S.X., Jung, D., and Yao, R. (2020). ShinyGO: a graphical gene-set enrichment tool for animals and plants. Bioinformatics *36*, 2628-2629.

Gibbons, R.J., Bachoo, S., Picketts, D.J., Aftimos, S., Asenbauer, B., Bergoffen, J., Berry, S.A., Dahl, N., Fryer, A., Keppler, K., *et al.* (1997). Mutations in transcriptional regulator ATRX establish the functional significance of a PHD-like domain. Nat Genet *17*, 146-148.

Gibbons, R.J., Suthers, G.K., Wilkie, A.O., Buckle, V.J., and Higgs, D.R. (1992). X-linked alpha-thalassemia/mental retardation (ATR-X) syndrome: localization to Xq12-q21.31 by X inactivation and linkage analysis. Am J Hum Genet *51*, 1136-1149.

Grassian, A.R., Parker, S.J., Davidson, S.M., Divakaruni, A.S., Green, C.R., Zhang, X., Slocum, K.L., Pu, M., Lin, F., Vickers, C., *et al.* (2014a). IDH1 mutations alter citric acid cycle metabolism and increase dependence on oxidative mitochondrial metabolism. Cancer Res *74*, 3317-3331.

Grassian, A.R., Parker, S.J., Davidson, S.M., Divakaruni, A.S., Green, C.R., Zhang, X., Slocum, K.L., Pu, M., Lin, F., Vickers, C., *et al.* (2014b). IDH1 mutations alter citric acid cycle metabolism and increase dependence on oxidative mitochondrial metabolism. Cancer research *74*, 3317-3331.

Halazonetis, T.D., and Kandil, A.N. (1993). Conformational shifts propagate from the oligomerization domain of p53 to its tetrameric DNA binding domain and restore DNA binding to select p53 mutants. EMBO J *12*, 5057-5064.

Hall, B., Limaye, A., and Kulkarni, A.B. (2009). Overview: Generation of Gene Knockout Mice. Current Protocols in Cell Biology *44*, 19.12.11-19.12.17.

Han, S., Liu, Y., Cai, S.J., Qian, M., Ding, J., Larion, M., Gilbert, M.R., and Yang, C. (2020). IDH mutation in glioma: molecular mechanisms and potential therapeutic targets. British Journal of Cancer *122*, 1580-1589.

Hanahan, D., and Weinberg, Robert A. (2011). Hallmarks of Cancer: The Next Generation. Cell *144*, 646-674.

Harris, C.C. (1996). Structure and function of the p53 tumor suppressor gene: clues for rational cancer therapeutic strategies. J Natl Cancer Inst *88*, 1442-1455.

Heaphy, C.M., de Wilde, R.F., Jiao, Y., Klein, A.P., Edil, B.H., Shi, C., Bettegowda, C., Rodriguez, F.J., Eberhart, C.G., Hebbar, S., *et al.* (2011). Altered telomeres in tumors with ATRX and DAXX mutations. Science *333*, 425.

Hoess, R., Abremski, K., Irwin, S., Kendall, M., and Mack, A. (1990). DNA specificity of the cre recombinase resides in the 25 kDa carboxyl domain of the protein. Journal of Molecular Biology *216*, 873-882.

Hoess, R.H., Wierzbicki, A., and Abremski, K. (1986). The role of the loxP spacer region in PI site-specific recombination. Nucleic Acids Research *14*, 2287-2300.

Huang, L.E. (2019). Friend or foe—IDH1 mutations in glioma 10 years on. Carcinogenesis *40*, 1299-1307.

Hupp, T.R., Meek, D.W., Midgley, C.A., and Lane, D.P. (1992). Regulation of the specific DNA binding function of p53. Cell *71*, 875-886.

Indra, A.K., Warot, X., Brocard, J., Bornert, J.M., Xiao, J.H., Chambon, P., and Metzger, D. (1999). Temporally-controlled site-specific mutagenesis in the basal layer of the epidermis: comparison of the

recombinase activity of the tamoxifen-inducible Cre-ER(T) and Cre-ER(T2) recombinases. Nucleic Acids Res *27*, 4324-4327.

Irizarry, R.A., Ladd-Acosta, C., Wen, B., Wu, Z., Montano, C., Onyango, P., Cui, H., Gabo, K., Rongione, M., Webster, M.*, et al.* (2009). The human colon cancer methylome shows similar hypo- and hypermethylation at conserved tissue-specific CpG island shores. Nat Genet *41*, 178-186.

Jiang, B., Zhang, J., Xia, J., Zhao, W., Wu, Y., Shi, M., Luo, L., Zhou, H., Chen, A., Ma, H.*, et al.* (2017). IDH1 Mutation Promotes Tumorigenesis by Inhibiting JNK Activation and Apoptosis Induced by Serum Starvation. Cell Rep *19*, 389-400.

Jiao, Y., Killela, P.J., Reitman, Z.J., Rasheed, A.B., Heaphy, C.M., de Wilde, R.F., Rodriguez, F.J., Rosemberg, S., Oba-Shinjo, S.M., Nagahashi Marie, S.K.*, et al.* (2012). Frequent ATRX, CIC, FUBP1 and IDH1 mutations refine the classification of malignant gliomas. Oncotarget *3*, 709-722.

Jiao, Y., Shi, C., Edil, B.H., de Wilde, R.F., Klimstra, D.S., Maitra, A., Schulick, R.D., Tang, L.H., Wolfgang, C.L., Choti, M.A.*, et al.* (2011). DAXX/ATRX, MEN1, and mTOR pathway genes are frequently altered in pancreatic neuroendocrine tumors. Science *331*, 1199-1203.

Jin, G., Reitman, Z.J., Duncan, C.G., Spasojevic, I., Gooden, D.M., Rasheed, B.A., Yang, R., Lopez, G.Y., He, Y., McLendon, R.E.*, et al.* (2013). Disruption of wild-type IDH1 suppresses D-2-hydroxyglutarate production in IDH1-mutated gliomas. Cancer research *73*, 496-501.

Juhász, S., Elbakry, A., Mathes, A., and Löbrich, M. (2018). ATRX Promotes DNA Repair Synthesis and Sister Chromatid Exchange during Homologous Recombination. Mol Cell *71*, 11-24.e17.

Karpel-Massler, G., Nguyen, T.T.T., Shang, E., and Siegelin, M.D. (2019). Novel IDH1-Targeted Glioma Therapies. CNS Drugs *33*, 1155-1166.

Koivunen, P., Lee, S., Duncan, C.G., Lopez, G., Lu, G., Ramkissoon, S., Losman, J.A., Joensuu, P., Bergmann, U., Gross, S.*, et al.* (2012). Transformation by the (R)-enantiomer of 2-hydroxyglutarate linked to EGLN activation. Nature *483*, 484-488.

Konteatis, Z., Artin, E., Nicolay, B., Straley, K., Padyana, A.K., Jin, L., Chen, Y., Narayaraswamy, R., Tong, S., Wang, F.*, et al.* (2020). Vorasidenib (AG-881): A First-in-Class, Brain-Penetrant Dual Inhibitor of Mutant IDH1 and 2 for Treatment of Glioma. ACS Med Chem Lett *11*, 101-107.

Koschmann, C., Calinescu, A.A., Nunez, F.J., Mackay, A., Fazal-Salom, J., Thomas, D., Mendez, F., Kamran, N., Dzaman, M., Mulpuri, L.*, et al.* (2016). ATRX loss promotes tumor growth and impairs nonhomologous end joining DNA repair in glioma. Sci Transl Med *8*, 328ra328.

Kristianto, J., Johnson, M., Zastrow, R., Radcliff, A., and Blank, R. (2017). Spontaneous recombinase activity of Cre–ERT2 in vivo. Transgenic Research *26*, 1-7.

Lee, J., Kotliarova, S., Kotliarov, Y., Li, A., Su, Q., Donin, N.M., Pastorino, S., Purow, B.W., Christopher, N., Zhang, W.*, et al.* (2006). Tumor stem cells derived from glioblastomas cultured in bFGF and EGF more closely mirror the phenotype and genotype of primary tumors than do serum-cultured cell lines. Cancer Cell *9*, 391-403.

Lee, S.M., Koh, H.-J., Park, D.-C., Song, B.J., Huh, T.-L., and Park, J.-W. (2002). Cytosolic NADP+-dependent isocitrate dehydrogenase status modulates oxidative damage to cells. Free Radical Biology and Medicine *32*, 1185-1196.

Lenting, K., Khurshed, M., Peeters, T.H., van den Heuvel, C., van Lith, S.A.M., de Bitter, T., Hendriks, W., Span, P.N., Molenaar, R.J., Botman, D.*, et al.* (2019). Isocitrate dehydrogenase 1-mutated human gliomas depend on lactate and glutamate to alleviate metabolic stress. Faseb j *33*, 557-571.

Liang, J., Liu, H., Li, G., Qian, J., Gao, R., Zhou, Y., and Wang, X. (2020). Global changes in chromatin accessibility and transcription following ATRX inactivation in human cancer cells. FEBS Lett *594*, 67-78.

Liu, X.Y., Gerges, N., Korshunov, A., Sabha, N., Khuong-Quang, D.A., Fontebasso, A.M., Fleming, A., Hadjadj, D., Schwartzentruber, J., Majewski, J.*, et al.* (2012). Frequent ATRX mutations and loss of expression in adult diffuse astrocytic tumors carrying IDH1/IDH2 and TP53 mutations. Acta Neuropathol *124*, 615-625.

Loenarz, C., and Schofield, C.J. (2008). Expanding chemical biology of 2-oxoglutarate oxygenases. Nat Chem Biol *4*, 152-156.

Losman, J.A., and Kaelin, W.G., Jr. (2013). What a difference a hydroxyl makes: mutant IDH, (R)-2-hydroxyglutarate, and cancer. Genes Dev *27*, 836-852.

Louis, D.N. (1994). The p53 gene and protein in human brain tumors. J Neuropathol Exp Neurol *53*, 11-21.

Louis, D.N., Perry, A., Reifenberger, G., von Deimling, A., Figarella-Branger, D., Cavenee, W.K., Ohgaki, H., Wiestler, O.D., Kleihues, P., and Ellison, D.W. (2016). The 2016 World Health Organization Classification of Tumors of the Central Nervous System: a summary. Acta Neuropathol *131*, 803-820.

Louis, D.N., Perry, A., Wesseling, P., Brat, D.J., Cree, I.A., Figarella-Branger, D., Hawkins, C., Ng, H.K., Pfister, S.M., Reifenberger, G.*, et al.* (2021). The 2021 WHO Classification of Tumors of the Central Nervous System: a summary. Neuro-Oncology *23*, 1231-1251.

Lu, C., Ward, P.S., Kapoor, G.S., Rohle, D., Turcan, S., Abdel-Wahab, O., Edwards, C.R., Khanin, R., Figueroa, M.E., Melnick, A.*, et al.* (2012). IDH mutation impairs histone demethylation and results in a block to cell differentiation. Nature *483*, 474-478.

Luchman, H.A., Chesnelong, C., Cairncross, J.G., and Weiss, S. (2013). Spontaneous loss of heterozygosity leading to homozygous R132H in a patient-derived IDH1 mutant cell line. Neuro-oncology *15*, 979-980.

Luchman, H.A., Stechishin, O.D., Dang, N.H., Blough, M.D., Chesnelong, C., Kelly, J.J., Nguyen, S.A., Chan, J.A., Weljie, A.M., Cairncross, J.G.*, et al.* (2012). An in vivo patient-derived model of endogenous IDH1-mutant glioma. Neuro Oncol *14*, 184-191.

Magzoub, M.M., Prunello, M., Brennan, K., and Gevaert, O. (2019). The impact of DNA methylation on the cancer proteome. PLOS Computational Biology *15*, e1007245.

Mardis, E.R., Ding, L., Dooling, D.J., Larson, D.E., McLellan, M.D., Chen, K., Koboldt, D.C., Fulton, R.S., Delehaunty, K.D., McGrath, S.D.*, et al.* (2009). Recurring Mutations Found by Sequencing an Acute Myeloid Leukemia Genome. New England Journal of Medicine *361*, 1058-1066.

Margueron, R., Trojer, P., and Reinberg, D. (2005). The key to development: interpreting the histone code? Curr Opin Genet Dev *15*, 163-176.

Martinou, J.-C., Desagher, S., and Antonsson, B. (2000). Cytochrome c release from mitochondria: all or nothing. Nature Cell Biology *2*, E41-E43.

Mazor, T., Chesnelong, C., Pankov, A., Jalbert, L.E., Hong, C., Hayes, J., Smirnov, I.V., Marshall, R., Souza, C.F., Shen, Y.*, et al.* (2017). Clonal expansion and epigenetic reprogramming following deletion or amplification of mutant IDH1. Proceedings of the National Academy of Sciences of the United States of America *114*, 10743-10748.

McClellan, J., Macasocal, R., Hare, T., and Horn, M. (2017). Characterization of Immunodeficient Mouse Models. The FASEB Journal *31*, 807.814-807.814.

Mellinghoff, I.K., Ellingson, B.M., Touat, M., Maher, E., De La Fuente, M.I., Holdhoff, M., Cote, G.M., Burris, H., Janku, F., Young, R.J.*, et al.* (2020). Ivosidenib in Isocitrate Dehydrogenase 1-Mutated Advanced Glioma. J Clin Oncol *38*, 3398-3406.

Metzger, D., and Chambon, P. (2001). Site- and Time-Specific Gene Targeting in the Mouse. Methods *24*, 71-80.

Miller, J.J., Loebel, F., Juratli, T.A., Tummala, S.S., Williams, E.A., Batchelor, T.T., Arrillaga-Romany, I., and Cahill, D.P. (2019). Accelerated progression of IDH mutant glioma after first recurrence. Neuro Oncol *21*, 669-677.

Miura, H., Quadros, R.M., Gurumurthy, C.B., and Ohtsuka, M. (2018). Easi-CRISPR for creating knock-in and conditional knockout mouse models using long ssDNA donors. Nat Protoc *13*, 195-215.

Modrek, A.S., Golub, D., Khan, T., Bready, D., Prado, J., Bowman, C., Deng, J., Zhang, G., Rocha, P.P., Raviram, R.*, et al.* (2017). Low-Grade Astrocytoma Mutations in IDH1, P53, and ATRX Cooperate to Block Differentiation of Human Neural Stem Cells via Repression of SOX2. Cell Rep *21*, 1267-1280.

Molenaar, R.J., Botman, D., Smits, M.A., Hira, V.V., van Lith, S.A., Stap, J., Henneman, P., Khurshed, M., Lenting, K., Mul, A.N.*, et al.* (2015). Radioprotection of IDH1-Mutated Cancer Cells by the IDH1-Mutant Inhibitor AGI-5198. Cancer Res *75*, 4790-4802.

Molinaro, A.M., Taylor, J.W., Wiencke, J.K., and Wrensch, M.R. (2019). Genetic and molecular epidemiology of adult diffuse glioma. Nature Reviews Neurology *15*, 405-417.

Mukherjee, J., Johannessen, T.-C., Ohba, S., Chow, T.T., Jones, L., Pandita, A., and Pieper, R.O. (2018). Mutant IDH1 Cooperates with ATRX Loss to Drive the Alternative Lengthening of Telomere Phenotype in Glioma. Cancer Research *78*, 2966-2977.

Mural, R.J., Adams, M.D., Myers, E.W., Smith, H.O., Miklos, G.L., Wides, R., Halpern, A., Li, P.W., Sutton, G.G., Nadeau, J.*, et al.* (2002). A comparison of whole-genome shotgun-derived mouse chromosome 16 and the human genome. Science *296*, 1661-1671.

Nagy, A. (2000). Cre recombinase: the universal reagent for genome tailoring. Genesis *26*, 99-109.

Needhamsen, M., Ewing, E., Lund, H., Gomez-Cabrero, D., Harris, R.A., Kular, L., and Jagodic, M. (2017). Usability of human Infinium MethylationEPIC BeadChip for mouse DNA methylation studies. BMC Bioinformatics *18*, 486.

Noushmehr, H., Weisenberger, D.J., Diefes, K., Phillips, H.S., Pujara, K., Berman, B.P., Pan, F., Pelloski, C.E., Sulman, E.P., Bhat, K.P.*, et al.* (2010). Identification of a CpG island methylator phenotype that defines a distinct subgroup of glioma. Cancer Cell *17*, 510-522.

Núñez, F.J., Mendez, F.M., Kadiyala, P., Alghamri, M.S., Savelieff, M.G., Garcia-Fabiani, M.B., Haase, S., Koschmann, C., Calinescu, A.A., Kamran, N.*, et al.* (2019). IDH1-R132H acts as a tumor suppressor in glioma via epigenetic up-regulation of the DNA damage response. Sci Transl Med *11*.

Ostrom, Q.T., Patil, N., Cioffi, G., Waite, K., Kruchko, C., and Barnholtz-Sloan, J.S. (2020). CBTRUS Statistical Report: Primary Brain and Other Central Nervous System Tumors Diagnosed in the United States in 2013-2017. Neuro Oncol *22*, iv1-iv96.

Pantelouris, E.M. (1968). Absence of thymus in a mouse mutant. Nature *217*, 370-371.

Park, J.-W., and Turcan, Ş. (2019). Epigenetic Reprogramming for Targeting IDH-Mutant Malignant Gliomas. Cancers *11*, 1616.

Parsons, D.W., Jones, S., Zhang, X., Lin, J.C., Leary, R.J., Angenendt, P., Mankoo, P., Carter, H., Siu, I.M., Gallia, G.L.*, et al.* (2008). An integrated genomic analysis of human glioblastoma multiforme. Science *321*, 1807-1812.

Paschka, P., Schlenk, R.F., Gaidzik, V.I., Habdank, M., Krönke, J., Bullinger, L., Späth, D., Kayser, S., Zucknick, M., Götze, K.*, et al.* (2010). IDH1 and IDH2 Mutations Are Frequent Genetic Alterations in Acute Myeloid Leukemia and Confer Adverse Prognosis in Cytogenetically Normal Acute Myeloid Leukemia With NPM1 Mutation Without FLT3 Internal Tandem Duplication. Journal of Clinical Oncology *28*, 3636-3643.

Philip, B., Yu, D.X., Silvis, M.R., Shin, C.H., Robinson, J.P., Robinson, G.L., Welker, A.E., Angel, S.N., Tripp, S.R., Sonnen, J.A*., et al.* (2018). Mutant IDH1 Promotes Glioma Formation In Vivo. Cell Rep *23*, 1553-1564.

Piaskowski, S., Bienkowski, M., Stoczynska-Fidelus, E., Stawski, R., Sieruta, M., Szybka, M., Papierz, W., Wolanczyk, M., Jaskolski, D.J., Liberski, P.P*., et al.* (2011). Glioma cells showing IDH1 mutation cannot be propagated in standard cell culture conditions. British journal of cancer *104*, 968-970.

Picketts, D.J., Higgs, D.R., Bachoo, S., Blake, D.J., Quarrell, O.W., and Gibbons, R.J. (1996). ATRX encodes a novel member of the SNF2 family of proteins: mutations point to a common mechanism underlying the ATR-X syndrome. Hum Mol Genet *5*, 1899-1907.

Pinto, B., Henriques, A.C., Silva, P.M.A., and Bousbaa, H. (2020). Three-Dimensional Spheroids as In Vitro Preclinical Models for Cancer Research. Pharmaceutics *12*, 1186.

Pirozzi, C.J., Carpenter, A.B., Waitkus, M.S., Wang, C.Y., Zhu, H., Hansen, L.J., Chen, L.H., Greer, P.K., Feng, J., Wang, Y*., et al.* (2017). Mutant IDH1 Disrupts the Mouse Subventricular Zone and Alters Brain Tumor Progression. Mol Cancer Res *15*, 507-520.

Platten, M., Schilling, D., Bunse, L., Wick, A., Bunse, T., Riehl, D., Karapanagiotou-Schenkel, I., Harting, I., Sahm, F., Schmitt, A*., et al.* (2018). A mutation-specific peptide vaccine targeting IDH1R132H in patients with newly diagnosed malignant astrocytomas: A first-in-man multicenter phase I clinical trial of the German Neurooncology Working Group (NOA-16). Journal of Clinical Oncology *36*, 2001-2001.

Pusch, S., Krausert, S., Fischer, V., Balss, J., Ott, M., Schrimpf, D., Capper, D., Sahm, F., Eisel, J., Beck, A.C*., et al.* (2017). Pan-mutant IDH1 inhibitor BAY 1436032 for effective treatment of IDH1 mutant astrocytoma in vivo. Acta Neuropathol *133*, 629-644.

Raudvere, U., Kolberg, L., Kuzmin, I., Arak, T., Adler, P., Peterson, H., and Vilo, J. (2019). g:Profiler: a web server for functional enrichment analysis and conversions of gene lists (2019 update). Nucleic Acids Research *47*, W191-W198.

Reitman, Z.J., Jin, G., Karoly, E.D., Spasojevic, I., Yang, J., Kinzler, K.W., He, Y., Bigner, D.D., Vogelstein, B., and Yan, H. (2011). Profiling the effects of isocitrate dehydrogenase 1 and 2 mutations on the cellular metabolome. Proc Natl Acad Sci U S A *108*, 3270-3275.

Ren, F., Zhao, Q., Huang, L., Zheng, Y., Li, L., He, Q., Zhang, C., Li, F., Maimela, N.R., Sun, Z*., et al.* (2019). The R132H mutation in IDH1 promotes the recruitment of NK cells through CX3CL1/CX3CR1 chemotaxis and is correlated with a better prognosis in gliomas. Immunol Cell Biol *97*, 457-469.

Reuss, D.E., Sahm, F., Schrimpf, D., Wiestler, B., Capper, D., Koelsche, C., Schweizer, L., Korshunov, A., Jones, D.T., Hovestadt, V*., et al.* (2015). ATRX and IDH1-R132H immunohistochemistry with subsequent copy number analysis and IDH sequencing as a basis for an "integrated" diagnostic approach for adult astrocytoma, oligodendroglioma and glioblastoma. Acta Neuropathol *129*, 133-146.

Reynolds, B.A., and Weiss, S. (1992). Generation of neurons and astrocytes from isolated cells of the adult mammalian central nervous system. Science *255*, 1707-1710.

Richardson, L.G., Choi, B.D., and Curry, W.T. (2019). (R)-2-hydroxyglutarate drives immune quiescence in the tumor microenvironment of IDH-mutant gliomas. Transl Cancer Res *8*, S167-S170.

Richmond, A., and Su, Y. (2008). Mouse xenograft models vs GEM models for human cancer therapeutics. Dis Model Mech *1*, 78-82.

Rivera, J., and Tessarollo, L. (2008). Genetic Background and the Dilemma of Translating Mouse Studies to Humans. Immunity *28*, 1-4.

Rohle, D., Popovici-Muller, J., Palaskas, N., Turcan, S., Grommes, C., Campos, C., Tsoi, J., Clark, O., Oldrini, B., Komisopoulou, E*., et al.* (2013). An inhibitor of mutant IDH1 delays growth and promotes differentiation of glioma cells. Science *340*, 626-630.

Rose, N.R., McDonough, M.A., King, O.N.F., Kawamura, A., and Schofield, C.J. (2011). Inhibition of 2-oxoglutarate dependent oxygenases. Chemical Society Reviews *40*, 4364-4397.

Rosiak, K., Smolarz, M., Stec, W.J., Peciak, J., Grzela, D., Winiecka-Klimek, M., Stoczynska-Fidelus, E., Krynska, B., Piaskowski, S., and Rieske, P. (2016). IDH1R132H in Neural Stem Cells: Differentiation Impaired by Increased Apoptosis. PLOS ONE *11*, e0154726.

Ruiz-Rodado, V., Seki, T., Dowdy, T., Lita, A., Zhang, M., Han, S., Yang, C., Cherukuri, M.K., Gilbert, M.R., and Larion, M. (2020). Metabolic Landscape of a Genetically Engineered Mouse Model of IDH1 Mutant Glioma. Cancers (Basel) *12*.

Sakamuro, D., Sabbatini, P., White, E., and Prendergast, G.C. (1997). The polyproline region of p53 is required to activate apoptosis but not growth arrest. Oncogene *15*, 887-898.

Salamanca-Cardona, L., Shah, H., Poot, A.J., Correa, F.M., Di Gialleonardo, V., Lui, H., Miloushev, V.Z., Granlund, K.L., Tee, S.S., Cross, J.R.*, et al.* (2017). In Vivo Imaging of Glutamine Metabolism to the Oncometabolite 2-Hydroxyglutarate in IDH1/2 Mutant Tumors. Cell Metab *26*, 830-841.e833.

Sanai, N., Alvarez-Buylla, A., and Berger, M.S. (2005). Neural Stem Cells and the Origin of Gliomas. New England Journal of Medicine *353*, 811-822.

Sanai, N., Tramontin, A.D., Quiñones-Hinojosa, A., Barbaro, N.M., Gupta, N., Kunwar, S., Lawton, M.T., McDermott, M.W., Parsa, A.T., Manuel-García Verdugo, J.*, et al.* (2004). Unique astrocyte ribbon in adult human brain contains neural stem cells but lacks chain migration. Nature *427*, 740-744.

Sandlesh, P., Juang, T., Safina, A., Higgins, M.J., and Gurova, K.V. (2018). Uncovering the fine print of the CreERT2-LoxP system while generating a conditional knockout mouse model of Ssrp1 gene. PLOS ONE *13*, e0199785.

Sandoval, J., Heyn, H., Moran, S., Serra-Musach, J., Pujana, M.A., Bibikova, M., and Esteller, M. (2011). Validation of a DNA methylation microarray for 450,000 CpG sites in the human genome. Epigenetics *6*, 692-702.

Sasaki, M., Knobbe, C.B., Itsumi, M., Elia, A.J., Harris, I.S., Chio, II, Cairns, R.A., McCracken, S., Wakeham, A., Haight, J.*, et al.* (2012). D-2-hydroxyglutarate produced by mutant IDH1 perturbs collagen maturation and basement membrane function. Genes Dev *26*, 2038-2049.

Sauer, B. (1998). Inducible gene targeting in mice using the Cre/lox system. Methods *14*, 381-392.

Schumacher, T., Bunse, L., Pusch, S., Sahm, F., Wiestler, B., Quandt, J., Menn, O., Osswald, M., Oezen, I., Ott, M.*, et al.* (2014). A vaccine targeting mutant IDH1 induces antitumour immunity. Nature *512*, 324-327.

Serrano, M., Lin, A.W., McCurrach, M.E., Beach, D., and Lowe, S.W. (1997). Oncogenic ras provokes premature cell senescence associated with accumulation of p53 and p16INK4a. Cell *88*, 593-602.

Shibata, T., Kokubu, A., Miyamoto, M., Sasajima, Y., and Yamazaki, N. (2011). Mutant IDH1 Confers an in Vivo Growth in a Melanoma Cell Line with BRAF Mutation. The American Journal of Pathology *178*, 1395-1402.

Shirahata, M., Ono, T., Stichel, D., Schrimpf, D., Reuss, D.E., Sahm, F., Koelsche, C., Wefers, A., Reinhardt, A., Huang, K.*, et al.* (2018). Novel, improved grading system(s) for IDH-mutant astrocytic gliomas. Acta Neuropathol *136*, 153-166.

Siebzehnrubl, F.A. (2021). Proteoglycans in Glioma Stem Cells. In Proteoglycans in Stem Cells: From Development to Cancer, M. Götte, and K. Forsberg-Nilsson, eds. (Cham: Springer International Publishing), pp. 263-278.

Singh, S.K., Clarke, I.D., Hide, T., and Dirks, P.B. (2004). Cancer stem cells in nervous system tumors. Oncogene *23*, 7267-7273.

Stratton, M.R., Campbell, P.J., and Futreal, P.A. (2009). The cancer genome. Nature *458*, 719-724.

Strickland, M., and Stoll, E.A. (2017). Metabolic Reprogramming in Glioma. Front Cell Dev Biol *5*, 43.

Sulkowski, P.L., Corso, C.D., Robinson, N.D., Scanlon, S.E., Purshouse, K.R., Bai, H., Liu, Y., Sundaram, R.K., Hegan, D.C., Fons, N.R.*, et al.* (2017). 2-Hydroxyglutarate produced by neomorphic IDH mutations suppresses homologous recombination and induces PARP inhibitor sensitivity. Sci Transl Med *9*.

Takami, H., Yoshida, A., Fukushima, S., Arita, H., Matsushita, Y., Nakamura, T., Ohno, M., Miyakita, Y., Shibui, S., Narita, Y.*, et al.* (2015). Revisiting TP53 Mutations and Immunohistochemistry—A Comparative Study in 157 Diffuse Gliomas. Brain Pathology *25*, 256-265.

Tang, J., Wu, S., Liu, H., Stratt, R., Barak, O.G., Shiekhattar, R., Picketts, D.J., and Yang, X. (2004). A novel transcription regulatory complex containing death domain-associated protein and the ATR-X syndrome protein. J Biol Chem *279*, 20369-20377.

Triche, T.J., Jr., Weisenberger, D.J., Van Den Berg, D., Laird, P.W., and Siegmund, K.D. (2013). Low-level processing of Illumina Infinium DNA Methylation BeadArrays. Nucleic Acids Res *41*, e90.

Trinh, K.R., and Morrison, S.L. (2000). Site-specific and directional gene replacement mediated by Cre recombinase. Journal of Immunological Methods *244*, 185-193.

Tunici, P., Bissola, L., Lualdi, E., Pollo, B., Cajola, L., Broggi, G., Sozzi, G., and Finocchiaro, G. (2004). Genetic alterations and in vivo tumorigenicity of neurospheres derived from an adult glioblastoma. Mol Cancer *3*, 25-25.

Turcan, S., Rohle, D., Goenka, A., Walsh, L.A., Fang, F., Yilmaz, E., Campos, C., Fabius, A.W., Lu, C., Ward, P.S.*, et al.* (2012). IDH1 mutation is sufficient to establish the glioma hypermethylator phenotype. Nature *483*, 479-483.

Unruh, D., Zewde, M., Buss, A., Drumm, M.R., Tran, A.N., Scholtens, D.M., and Horbinski, C. (2019). Methylation and transcription patterns are distinct in IDH mutant gliomas compared to other IDH mutant cancers. Scientific Reports *9*, 8946.

van den Bent, M.J., Weller, M., Wen, P.Y., Kros, J.M., Aldape, K., and Chang, S. (2017). A clinical perspective on the 2016 WHO brain tumor classification and routine molecular diagnostics. Neuro-oncology *19*, 614-624.

Venugopal, S., Maiti, A., DiNardo, C.D., Loghavi, S., Daver, N.G., Kadia, T.M., Rausch, C.R., Alvarado, Y., Ohanian, M., Sasaki, K.*, et al.* (2021). Decitabine and venetoclax for IDH1/2-mutated acute myeloid leukemia. American Journal of Hematology *96*, E154-E157.

Voon, H.P., and Wong, L.H. (2016). New players in heterochromatin silencing: histone variant H3.3 and the ATRX/DAXX chaperone. Nucleic Acids Res *44*, 1496-1501.

Waitkus, M.S., Diplas, B.H., and Yan, H. (2016). Isocitrate dehydrogenase mutations in gliomas. Neuro-oncology *18*, 16-26.

Wakimoto, H., Tanaka, S., Curry, W.T., Loebel, F., Zhao, D., Tateishi, K., Chen, J., Klofas, L.K., Lelic, N., Kim, J.C.*, et al.* (2014a). Targetable Signaling Pathway Mutations Are Associated with Malignant Phenotype in IDH-Mutant Gliomas. Clinical Cancer Research *20*, 2898-2909.

Wakimoto, H., Tanaka, S., Curry, W.T., Loebel, F., Zhao, D., Tateishi, K., Chen, J., Klofas, L.K., Lelic, N., Kim, J.C.*, et al.* (2014b). Targetable signaling pathway mutations are associated with malignant phenotype in IDH-mutant gliomas. Clin Cancer Res *20*, 2898-2909.

Wang, Z., Zhang, C., Liu, X., Wang, Z., Sun, L., Li, G., Liang, J., Hu, H., Liu, Y., Zhang, W.*, et al.* (2016). Molecular and clinical characterization of PD-L1 expression at transcriptional level via 976 samples of brain glioma. Oncoimmunology *5*, e1196310.

Watanabe, T., Nobusawa, S., Kleihues, P., and Ohgaki, H. (2009). IDH1 mutations are early events in the development of astrocytomas and oligodendrogliomas. Am J Pathol *174*, 1149-1153.

Wei, S., Wang, J., Oyinlade, O., Ma, D., Wang, S., Kratz, L., Lal, B., Xu, Q., Liu, S., Shah, S.R.*, et al.* (2018). Heterozygous IDH1(R132H/WT) created by "single base editing" inhibits human astroglial cell growth by downregulating YAP. Oncogene *37*, 5160-5174.

Weller, M., van den Bent, M., Preusser, M., Le Rhun, E., Tonn, J.C., Minniti, G., Bendszus, M., Balana, C., Chinot, O., Dirven, L.*, et al.* (2021). EANO guidelines on the diagnosis and treatment of diffuse gliomas of adulthood. Nature Reviews Clinical Oncology *18*, 170-186.

Wesseling, P., Kros, J.M., and Jeuken, J.W.M. (2011). The pathological diagnosis of diffuse gliomas: towards a smart synthesis of microscopic and molecular information in a multidisciplinary context. Diagnostic Histopathology *17*, 486-494.

Xu, W., Yang, H., Liu, Y., Yang, Y., Wang, P., Kim, S.H., Ito, S., Yang, C., Wang, P., Xiao, M.T.*, et al.* (2011). Oncometabolite 2-hydroxyglutarate is a competitive inhibitor of α-ketoglutarate-dependent dioxygenases. Cancer Cell *19*, 17-30.

Xue, Y., Gibbons, R., Yan, Z., Yang, D., McDowell, T.L., Sechi, S., Qin, J., Zhou, S., Higgs, D., and Wang, W. (2003). The ATRX syndrome protein forms a chromatin-remodeling complex with Daxx and localizes in promyelocytic leukemia nuclear bodies. Proc Natl Acad Sci U S A *100*, 10635-10640.

Yan, H., Parsons, D.W., Jin, G., McLendon, R., Rasheed, B.A., Yuan, W., Kos, I., Batinic-Haberle, I., Jones, S., Riggins, G.J.*, et al.* (2009). IDH1 and IDH2 Mutations in Gliomas. New England Journal of Medicine *360*, 765-773.

Yan, Z., and Wang, S. (2020). Proteoglycans as Therapeutic Targets in Brain Cancer. Frontiers in Oncology *10*.

Yang, L., Venneti, S., and Nagrath, D. (2017). Glutaminolysis: A Hallmark of Cancer Metabolism. Annu Rev Biomed Eng *19*, 163-194.

Yang, R.R., Shi, Z.-f., Zhang, Z.-y., Chan, A.K.-Y., Aibaidula, A., Wang, W.-w., Kwan, J.S.H., Poon, W.S., Chen, H., Li, W.-c.*, et al.* (2020). IDH mutant lower grade (WHO Grades II/III) astrocytomas can be stratified for risk by CDKN2A, CDK4 and PDGFRA copy number alterations. Brain Pathology *30*, 541-553.

Ye, D., Guan, K.-L., and Xiong, Y. (2018). Metabolism, Activity, and Targeting of D- and L-2-Hydroxyglutarates. Trends Cancer *4*, 151-165.

Zhang, Y., Pusch, S., Innes, J., Sidlauskas, K., Ellis, M., Lau, J., El-Hassan, T., Aley, N., Launchbury, F., Richard-Loendt, A.*, et al.* (2019). Mutant IDH Sensitizes Gliomas to Endoplasmic Reticulum Stress and Triggers Apoptosis via miR-183-Mediated Inhibition of Semaphorin 3E. Cancer Research *79*, 4994-5007.

Zhao, S., Lin, Y., Xu, W., Jiang, W., Zha, Z., Wang, P., Yu, W., Li, Z., Gong, L., Peng, Y.*, et al.* (2009). Glioma-derived mutations in IDH1 dominantly inhibit IDH1 catalytic activity and induce HIF-1alpha. Science *324*, 261-265.

Zhou, W., Triche, T.J., Jr, Laird, P.W., and Shen, H. (2018). SeSAMe: reducing artifactual detection of DNA methylation by Infinium BeadChips in genomic deletions. Nucleic Acids Research *46*, e123-e123.

6. Supplement

The supplement contains all data that complement the above shown data, but are not essential for the statement.

Supplement 1: ***Apoptotic activity in p53^{ko} NSCs.*** *complements figure 4 Caspase assay n=2 with each 2-3 technical replicates, One sample t-test p=0.29; in the total comparison only * significant different from Idh1 alone*

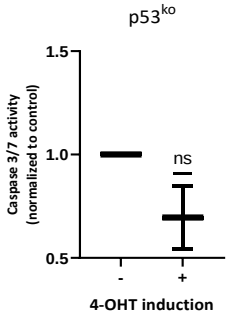

Supplement 2: ***Gradual shift towards hypermethylation.*** *First density plots figure 7; 500 most different CpGs for Idh1^{R132H}p53^{ko}Atrx^{ko}*

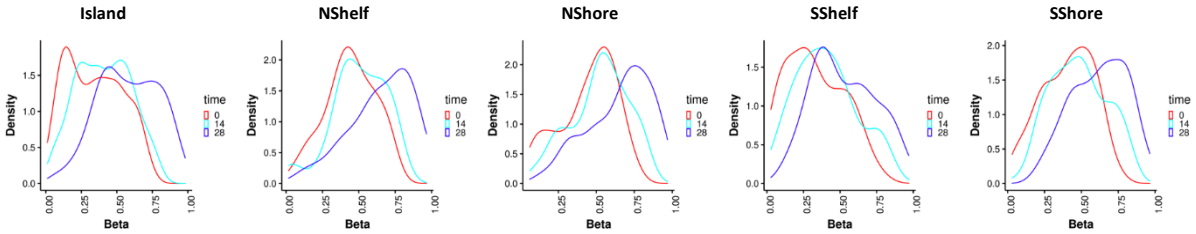

Supplement 3: ***High-level GO term categorization of same direction CpGs.*** *Fits to figure 11. ShinyGOv0.741*

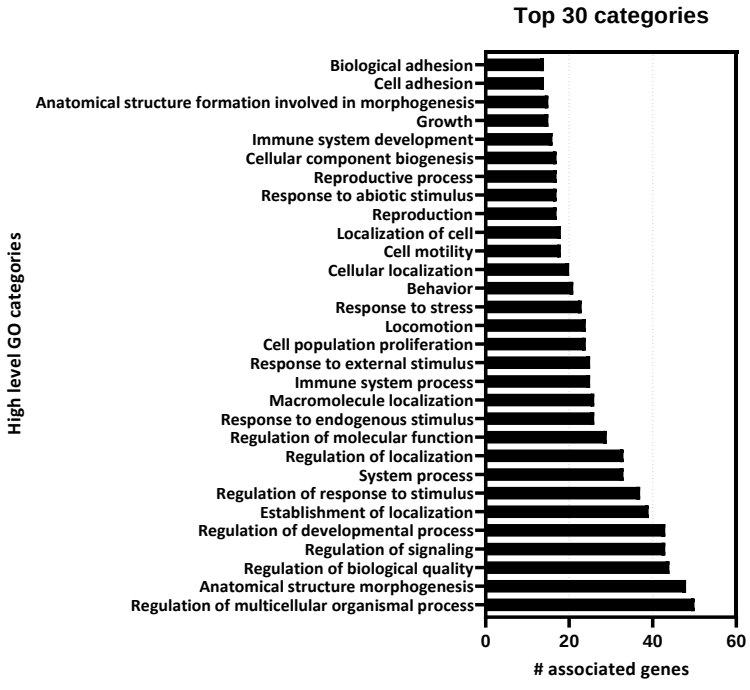

Supplement 4: List of the 166 differentially methylated genes overlapping between human and mouse in KEGG (Figure 14)

Traf5	Zbtb16	Txnrd1	Ddb2	Birc3	Zbtb17	Rasgrp1	Ptch2	Lpar2	Bcl2
Axin1	Gnai2	Stat6	Ptk2	Ralgds	Ptger4	Pik3R2	Tgfbr1	Smad2	Cul1
Traf1	Ifnar2	Ccnd3	Ccna2	Calm1	Tgfb2	Stat1	Bbc3	Egln2	Casp8
Rasgrp2	Pgf	Dapk2	Cdk2	Ccnd2	Tcf7	Rac1	Pten	Vegfa	Adcy4
Ccdc6	Gadd45G	Axin2	Gnb1	Stat4	Hdac1	Hras	Bax	Rac2	Mapk1
Itga6	Bcr	Hif1A	Traf4	Il15	Stat5A	Abl1	Rassf5	Rara	Apc
Arhgef1	Bcl2L1	Foxo1	Rassf1	Plcb3	Ets1	Rasgrp3	Gstp1	Cdkn1B	Il12Rb2
Tgfb3	Keap1	Plcg1	Il12A	Prkaca	Pik3Cd	Traf6	Fzd8	Ccnd1	Gna13
E2F1	Wnt2B	Arnt	Jak1	Epor	Ppard	Traf2	Gstm4	Gna12	Gnb2
Il23A	Tgfb1	Lpar5	Brca2	Cks2	Slc2A1	Igf1R	Il15Ra	Akt2	Grb2
Map2K2	Stat3	Gng4	Il6St	Prkca	Nfkbia	Cdkn2A	Txnrd2	Sufu	Runx1
Nkx3-1	Spi1	Cebpa	Cdk6	Notch1	Prkacb	Gsto2	Nqo1	Rps6Ka5	Esr2
Ncoa4	Eml4	Rhoa	Msh6	Ncoa3	Ralb	Crk	Dvl1	Pik3R1	Birc5
Max	Fadd	Rb1	Ikbkb	Smad3	Plcb2	Cdc42	Wnt3A	Gnai3	Crkl
Pim1	Mapk3	Il12Rb1	Egln1	Gsk3B	Tgfa	Ccne2	Jak2	Map2K1	E2F3
Chuk	Mgst3	Braf	Rock1	Cxcr4	Plcg2	Nfkb2	Gnas	Ifnar1	Mapk9
Wnt1	Skp2	Ctbp1	Gsta4	Msh2	Rbx1				

Supplement 5: KEGG analysis of Pathways in Cancer with 431 genes (reduced from 6017 genes, filtered 50% CpGs methylated) done with ShinyGO v0.741

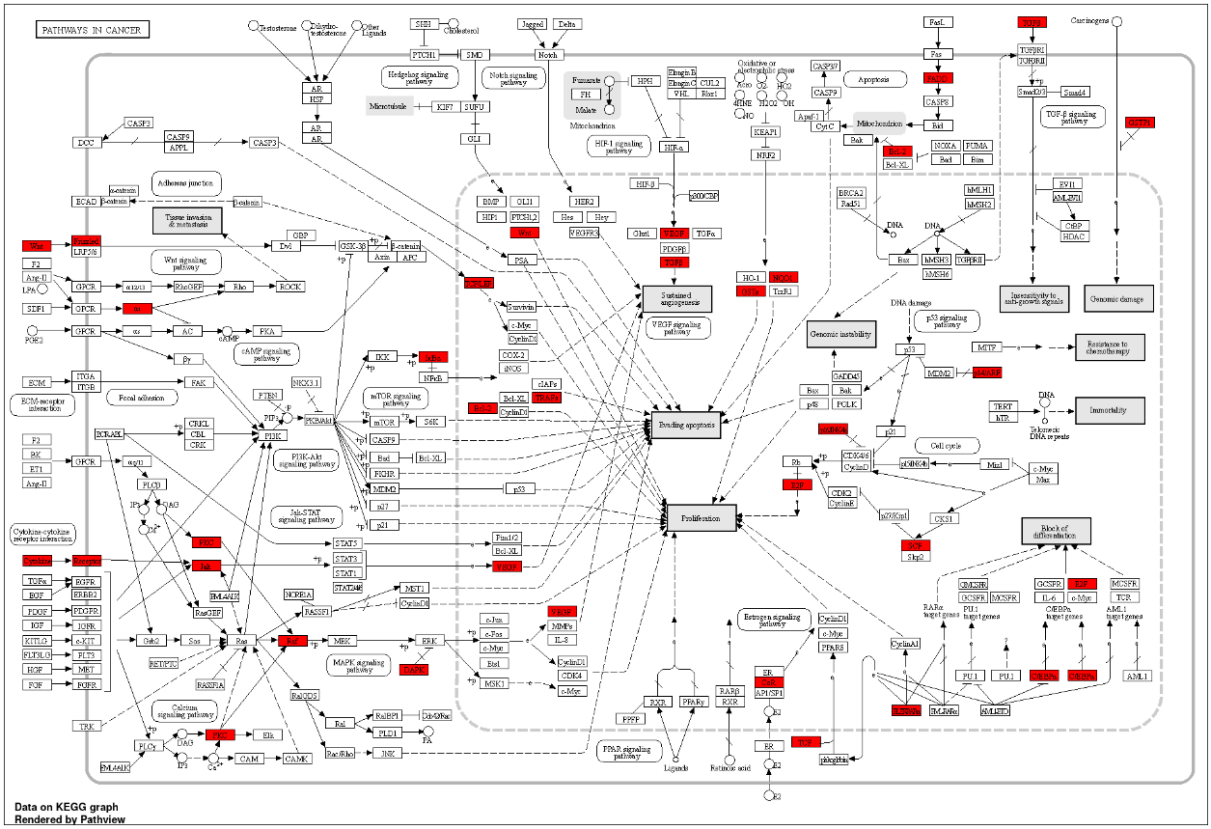

Supplement 6: ***Detailed enrichment analysis****. Here the 30 top hits of GO-terms (upper graph) and KEGG pathways (lower graph) are represented applying the significant proteins under Idh1^{R132H}p53^{ko}Atrx^{ko} influence. This data complement the high level analysis of Figure 17*

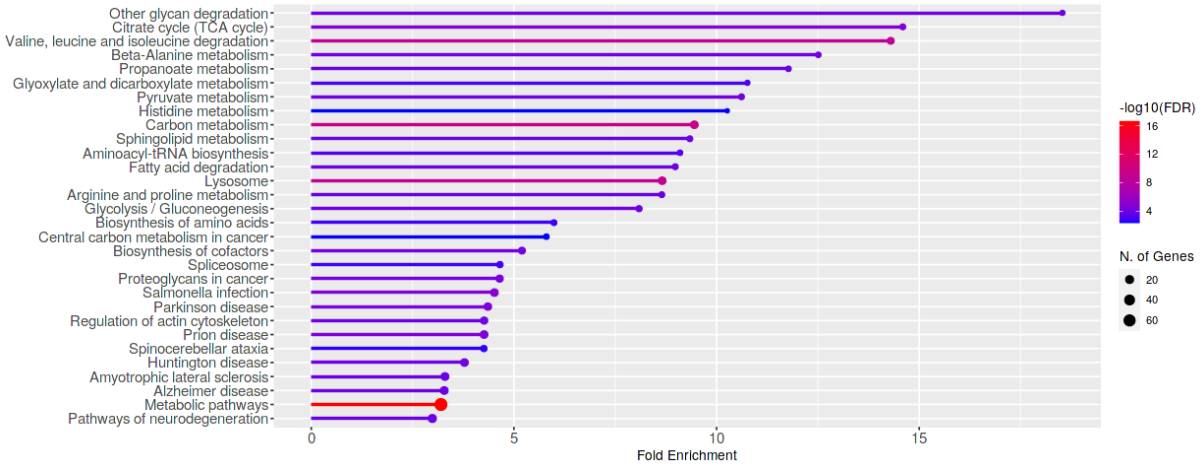

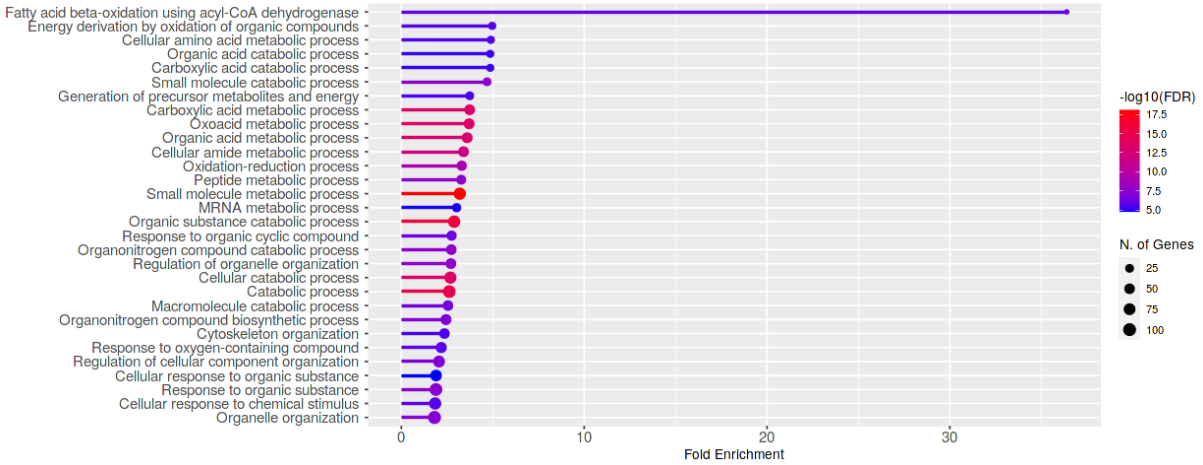

Supplement 7 ***Post-mortem 2-HG measurement.*** *To determine 2-HG levels of the in vivo tumors developed after implantation of IDH-mut NCH 551b three samples each were taken from tumor and control hemisphere. Here the results of the 2-HG assay is presented showing the three biological replicates (points), the mean and SD. Normal distribution was tested by Shapiro-Wilk test and 2-HG concentrations were compared with an unpaired t-test with Welch's correction (p=0.0214).*

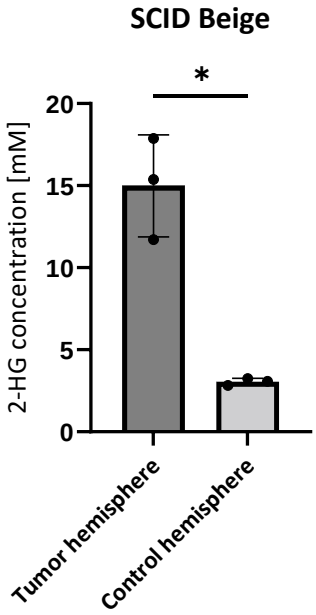

Supplement 8: ***Methylation change exclusively induced by Atrx^{ko}.*** *Some specific CpGs showed a very unique hypomethylation only identified for the genotypes with Atrx^{ko} impact*

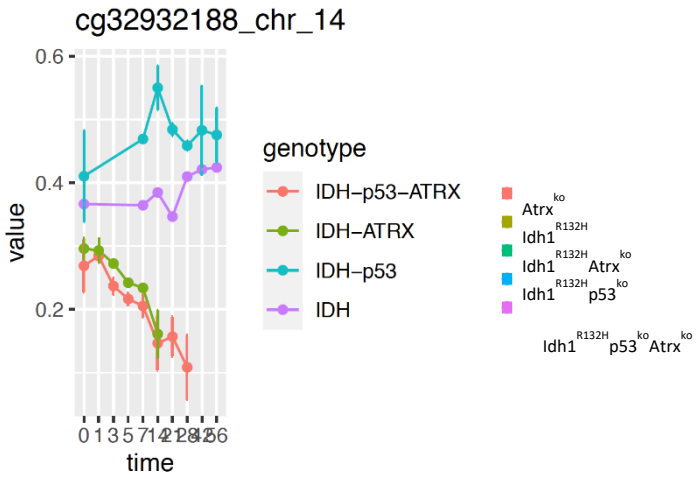

Supplement 9: ***Spectra of tumor and contralateral hemisphere.*** *Preliminary data received from the MR spectroscopy approach by Dr. Andreas Korzowski comparing the metabolites in the tumor and the healthy tissue calculated in relation to the total creatin. 2-HG values of 0.78 compared to 0 support successful 2-HG detection.*

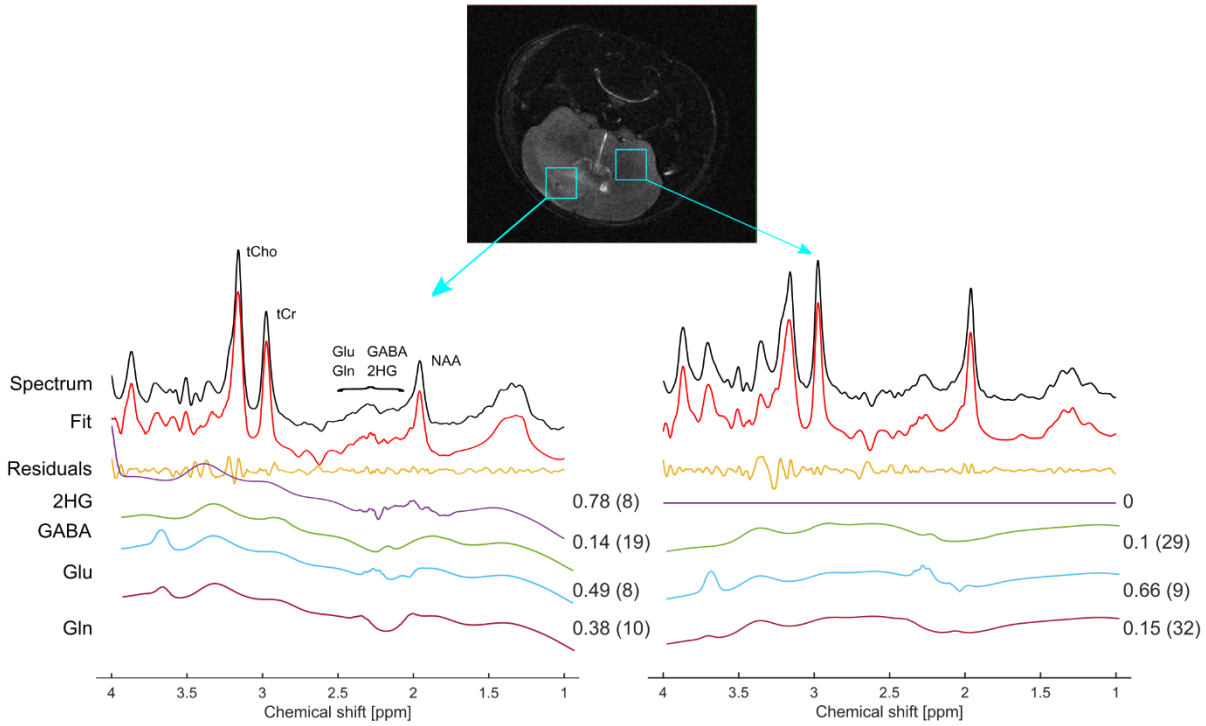

Acknowledgments

Realizing the project, that is only partly reflected in this doctoral thesis, was only possible with the incredible supporting effort from various sides.

To begin with I want to thank my supervisor Stefan Pusch for the opportunity to do my PhD in the CCU Neuropathology even though I was considered to be too immature by some and despite knowing what you were getting into with me. I am thankful for your unrestricted support during my entire project, probably the most fascinating time of my life. You let me make my own experiences and always assumed the role of the pessimist so that it was quite easy for me to stay optimistic, which helped me believe in myself along the way. I really appreciate all the inspiring discussions, that often arose suddenly and escalated quickly, that I was never prepared for so that you frequently had to lend me a pink post-it note.

I would also like to thank Andreas von Deimling for all the support, opportunities and trust to successfully develop the IDH1 project to the next level, especially knowing how important the topic is to him. Particularly helpful for me was the chance to learn from your valuable advice and your guidance on which questions to ask and where to lay my focus.

I also want to express my gratitude to all my TAC members Christel Herold-Mende, Till Milde and Lukas Bunse as well as members of my defense committee Karin Müller-Decker, Walter Haefeli and Moritz Mall for faithfully undertaking their tasks.

Special thanks go to my whole lab. Starting chronologically with the old crew I have to thank Viktoria Brendel for choosing me when everything started and later, for trustfully leaving the project and all your knowledge with me. You know I have to stay friends… I am also grateful to Jessica Eisel for playing a decisive role, particularly in the first phase of my PhD. What would this time have been without both of you: no fruitful discussions concerning complex scientific issues or puzzling other problems, no after-work beer, no Ben and Jerry's Botanik sessions, and all the other unforgetaable times.

Moritz and Johannes for being my inspiration to not take five years for my PhD and for Austria, Pizza, Uno and Happy Hours. Especially Moritz for our evening walks and always supporting me when it was needed.

Though I still don't understand your pathways, I very much appreciate your unwavering support Antoni Martija, from starting our PhD together to today.

Thanks should also go the new lab gang composed of Lars Noller (for your relentless support), Caro Birr (for our unforgettable Kubatzky-reunion), David Vonhören (for sharing whatever comes to your mind, scientifically and non-scientifically), Sonja Herter (for your contribution to my general fitness and

the great talks), Philipp Sievers (my new senior office mate, for matching my crazy moods – with chocolate-coffee beans, if necessary), Amelie Muth (for your commitment in your and Sonjas' battle against Otto), Jana Quadrizius (for your great assistance during your time in our lab and our squash evenings), Antonia Tietzel (for the world's best carrot cake), Annika Reineke (for enriching our team so quickly and easily), Lisa Rösch (for our corona-connection and elevating the average age). And all my other students who supported my project and taught me a lot.

I must also thank my bioinformatic 3Ds whose help cannot be underestimated: Damian Stichel for IPA and a sexy title, Dennis Friedel for his incredible patience and David Vonhören for giving proteomics a chance.

I also wish to acknowledge the effort of Antje Habel, Ulrike Laß, Ulrike Vogel, Viktoria Zeller and I want to thank the whole neuropathology department in general, for being amazing colleagues.

My gratitude goes out to everyone who helped make my project possible and gave me their support along the way, including Andreas Korzowski, Justyna Platek, the transgenic service, the animal imagine people, animal facility,

I would also like to thank all of my other friends for their care and for making my life outside of the DKFZ colorful: Tania, Clara, Svenja, Svenja, Sonja, Viki, Nadine, Kira, Ronny, Steffen, Sebastian and everyone I forgot… by encouraging phone calls, satisfying sports, walks, lovely day trips, essential coffees, excessive cooking and all in all for reminding me that there's a life away from the lab.

Special thanks also to Joy and Cosima, the two beings with the amazing nature to bring me back to myself and to reflect on the truly important things again.

Finally and foremost I am deeply grateful to my family, especially my Mum for your profound belief in me from wherever, and my siblings Alex (now knowing more than ever wanted about IDH) and Rouven for everything sibling love encompasses.